Engineering PNIPAAm Biomaterial Scaffolds to Model Microenvironmental Regulation of Glioblastoma Stem-Like Cells

by

John Michael Heffernan

A Dissertation Presented in Partial Fulfillment
of the Requirements for the Degree
Doctor of Philosophy

Approved October 2017 by the
Graduate Supervisory Committee

Rachael W. Sirianni, Co-Chair
Brent L. Vernon, Co-Chair
Sarah Stabenfeldt
Stephen Massia
Shwetal Mehta

ARIZONA STATE UNIVERSITY

December 2017

ABSTRACT

Following diagnosis of a glioblastoma (GBM) brain tumor, surgical resection, chemotherapy and radiation together yield a median patient survival of only 15 months. Importantly, standard treatments fail to address the dynamic regulation of the brain tumor microenvironment that actively supports tumor progression and treatment resistance. Moreover, specialized niches within the tumor microenvironment maintain a population of highly malignant glioblastoma stem-like cells (GSCs). GSCs are resistant to traditional chemotherapy and radiation therapy and are likely responsible for near universal rates of tumor recurrence and associated morbidity. Thus, disrupting microenvironmental support for GSCs could be critical to more effective GBM therapies. Three-dimensional (3D) culture models of the tumor microenvironment are powerful tools for identifying key biochemical and biophysical inputs that may support or inhibit malignant behaviors. Here, we developed synthetic poly(N-isopropylacrylamide-co-Jeffamine M-1000® acrylamide) or PNJ copolymers as a model 3D system for culturing GBM cell lines and low-passage patient-derived GSCs *in vitro*. These temperature responsive scaffolds reversibly transition from soluble to insoluble in aqueous solution by heating from room temperature to body temperature, thereby enabling easy encapsulation and release of cells in a 3D scaffold. We also designed this system with the capacity for presenting the cell-adhesion peptide sequence RGD for adherent culture conditions. Using this system, we identified conditions that promoted GBM proliferation, invasion, GSC phenotypes, and radiation resistance. In particular, using two separate patient-derived GSC models, we observed that PNJ scaffolds regulated self-renewal, provided protection from radiation induced cell death, and may promote stem cell plasticity in response to radiation. Furthermore, PNJ scaffolds produced *de novo* activation of the transcription factor HIF2α, which is critical to GSC tumorigenicity and

stem plasticity. All together, these studies establish the robust utility of PNJ biomaterials as *in vitro* models for studying microenvironmental regulation of GSC behaviors and treatment resistance.

DEDICATION

First and foremost, I want to give my deepest thanks to my cousin Kyle. Five years ago, I invaded your life and have shamelessly mooched off of your goodwill ever since. I am so appreciative and will never forget the kindness and hospitality that you've shown me. The past few years have been challenging for our family, with probably none more difficult than the last 6 months for both of us. You've dealt with unimaginable difficulty, and have done so with compassion, thoughtfulness, and courage. I truly admire you, and am forever grateful for your friendship in the times I needed it most.

To Mom and Dad, thank you for your continuous outpouring of love, prayers, and support. I know it has been difficult living so far apart, but you have always remained rock steady sources of guidance and encouragement. Thank you for believing in me, and for providing an exceptional example for how to live a full and healthy life. To my brother Patrick, thank you for always being your genuine self. I am looking forward to seeing you more often, and to many more future ski trips together. You guys are the best, and know that I would never have made it this far without your love.

To my friends in the "Trails", Kyle, Tyler, Krystal, Tristan, Billy, and Chris, thank you for being supportive, for picking me up when I'm down, and for your collective sense of humor. To my friends in the climbing community, Chris, Sergio, Laura, Lisa, Blakeslee, Kevin, Chara, Tony, and many more, thank you for constantly reaching out and including me in your plans, for loving the outdoors as much as I do, and most of all for being amazing people. To the LMIC soccer club, Roger, Alex, Greg, Greg, Paulo, Tavo, and many others, thank you for putting up with my constant injuries and mediocre play, for being social after the games, and for helping me to escape my work on the field.

Love you all.

ACKNOWLEDGMENTS

To my mentor Dr. Rachael Sirianni, thank you for being an incredible leader and boss these past years. Thank you for always being willing to take the time to be a teacher, for inspiring me to become a better scientist, for understanding when I needed to take time off, for exemplifying a healthy work/life balance, for your willingness to share and discuss your personal feelings on difficult topics, and for your friendship and constant encouragement. In starting your lab, I know that you took a leap of faith in hiring me as your first graduate student. Five years later, and I have developed a strong scientific mindset, and benefited greatly from your thoughtful guidance. Thank you for giving me the opportunity to work with you. I truly cherish your mentorship, and cannot fully express how much I appreciate the investment that you have made in me. I look forward to the great projects and ideas coming from your lab in the future.

I would also like to acknowledge my other committee members Drs. Brent Vernon, Shwetal Mehta, Sarah Stabenfeldt, and Stephen Massia. Thank you all for always making yourselves available to answer my questions, and for challenging me to broaden my scientific perspectives. I truly appreciate all of your contributions to my academic success.

To Dr. Derek Overstreet, thank you being a great friend and mentor. Your guidance when I started in lab was invaluable as you taught me how to be an effective scientist. I really appreciate the time that we've spent on the golf course, commiserating about our irrational love for terrible (terrible!) sports teams, and wide ranging scientific discussions. To James McNamara, it has been great working with you, and watching your growth as a scientist. Thank you for all of your hard work in lab, and for your consistently positive influence on myself and the other lab members. I really appreciate all of your contributions, and this dissertation would not have been completed without

your help. To Rebecca Cook, thank you for being so welcoming and helpful when I started in lab. You made my transition extremely easy, and it is always a pleasure to work with you. I would also like to acknowledge the rest of the many Sirianni lab members. Science is a team sport, and you all make an incredible team. I am grateful for all of our thoughtful discussions about science, but most of all, for your friendship. You have made coming to work every day a more pleasant experience than I could realistically imagine. It has been a pleasure getting to know and work with you. Thank you for all of your help over these years, and keep up the good work. I would also like to acknowledge the members of the Vernon lab at ASU, the Mehta lab at BNI, the Sanai lab at BNI, and Sara Bowen in the Flow Cytometry CORE at BNI. Thank you all for your help and generosity in supporting my scientific pursuits.

Finally, I would like to acknowledge the funding that has supported this project. Fellowships were provided by the Arizona State University Ira A. Fulton Schools of Engineering, the Achievement Rewards for College Scientists Foundation, as well as the Ben and Catherine Ivy Foundation. Funding support was also provided through Dr. Rachael Sirianni's start-up funds, the Barrow Neurological Foundation, the Arizona State University School of Biological and Health Systems Engineering, and the Arizona State University Graduate and Professional Student Association. Thank you for enabling my research, and for also allowing me to travel and present this work at numerous conferences and academic meetings.

TABLE OF CONTENTS

Page

CHAPTER Page

Page

LIST OF TABLES

LIST OF FIGURES

Figure Page

PREFACE

This dissertation includes original research articles previously published by the primary author. Chapter 2 describes the synthesis and characterization of synthetic temperature responsive PNIPAAm based scaffolds for culturing and passaging Glioblastoma cells in three-dimensional culture [1]. Chapter 3 describes the capacity of PNIPAAm based scaffolds to promote enrichment of Glioblastoma stem-like cells in three-dimensional culture [2]. The use of these previously published works was approved by all co-authors (Appendix A).

CHAPTER 1

Introduction

1.1. Glioblastoma

Glioblastoma (GBM) is the most common and deadly pathological classification of malignant primary brain tumors. Epidemiological data collected for the United States between 2009-2013 indicate that GBM represents 46.6% of these diagnoses and 14.9% of all malignant and non-malignant primary brain tumor diagnoses [3]. Overall age adjusted incidence rates are 3.2 per 100,000, with a median age of diagnosis of 64.0 years; risk rises with age [3]. Symptoms of a GBM vary widely depending on tumor location and size but may include severe headaches, seizures, vision and speech impairment, or loss of cognitive and motor functions. Standard treatment modalities include removal of the bulk tumor via surgical resection, followed by radiotherapy and concomitant chemotherapy. However, treatment is rarely curative, and the prognosis is poor. Median survival remains stagnated at only 15 months [4], and the 5-year survival rate is reported between 4.7 – 5.5% [3,5].

1.1.1. Barriers to Treatment

From a clinical perspective, successful treatment of GBM remains challenging due to several factors. Complete surgical resection, while the best treatment for GBM, is often impossible as a result of tumor location, as well as the potential for irreparable damage to healthy brain tissue during surgery [6]. Radiation treatment can often be targeted to areas of the brain that would be otherwise difficult to access surgically. Although radiation is an effective means for killing remaining tumor cells, simultaneous damage incurred on surrounding healthy tissue limits tolerability and may worsen patient outcome. Treatment of GBM with chemotherapeutics is inhibited by the blood-brain barrier, which segregates the brain from systemic circulation and prevents the vast

majority of drugs from effectively reaching malignant cells in the brain. The primary chemotherapeutic currently used in GBM treatment is the DNA alkylating agent temozolomide, which is administered orally, brain available and generally well tolerated, but imparts only a modest improvement in patient outcome [4]. Overall, current treatment options remain inadequate.

One of the key biological features of GBM is that, unlike other tumor types tumors, it does not metastasize through the blood to peripheral organs; instead, individual cells invade healthy brain, preferentially migrating along white matter tracts and perivascular spaces [7]. These cells are responsible for initiating secondary tumors that most often arise within centimeters of the original tumor [8], but may manifest even on the contralateral side of the brain [9,10]. Invasive cells are undetectable by current imaging methods, and almost impossible to remove via surgical resection without damaging healthy brain. Radiation and chemotherapy fail to address invasive cells that are shielded by radio-sensitive healthy tissue and an intact blood-brain barrier. Thus, the invasive nature of GBM drives near universal rates of tumor recurrence as secondary tumors arise from seemingly healthy brain [5,8].

A factor that further complicates the treatment landscape is that GBM tumors display a high degree of genetic, epigenetic, and cellular diversity. Presently, GBM are classified into 4 distinct subtypes: Proneural, Neural, Classical, and Mesenchymal; each of which corresponds to a common set of neoplastic genetic alterations [11]. However, individual subtype classifications may not be relevant to all cells found in a single tumor, as intratumoral heterogeneity is also a common feature of GBM [12]. This heterogeneity is a primary source of treatment resistance, whereby one tumor region that is sensitive to treatment is sustained or replaced by another region that is tolerant [13]. Tumor

heterogeneity is therefore an adaptive growth pattern that is challenging to address through monotherapy, even when targeted.

1.2. GBM Tumor Microenvironment

The tissue of the GBM tumor microenvironment contains cellular and non-cellular components that collectively contribute to disease progression. The extracellular matrix (ECM) of the tumor microenvironment is primarily composed of the glycosaminoglycan hyaluronic acid (HA), and to a lesser degree, tenascin-C, collagen IV and V, fibronectin and laminin [9,14]. HA affects GBM growth and invasion via interaction with the cell surface receptor CD44, which is often overexpressed on GBM cells [9,15–19]; interactions with the other aforementioned ECM components promote GBM malignancy through a variety of biochemical pathways [14,20,21]. Additionally, the concentration of these non-cellular components is increased in the tumor microenvironment as GBM cells manufacture them to promote malignancy [9,17,19,21,22]. The increased density of the tumor ECM also contributes to increased mechanical stiffness of the microenvironment; stiffness is a well-characterized regulator of GBM proliferation and invasion [14,22–28]. Cells sense microenvironmental stiffness primarily through integrins and focal adhesion complexes in a process called mechanosensation [14]. Moreover, integrins that construct focal adhesion complexes with the tumor ECM play a significant role in GBM progression and have been proposed as a biomarker target for treatment [29–32].

The tumor-associated cells within the tumor microenvironment are key regulators of GBM growth and tumor vascularization. Cells that commonly provide support to GBM include tumor associated endothelial cells, pericytes, astrocytes, fibroblasts and infiltrating immune cells such as macrophages and microglia [33]. One of

the primary modes of support from tumor and tumor associated cells is secretion of soluble signaling factors that stimulate malignant phenotypes i.e. proliferation (EGF, FGF, IGF, HGF), angiogenesis (VEGF), and invasion (IGF, HGF, TGF-β) [34]. These secreted signaling factors may be sequestered within the dense network of ECM and serve as a depot for GBM cells [22,34]. Tumor vascularization is achieved in part by recruitment of vascular associated endothelial cells, pericytes, and astrocytes, to meet the nutrient demands of a growing tumor [33–35]. Specifically, endothelial cells are stimulated to proliferate and migrate toward tumor regions with poor oxygenation as a result of VEGF productions by hypoxic tumor cells [35]. However, the resulting tumor associated neovasculature is significantly different from healthy vessels as it forms a dense and disordered network of leaky vessels with necrosis developing in regions of severe chronic hypoxia (< 1% O_2) [35,36].

1.3. Glioblastoma Stem-like Cells

Prior to 2003, GBM, like most solid tumors, was widely believed to be driven by a stochastic model of clonal evolution in which tumors were initiated via neoplastic transformation of glia. The identification and characterization of tumorigenic Glioblastoma stem-like cells (GSCs) within human brain tumors has since reshaped conventional wisdom over the architecture of GBM biology [37–40]. This discovery supports the hypothesis that cells within a tumor display a hierarchical order of tumorigenic potential that is maintained by cancer stem cells (CSCs) [41,42]. It is now widely recognized that within GBM tumors, GSCs are essential to tumor maintenance, drivers of heterogeneity, and also may represent the cell of origin [41,43].

1.3.1. GSC Characteristics

GSCs display many biological similarities to NSCs; they are capable of indefinite self-renewal and multipotent differentiation, and they express genes that promote neural

stem phenotypes such as NESTIN, SOX2, and OLIG2 [37–40,43–45]. Identification and enrichment of GSCs can be achieved by sorting tumor cells that express validated cell surface biomarkers (CD133 [38], SSEA-1 [46], Integrin α6 [29]) followed by functional analysis of stem behaviors [47]. Of the stem behaviors, none is more important to GSC tumorigenicity than self-renewal. This was demonstrated when GSCs were first isolated and were observed to form orthotopic xenograft tumors from as few as 100 cells. In comparison, non-stem GBM cells (NGSCs) from the same tumor sample were incapable of forming tumors from injections of 100,000 cells [39]. GSCs also display a capacity for multipotent differentiation into non-tumorigenic cancer associated cells, such as vascular cells, that provide critical support for tumor growth [48–51]. Multipotency contributes to cellular heterogeneity observed in primary GBM; this behavior has been recapitulated in experimental orthotopic xenograft tumor models [39].

Ex vivo purification of GSCs requires a multi-step process that tests self-renewal, multipotency, and stem marker expression. Failure to test all three components often results in false positive identification [47]. Another method for identifying GSCs has been through the use of label retaining assays to identify quiescent or slow-cycling cells [52,53]. Using robust verification, long-term established GBM cell lines are found to lack fully functional GSCs, even in NSC culture conditions [44,47]. Thus to properly research GSC behaviors, experiments should ideally be performed on low-passage patient-derived cells that have been validated as a stem population.

1.3.2. GSC Response to Treatment

GSCs are highly treatment resistant, which is facilitated by their propensity to invade healthy brain [54], potential quiescence [55], and activation of molecular machinery that is protective against radiation [56] and cytotoxic insult [57]. Many of the invasive mechanisms utilized by GSCs mimic NSC motility along white matter tracts and

blood vessels [43]. Thus, GBM tumors characteristically display an infiltrative leading edge that disseminates into healthy tissue. GSC derived orthotopic xenograft tumors recapitulate this invasive behavior with GSCs concentrated at the tumor edge [58], whereas NGSCs from the same patient tumor sample are minimally invasive [54]. Resistance to both radiation [56] as well as many conventional chemotherapeutics, including temozolomide [55,57], has been reported in the GSC population. This resistance is ascribed to increased activation of DNA damage checkpoint and repair proteins [56], as well as increased expression of ATP-binding cassette (ABC) drug transporters, which contribute to increased drug efflux and chemoresistance [59]. Recurrent tumors are also enriched for GSCs compared to the primary tumor suggesting that GSCs evade conventional therapy and play a prominent role in the high rates of GBM relapse [57].

1.4. GSC Niche Microenvironments

Similar to NSCs, which are primarily found in the subventricular zone and hippocampus of the adult brain, GSCs are also concentrated in niche microenvironments [43]. One notable difference is that GSC niche microenvironments appear to be mitogenic, encouraging growth, while NSCs are generally sustained in quiescence [51]. These physical regions within the larger tumor microenvironment include a range of microenvironmental features that sustain and regulate GSC phenotypes through hypoxia, growth factor signaling, and adhesion to the ECM [51]. It is thus unsurprising that the microenvironment plays a role in provoking treatment resistance [21,60–64].

1.4.1. Perivascular Niche

A niche microenvironment has been identified in regions directly adjacent to blood vessels known as the vascular or perivascular niche [60,65]. Tumor vascularization is a requisite process to provide GBM tumors with adequate oxygen and nutrients that

sustain rapid growth. Bao et al. determined that GSCs initiate neovascularization by stimulating endothelial cell proliferation, migration, and tube formation through secretion of vascular endothelial growth factor (VEGF) and stromal-derived factor 1 (SDF-1) [66,67]. In parallel, vascular endothelial cells promote GSC self-renewal and proliferation, through secretion of soluble signaling factors such as nitric oxide, as well as via activation of NOTCH signaling [65,68–70]. This support appears to be unique to endothelial cells. For example, Calabrese et al. determined that neither NGSCs, astrocytes, nor fibroblasts were able to produce comparable enrichment of GSCs *in vitro* [65]. Importantly, GSCs are also capable of transdifferentiation into tumor-derived vascular cells. In experimental tumor models, GSCs have been observed to differentiate into pericytes and endothelial cells that participate in the formation and maintenance of neovasculature [48–51,71]. Therefore, interactions between endothelial cells and GSCs in the perivascular niche may create a self-sustaining paracrine signaling cycle that is critical for tumor maintenance and progression [71].

1.4.2. Hypoxic Niche

In juxtaposition to the nutrient-rich perivascular niche, GSCs are also found concentrated surrounding tumor regions that have limited access to blood vessels and are often necrotic [72]. The disorganized vasculature of GBM tumors leads to regional oxygen concentration gradients that have significant effects on GSC phenotypes. The primary molecular response to oxygen deprivation involves activation of the hypoxia inducible factor (HIF) family of transcription factors whose canonical downstream targets are proangiogenic [73]. As a result, the hypoxic niche may in some cases exist as a transitional microenvironment in which GSCs use proangiogenic factors such as VEGF to recruit blood vessels and establish a perivascular niche [41].

HIF activation has also been found to be a potent regulator of various GSC behaviors. HIF1α and HIF2α exhibit overlapping functions in both vasculogenesis and enriching stem phenotypes [72–77]. However, unique downstream target genes have also been identified particularly for HIF2α, which include stem markers Oct4, c-Myc, and Nanog [72,74,78]. Importantly, Li et al. reported that while HIF1α is expressed in both NSC and GSC populations, HIF2α expression is restricted to GSCs and is required for GSC tumorigenicity *in vivo* [72]. HIF2α induction also promotes stem plasticity in the pool of NGSCs, which may be particularly important for repopulating the GSC pool in response to treatment [74]. HIF expression also appears to be regulated by distinct components of the microenvironment. HIF1α expressing cells are enriched in regions of chronic hypoxia (> 1% O_2), while HIF2α expression is more sporadically identified in both hypoxic and normoxic regions surrounding blood vessels [36,72]. In addition, tumor acidity, a byproduct of overactive glycolytic energy production, increases HIF2α stabilization independent of oxygen concentration, and also promotes stem plasticity [79]. Thus, the hypoxic niche regulates GSC phenotypes primarily through HIF activity, which is essential to stem maintenance and tumorigenicity.

1.4.3. Invasive Niche

GSC populations have been identified at the leading edge of GBM tumors suggesting that this invasive front also contributes to GSC maintenance [44,51,54,80–82]. Therefore, while an invasive niche has yet to be definitively established, microenvironmental interactions particularly with the ECM protein laminin have been identified that regulate both invasive behaviors and stem phenotypes. For example, laminin receptor integrins α6 and α7 have been proposed as biomarkers for functional GSCs [29,30], while GSC regulation has also been described through interactions with the laminin subunit α2 [21]. In healthy brain, laminin is primarily located on the outside

of blood vessels, which are primary routes of GBM invasion [9]. Moreover, the interactions with vascular associated laminins are an important factor for GSC regulation in the perivascular niche [21]. *In vivo*, orthotopic GSC tumors recapitulate the invasive profile observed in patient tumors compared to NGSCs, which generally form noninvasive tumors [54]. Furthermore, recurrent tumors are enriched with GSCs indicating that these cells are likely responsible for infiltrative growth that is characteristic of GBM [57].

1.4.4. Therapeutic Challenges and Opportunities

Along with regulatory inputs, niche microenvironments provide GSCs with protection from cytotoxic treatments [60]. The perivascular niche has been described as radio-protective for medulloblastoma tumors [83]. This resistance was initiated by signaling through the oncogenic PI3K/Akt pathway which is a downstream target of the epidermal growth factor receptor (EGFR). In relation to GBM biology, EGFR is one of the most important biomarkers for malignancy [11], and is critical to the maintenance of stem phenotypes *in vitro* [44]. Moreover, inhibiting EGFR has been observed to sensitize otherwise radioresistant GSCs to treatment [84]. Therefore, activation of this receptor in the nutrient-rich perivascular niche would conceivably negatively impact the efficacy of radiotherapy on GSCs. VEGF signaling, which is critical for tumor vascularization and establishment of the perivascular niche, has also been shown to enhance resistance to radiation [85]. Similarly, Notch signaling, which functions through direct cell-cell contact of transmembrane proteins, also supports radioresistant behaviors in GSCs and is an integral signaling pathway in the vascular niche [86].

The hypoxic niche provides some of the best direct evidence of niche protection from chemotherapy and radiation. For both treatments, a common mode of action is through the generation of reactive oxygen species (ROS) induces double strand breaks in

DNA [87]. However, due to the relative lack of oxygen, ROS generation is attenuated thereby limiting this mechanism. Additionally, hypoxia is capable of promoting downstream activation of numerous survival pathways that may further limit treatment efficacy [87–89]. For example, GSCs identified in hypoxia have been observed to highly express MGMT, which functions to repair DNA and promotes resistance to TMZ [90].

Targeting niche microenvironments may provide an opportunity to disrupt GSC regulation and increase GBM treatment efficacy. Recently, inhibition of vascular niche formation initially appeared to be a promising direction for the development of new treatments; in experimental tumors, GSCs were depleted and tumor growth retarded by the antiangiogenic therapy bevacizumab, which is a VEGF function blocking antibody [65,66]. However, bevacizumab was subsequently found to effect an increase invasion of GBM cells in response to increased hypoxia resulting from the inhibition of blood vessel formation [91,92]. In a phase III clinical trial this treatment failed as a first-line therapy, but remains an approved and viable option as a salvage treatment for increasing progression free survival in recurrent GBM [93]. Bevacizumab fails as a GBM treatment primarily as a result of the strong hypoxia response of these tumors, and thus any approach seeking to inhibit blood supply to GBM must consider molecular responses of cells to hypoxic environments. For example, HIF2α may present a potential co-therapeutic target due to its specificity for GSCs, prominent role in GSC tumorigenicity, and regulation of responses to oxygen [72,79].

GSC niches are complex and diverse microenvironments that provide adaptive regulation of stem functions along with protective support against GBM treatments. The striking capacity of these cells to survive insults decreases the likelihood that any monotherapy will be significantly effective. Therefore, although clinical results have thus

far been disappointing, targeting and disrupting microenvironmental mechanisms of GSC regulation should remain a focus of novel treatment designs.

1.5. GBM Research Models

1.5.1. Cell Lines and In Vitro Culture

In vitro cell culture models have been fundamental to GBM research since the first tumor cell lines were isolated and immortalized in the 1960s [94]. A variety of immortalized cell lines are now widely available for research, and provide a platform for disease research that ideally enables reproducible testing. Propagation *in vitro* is performed using a simplified two-dimensional (2D) isotropic plate (often poly(styrene)) that is treated to present a negative charge, or coated with poly-d-lysine, or ECM proteins to promote anchorage dependent cell growth. This 2D design is optimized for cells to experience consistency in their access to adhesion sites, nutrients, soluble signaling factors, and oxygen in culture [95]. These cultures enable biologically instructive assays that measure behaviors such as proliferation, migration, stem cell status, and drug sensitivity under a variety of discrete conditions [96,97].

Although immortalized GBM cell lines have provided invaluable understanding of aspects of the disease process in GBM, their utility in generating new therapies for clinical application is limited. *In vitro*, cells are polarized and attach to the stiff culture substrate in a single plane that provides little to no resistance to proliferation or migration. In response, cells converge on a singular phenotype through a rapid loss of cellular heterogeneity, which is a fundamental feature of GBM [98]. Immortalized cell lines show significant differences in their molecular signature compared to primary GBM tissue, which is a direct result of prolonged propagation and genetic instability [98]. Another prominent issue with long-term cell lines is the potential for contamination with other cell lines that replace the original population. As an example, one of the most

widely used and first established *in vitro* models of GBM, the U-87 MG cell line, was originally isolated from a 44-year old female patient [94]. Recently, the genome of this line was compared to the original tumor sample, and was determined to be a GBM of male origin [99]. These problems, among others, illustrate that more representative disease models are necessary to overcome challenges in studying GBM biology.

The use of low-passage primary cells derived from patient tissue provides an improvement in the biological relevance of *in vitro* models. These are established by mechanical and enzymatic digestion of tumor tissue, whereby the resulting heterogeneous cell-mix is cultured *in vitro* using standard culture conditions. GSC lines may also be established from primary tissue through culture in serum-free NSC optimized media with the mitogenic growth factors EGF and FGF [100]. These conditions maintain the GSC population such that cells preserve genotypic and phenotypic features of the original tumor, whereas serum-supplemented cultures promote selection of differentiated GBM phenotypes and the GSC pool is subsequently depleted [47,101].

Standard 2D cultures may also be modified to produce models that better represent native GBM biology. For example, GBM has been co-cultured with a secondary cell type such as astrocytes [102,103] or endothelial cells [69] to promote malignant phenotypes. The most common method for establishing co-cultures is through a transwell or boyden chamber system. In these cultures, cells are separated by a semi-permeable membrane that allows access to signaling factors secreted by the otherwise physically separated cell populations. Co-culture studies have indicated that supporting cells are well capable of directing the behavior of tumor cells, including provocation of invasion and treatment resistance [69,102,103].

Similar to co-culture methods, three-dimensional (3D) cell cultures model aspects of the tumor microenvironment to elicit interactions that are generally absent from 2D cultures. Techniques such as hanging drop culture or culture on soft agar gels generates multicellular GBM spheroids that exhibit proliferation and invasion that better recapitulates *in vivo* scenarios [27,104,105]. Suspension culture, in which non-adherent cells are free-floating in media, is most often used to propagate GSCs where, similar to NSCs, stem-like cells form multicellular neurospheres (also called tumorspheres) [37,38,40,44,100,106]. Spheroid cultures can also be initiated as co-cultures in which GBM cells are combined with endothelial or glial cells and incorporated into spheroid structures [107]. Brain slice cultures further improve the relevance of the *in vitro* culture by enabling GBM cells to be analyzed in live brain tissue *ex vivo*. Here, viable brain slices are cultured and inoculated with tumor cells to enable tracking of GBM proliferation and invasion within a complete brain microenvironment. The primary drawbacks to brain slice culture include technical challenges with maintaining the tissue, reproducibility, and rapid cell death and/or alterations in the tissue during cultures [108,109]. Taken in sum, each of these approaches to culturing GBM have been valuable to isolate specific cellular responses under defined experimental conditions, although the degree to which neurosphere or hanging drop cultures can be engineered to capture essential aspects of the niche remain limited.

1.5.2. Preclinical In Vivo Models

In vivo models of GBM are the gold-standard for analyzing tumor growth and response to therapy within a physiologically relevant system. *In vivo* models are either syngeneic or xenograft. Syngeneic murine GBM models have been established via development of native GBM cell lines (e.g., through chemical insult) or genetic engineering that induces spontaneous and reproducible tumor formation [110]. Primary

advantages of syngeneic models include the ability to analyze tumors in the context of a fully functional immune system, and in genetic models, alterations in signaling pathways that are known to drive GBM malignancy (EGFR, PDGFR, Rb, Ras, Akt) [110,111]. Alternatively, xenograft models are established by the transplantation of human derived cell lines into an immunocompromised mouse host. The primary advantage of xenograft models is that they enable study of human GBM progression within a functional albeit immunodeficient brain.

Human xenograft models may be established from long-term cell lines or from freshly isolated patient-derived GBM tissue. Tumors can be induced in either the flank or directly in the brain. Flank models enable rapid confirmation of tumorigenicity and rapid growth of tumor within an easy to access physical compartment, while also providing a more permissive paradigm for treatment studies due to the lack of a blood-brain-barrier protecting the tumor. Orthotopic models on the other hand, are best suited for studying GBM behaviors in the context of the native brain tumor microenvironment. A variety of immortalized cell lines (U87, U118 etc.) have been used to produce aggressive orthotopic tumors with reproducible cellular architecture [110,111]. However, tumors generated through orthotopic transplant of immortalized cells often present significant genetic and histological variations from patient tumors thereby limiting their translational relevance [44,111]. For example, U87 tumors are highly vascularized, possess a relatively leaky blood-brain barrier, and do not exhibit the infiltrative behavior that is characteristic of patient GBM tissue [111]. The generation of noninvasive tumors is one of the primary drawbacks common to using immortalized cells in preclinical models. Conversely, low-passage patient-derived xenografts, particularly those established in serum-free culture or via direct *in vivo* inoculation, are characterized by their maintenance of parental tumor genotypes, an invasive leading edge, and minimal

disruption of the blood-brain barrier [39,40,43,44,106]. Thus patient-derived xenografts are presently considered the most biologically relevant research model of the human disease [110].

1.6. Tissue Engineering the GBM Tumor Microenvironment

The reduction of microenvironmental complexity in 2D cell culture limits analysis of disease biology because the three-dimensional (3D) ECM regulates numerous essential cellular phenotypes [105]. Tissue engineering strategies address this gap in understanding by providing methods to model key components of the 3D tumor microenvironment such as insoluble ECM components, stiffness, matrix degradability, and soluble signaling factors. These tools are not a direct surrogate for the complex, anisotropic, and heterogeneous *in vivo* scenario; instead, they enable characterization of contributions from individual microenvironmental factors. Here, we review how these approaches have been utilized to understand important features of GBM and GSC biology.

1.6.1. Biomaterials in GBM Research

Both natural and synthetic polymers have been used to study GBM response to the microenvironment (relevant studies are summarized in Table 1.1). Natural materials are bioactive, degradable by enzymatic or hydrolytic mechanisms, and cells interact with them directly through specific and established biochemical pathways. One potential challenge with using ECM biomaterials derived from live hosts or cell cultures, such as Matrigel®, is the lack of experimental reproducibility. These multicomponent materials exhibit variation in composition across batches (e.g., growth factor content, ECM protein concentration), which may adversely impact the interpretation of results due to changes in the constituent materials [105]. Juxtaposed to natural materials, synthetic biomaterials used in GBM cultures are derived from organic sources, which enables a

high degree of control over their physical and chemical properties. Of these, poly(ethylene glycol) is by far the most common. Its hydrophilicity and chemical structure enable cell encapsulation and functionalization reactions that can be performed *in situ*. Synthetic biomaterials can be either degradable or non-degradable, and in general, are expected to possess lower intrinsic bioactivity than natural materials, since they do not possess cellular adhesion sites that would be expected elicit biological responses. Cells are capable of interfacing with a purely synthetic polymer either through surface adsorbed proteins (vitronectin, laminin, etc.) or through non-specific charge interactions [112]. Grafting synthetic polymers with bioactive proteins or peptides (e.g. RGD) is a common approach to enable cellular adhesion or biodegradation (Table 1.1). This method of combining natural and/or synthetic components into a composite biomaterial is useful for leveraging advantages of both classifications.

The majority of natural, synthetic, and composite scaffolds applied in GBM studies are hydrophilic hydrogels, which, like tissue, are composed of a high fraction of water and swell considerably in aqueous solution. However, in some instances hydrophobic polymers are also incorporated, often coated with hydrophilic ECM proteins [113–115]. Scaffolds of either classification can be further designed as porous, fibrous, anisotropic, or some combination, each with varying degrees of control of these physical properties dependent on the constituents. Chemical and physical crosslinking reactions are often necessary to increase the molecular weight of a biomaterial such that it forms an insoluble physical structure in aqueous solution. Strategies that do not negatively impact cell viability are particularly desirable. For chemically crosslinked biomaterials, click-chemistry, such as Michael addition [24,25,27,116–118], describes stepwise reactions that proceed efficiently at neutral pH, do not require biologically damaging solvents or reaction conditions, and do not produce any cytotoxic byproducts

[119]. Another common example of chemical crosslinking is UV free radical polymerization, which, unlike most free radical reactions, may utilize an aqueous compatible initiator that is photoreactive (e.g., Irgacure 2959). This method enables polymerization of reactive monomers such as terminal olefins (e.g. acrylates) [28,120–124]. Alternatively, physical crosslinking proceeds without a chemical reaction; alterations in pH or temperature produce electrostatic interactions that result in polymerization and/or precipitation [125]; typical examples include collagen (pH stimulus) or poly(N-isopropylacrylamide) (temperature stimulus). It is well known that the degree of crosslinking (chemical or physical) for any given material will affect the porosity, density, and stiffness of the scaffold, which are each independently important considerations in GBM tissue engineering.

1.6.2. 3D Culture Methods

Biomaterial cultures are performed with cells or spheroids either seeded on the scaffold surface or encapsulated within the scaffold during crosslinking. Surface cultures enable measurement of cellular behaviors (motility, invasion, proliferation, viability, etc.) in response to the biophysical and biochemical material properties. They also provide a set initial location for cells, and do not necessarily require biodegradation of the material to allow for cell proliferation or motility, since cells are capable of moving across the surface. Encapsulation cultures offer a more physiologically relevant scenario, but require biocompatible crosslinking and matrix degradation for cell growth and motility. Both scenarios are regularly used to measure invasive capacity, which cannot be fully recapitulated in 2D *in vitro* systems.

For both surface and encapsulation cultures, biological assays must be either performed *in situ* (e.g. immunofluorescence, cell tracking) or alternatively, on cells recovered from the scaffold (e.g. western blot, polymerase chain reaction (PCR),

fluorescence activated cell sorting (FACS)). Both culture approaches pose a variety of technical challenges to performing these assays that are specific to the biomaterial system; a significant consideration in designing a 3D culture format. For example, chemically crosslinked materials may require degradation or cell dissociation conditions that adversely affect cell viability or the presentation of surface proteins. Physical scaffolds, on the other hand, may offer reversible formation in response to mild environmental changes and thereby enable easy cell recovery for post-culture analysis.

1.6.3. Biophysical and Biochemical Regulation of GBM Behaviors

The *in vivo* tumor microenvironment provides critical regulatory functions for GBM tumors. As a result, there are many reports investigating how the physical microarchitecture and biochemical features of 3D biomaterials regulate or elicit specific GBM behaviors *in vitro* (summarized in detail in Table 1.1). Many of these studies have described the impact of matrix stiffness and topography (porosity, fibers, geometry) on altering malignant GBM phenotypes such as proliferation, migration, and invasion. Mechanosensation is a key component of GBM biology that mediates tumor growth and cell motility [14]. In considering how biochemical aspects of the microenvironment influence GBM biology, a variety of different scaffold components have been explored, one of the most prominent being hyaluronic acid (HA). Given that HA, as previously described, has many essential functions in GBM [9], it is unsurprising that HA hydrogels have been shown to regulate a wide variety of behaviors including proliferation, invasion, stem phenotypes, and treatment resistance. HA does not provide cellular adhesion sites, and as a result is regularly modified with cell adhesion peptides or combined with other biomaterials, such as collagen, that enable cell attachment. One of the more intriguing developments in 3D microenvironment models is the inclusion of fibers that mimic the structure of blood vessel mimicking and guide GBM invasion [114,115,126]. More

complex models have also been reported for developing high-throughput studies or co-cultures with microenvironmental support cells within a single *in vitro* system. Together, the current body of work illustrates the breadth of understanding that has developed in response to implementing *in vitro* biomaterial cultures. However, this is not an exhaustive review, because these and other engineering approaches applied to the GBM tumor microenvironment are covered in great detail in a number of extensive and wide ranging reviews [14,108,127].

1.7. Biomaterials for Probing GSC Biology

1.7.1. Engineering the Stem Cell Microenvironment

Engineering GSC instructive *in vitro* microenvironments is a relatively new approach derived from well-established tissue engineering research. Stem cells, are widely regarded for their potential to regenerate and establish functional tissues. Neural tissue engineering, which is most closely related to GBM tissue engineering, primarily focuses on developing novel techniques for directing NSC behaviors. In this field, biomaterials have been utilized to elucidate a variety of stem cell behaviors with a focus on understanding how biophysical and biochemical factors in 2D and 3D environments affect NSC maintenance, self-renewal, and differentiation mechanisms [128]. Through these studies, the mechanical stiffness of culture substrates and matrices has been identified as a potent regulator of NSC fate. Saha et al. reported that NSC differentiation could be directed with soft substrates (100-500 Pa) to promote neurogenesis, and stiff (>1000 Pa) matrices to promote gliogenesis [129]. In addition to matrix stiffness, Soen et al. and Nakajima et al. demonstrated that specific ECM components and growth factors were also capable of controlling stem cell fate and differentiation in culture [130,131]. Other cellular components of the NSC microenvironment, have been investigated as regulators of stem cell fate *in vitro*. For example, Shen et al. determined that endothelial

cells secrete soluble factors that promote and maintain stem phenotypes in NSC populations [132].

The regenerative capacity of NSCs has also been investigated in 3D microenvironment models with both matrix composition and stiffness again identified as key regulatory components. Here, Saha et al. described that very soft substrates (<100 Pa) promoted quiescent NSC phenotypes, while stiffening these substrates (≥100 Pa) promoted expansion of the NSC pool [129]. The structure of the ECM is also important to NSC neural regenerative properties, as Yang et al. described scaffolds composed of aligned poly(L-lactic acid) nanofibers promoted neuronal phenotypes and neurite outgrowth along the fibers [133]. More biomimetic approaches have also been tested using ECM components of the *in vivo* NSC niche as well. To this end, Cheng et al. described that a laminin-derived IKVAV peptide-based hydrogel supported NSC neuronal differentiation and improved tissue regeneration *in vivo* following a traumatic brain injury [134]. In addition, we reported that a HA-laminin composite hydrogels increase the migratory response of NSCs a result of increased sensitivity to stromal cell-derived factor 1α (SDF1α) both *in vitro* and *in vivo* [135,136].

Similar regulatory mechanisms govern both GSC and NSC biology [43], and as such, these examples have direct relevance to understanding and predicting how model microenvironments may affect malignant GSC phenotypes. In applying these same tissue engineering approaches to GSCs, conditions under which these cells acquire or enhance stem phenotypes, prefer to initiate invasive mechanisms, or exhibit treatment resistance have been identified. These results provide better understanding of the underlying mechanisms that drive microenvironmental support for GSC populations.

1.7.2. GBM Stem Plasticity in 3D Culture

GSCs and NGSCs are believed exist in a regulated state of plasticity where induction of differentiation is a bidirectional process regulated by the microenvironment, epigenetics, and response to treatment [74,137,138]. This stem-plasticity has been investigated using immortalized GBM cell lines as a model of NGSCs. Although, as previously described, these cell lines do not offer a complete and accurate depiction of GBM biology, the mechanisms that are employed to acquire stem phenotypes may mimic GSC plasticity [101,111].

Stem plasticity has been studied in GBM cell lines cultured in chitosan-based scaffolds; for example, Florczyk et al. developed a chitosan-HA composite scaffold that elucidated stem-like characteristics in U118 cells [139]. The authors reported that these scaffolds promoted sphere formation, expression of stem markers (NESTIN, Musashi-1, and CD44), and increased invasive capacity compared to traditional 2D cultures. In addition, scaffold-cultured cells displayed increased resistance to both TMZ and doxorubicin, coupled with increased expression of the ABCG2 drug efflux pump, suggesting a phenotypic switch toward a more GSC-like state [139]. In a follow-up study, Kievit et al. used a chitosan-alginate scaffold to also examine stem plasticity [140]. Using these models, U118 and U87 GBM cells again displayed increased stem protein and gene expression (CD133, NESTIN, CD44, Notch, among others) in scaffold environments, which was again a function of scaffold composition. Functionally, scaffold grown cells also exhibited increased tumorigenicity in a flank tumor model. Kieivit et al further optimized this approach by coating chitosan-alginate scaffolds with HA and establishing a 3D co-culture model of U87 and endothelial cells [141]. These conditions also increased expression of CD133, ID1, and CD44, but interestingly slowed the growth of spheroids.

Outside of GBM, Florczyk et al. employed this platform to enrich CD133 expression in prostate, breast, and liver cancer cells [142].

Chitosan-based scaffolds are also not the only biomaterial platform that has been reported to drive stem plasticity, as Ma et al. also identified stem specific responses to 3D electrospun polystyrene scaffolds coated with a library of 7 different isoforms of laminin [143]. The resulting behavior of U251 cells was, similar to the chitosan studies, contingent both on 3D context and matrix chemistry. Specifically, 3D scaffolds presenting the laminin isoforms 411, 421, 511 and 521 promoted an increase in expression of the GSC markers (including, for example, integrin α6, SOX2, and OLIG2) that coincided with an increase in clonogenicity of these cells [143].

Together, these works emphasize the significance of using engineered microenvironments to drive relevant GSC behaviors in culture. The use of immortalized cell lines provides some insight into how GBM cells exhibit plasticity in a shift from differentiated phenotypes to more stem-like behaviors.

1.7.3. Biomaterials Promoting GSC Expansion and Enrichment

Engineered tumor microenvironments have also been designed to assay conditions under which patient-derived GSCs may be enriched *in vitro*. GSCs are typically maintained in nonadherent neurosphere conditions [38] or in adherent cultures on laminin [97], with the desired condition often selected based on cellular affinity. In general, neurosphere conditions are most common as sphere forming capacity is regularly accompanied by a broader array of GSC specific phenotypes (self-renewal, multipotency, stem-marker expression) [100]. However, neurosphere culture has well-characterized drawbacks. Specifically, as spheres increase in size, the constituent cells experience differential access to oxygen and soluble signaling factors as a result of diffusion limitations [95]. This problem is amplified by variations in rates of cell

proliferation and fusion of adjacent spheres. As a result, a single neurosphere may contain a heterogeneous mixture of clonogenic, differentiated, apoptotic, and necrotic cells [95,97,144,145].

A number of biomaterials have been described as useful tools for addressing problems associated with neurosphere aggregation. For example, Yang et al. reported that gelatin foam scaffolds maintained GSC protein expression, while also increasing HIF1α and VEGF signaling to provide a GSC supportive microenvironment [146]. In a separate study, Oh et al. reported that GSCs encapsulated in an alginate-PEG hydrogel formed neurospheres with relative uniformity in size, which may improve nutrient and oxygen access [147]. Li et al. used a similar approach to expand patient-derived GSCs in a temperature-responsive PNIPAAm-based scaffold [148]. In this context, cells were capable of high density culture without aggregating, thus overcoming a key drawback to traditional neurosphere cultures. This system subsequently enabled improved cellular yield from GSC cultures while maintaining multipotency and stem marker expression.

Beyond GSC expansion, conditions under which GSC phenotypes are actively enriched have also been explored in 3D culture. Chitosan-HA scaffolds were recently applied to patient-derived GSCs by Wang et al., and were found to increase stem gene expression (SOX2, TAZ, NANOG), invasion gene expression (TWIST1, TWIST2, SNAIL1, SNAIL2, ZEB2), and expression of genes that drive drug resistance (MGMT, HIF1A, SOD1) compared to cells cultured as a 2D monolayer [149]. GSCs cultured in these scaffolds also exhibited higher tolerance to the chemotherapeutics TMZ, carmustin (BCNU), and lomustine (CCNU). Similarly, we recently reported another set of 3D culture conditions that promote GSC enrichment utilizing temperature responsive PNIPAAm-co-Jeffamine (PNJ) scaffolds [2]. This culture platform increased self-renewal capacity, expression of the stem marker NESTIN, and EGFR expression while

maintaining cellular multipotency in two genetically distinct models of GBM. In addition, we observed that PNJ cultured cells also exhibited increased resistance to clinical dosages of radiation following 3D culture.

In total, these studies suggest that there are a diverse set of biomaterials capable of maintaining GSCs cultures, and a subset of these materials are useful for actively enriching GSC specific phenotypes. Considering the differences in scaffold composition, it is also likely that GSCs are regulated via distinct mechanisms in the described culture systems.

1.7.4. In vitro Models of GSC Invasion

Invasion of neoplastic cells into healthy brain tissue has and continues to be considered the most clinically significant issue inhibiting effective GBM treatment [150]. Considering the role GSCs play in tumor recurrence and invasion, understanding how these cells respond to specific microenvironmental cues to promote invasive behaviors is of particular importance. In the seminal work of Cheng et al., GSC's were determined to exhibit a heightened propensity for invasion [54]. This characteristic was first identified *in vitro*, using a 3D Matrigel-transwell invasion assay, and was subsequently confirmed *in vivo* when compared to NGSCs from a matched tumor sample [54]. This description provided a foundation for employing *in vitro* microenvironments to determine how the biochemical, biophysical, and cellular components of the tumor microenvironment affect GSC invasion.

Biochemical input signals from the tumor microenvironment ECM influence GSC propensity for invasion, and this hypothesis has been supported in a variety of different *in vitro* paradigms. Using a library of Matrigel, collagen, and HA-collagen matrices, Herrera-Perez et al. determined that modes of GSC invasion were directly dependent on ECM chemistry [126]. These matrices accurately modeled the stiffness of healthy brain

tissue, and different preparations of collagen were used to separate the effects of matrix stiffness and collagen concentration. As a result, this study identified an interplay between matrix stiffness and chemistry that influenced invasion distance and velocity. Interestingly, soluble HA (non-immobilized) decreased GSC invasion in HA-collagen matrices, and Matrigel coated microfibers, mimicking the structure of blood vessels, encouraged directional strand motility reminiscent of white-matter tract invasion tendencies *in vivo* [126].

Identification of biochemical pathways that promote or inhibit GSC invasion is necessary for complete characterization of these behaviors, but is often underreported; a limitation of many 3D culture studies. As an example, Cha et al. explored a similar paradigm to Herrera-Perez et al. by measuring GSC invasion through collagen matrices that included soluble HA and PCL fibers to model blood vessels [115]. Yet, in apparent contrast to the prior study, Cha et al. reported that soluble HA increased GSC invasion in collagen matrices, while also exhibiting increased expression of CD44, and HA synthase [115]. In addition, treatment with an HA synthase inhibitor decreased invasion and effected an increase in FAK and MMP2 expression [115]. While the functional results of these studies (i.e. invasion) appear contradictory, it is important to recognize differences in methodology which include the source of patient-derived cells, and the concentrations of collagen and HA in the model systems. Therefore, molecular level descriptions may improve cross-study comparisons and allow for more robust descriptions of GSC invasive mechanisms.

From analysis of the *in vivo* tumor microenvironment, it is clear that non-GBM cells, such as endothelial cells, are capable of regulating GSC phenotypes and promoting invasion. This behavior was studied by Chonan et al. in which a 3D collagen gel was applied to separate a murine GSC line from endothelial cells in an engineered

microfluidic invasion model [151]. Here, endothelial cells stimulated increased invasion of NESTIN expressing cells through the 3D microenvironment. These GSCs also exhibited increased expression of integrin α2 and β3 in response to co-culture, suggesting a potential mechanistic role for endothelial cells in promoting motility of GSCs in this model. Meanwhile, cells expressing the neuronal differentiation marker tubulin β3 were less invasive, which agrees with prior reports of increased GSC invasive capacity versus NGSCs [54].

As previously stated, microenvironmental stiffness regulates the invasive capacity of GBM cell lines via mechanosensation mechanisms [24,25,27,28,152]. While the stiffness of healthy brain is generally characterized between 100 and 1,000 Pa, GBM tumors can present significantly increased stiffness due to their high cellularity and dense ECM [129,153–155]. At present, reports investigating the effects of matrix stiffness on GSC motility in both 2D and 3D paradigms describe a complex relationship [32,126,156,157]. Ruiz-Ontañon et al. reported that GSCs harvested from different tumor regions (peritumoral vs. bulk tumor) display invasive tendencies and sensitivity to microenvironmental stiffness that was a function of their regional origin [32]. Unsurprisingly, peritumoral GSCs were observed to have a heightened invasive capacity. These behaviors were modeled on 2D laminin functionalized polyacrylamide matrices, within 3D Matrigel and collagen I hydrogels, as well as in chicken embryo and mouse xenografts. Moreover, peritumoral invasion was insensitive to stiffness as a result of Rac and RhoA signaling activation, and integrin αVβ3, an RGD peptide binding integrin, was identified as a key regulator of GSC invasion and potential target for therapy [32]. Similarly, Wong et al. also reported that GSCs exhibited an insensitivity to matrix stiffness on 2D laminin coated polyacrylamide matrices [156]. Here, matrix stiffness ranging from 80 Pa to 119 kPa produced no effect on cellular migration. However, in

contrast to the previous study, activation of myosin II signaling via genetic constitutive activation of RhoA, ROCK, or MLCK sensitized cells to matrix stiffness and effected a decrease in motility on soft matrices.

Together these studies suggest that GSCs employ diverse invasion strategies that may be cell-type specific. This hypothesis was supported by Grundy et al. who suggested that a GSC subtype-specific relationship exists between invasive behavior and sensitivity to microenvironmental stiffness [157]. In this study, migration and invasion were measured on 2D Matrigel coated polyacrylamide matrices with varying stiffness (200 Pa – 50 kPa) and also within soft (~400 Pa) 3D Matrigel hydrogels. With this platform, the invasive behavior of neural subtype GSCs were observed to be insensitive to stiffness, while mesenchymal subtype GSCs exhibited stiffness dependent motility. The authors surmise that the cell of origin (neural GSCs - neuronal lineage; mesenchymal GSCs – astrocytic lineage) may be a primary factor influencing GSC motility in response to microenvironmental stiffness [157]. This hypothesis also draws relevance back to the NSC paradigm, in which neuronal phenotypes manifest on soft matrices while astrocytic phenotypes dominate on stiff substrates [129].

These 3D invasion studies provide unique opportunities to isolate specific microenvironmental features (chemistry, stiffness, architecture, cellular support, etc.), and may be instrumental in identifying targets for therapy to address GSC invasion at the clinical level. However, the wide range of reported results indicate that a more comprehensive picture of subtype specific and context specific molecular mechanisms of invasion may be necessary to develop predictive hypotheses.

1.7.5. Modeling Treatment Resistance and the Influence of Tumor Heterogeneity

Tumors generated through orthotopic transplant of human GSCs display treatment resistance that is supported by the tumor microenvironment [62]. Yet, similar

to challenges faced in studying GBM invasion, direct identification of specific resistance promoting factors remains challenging *in vivo*; the mechanisms underlying microenvironmental contributions to treatment resistance can be efficiently modeled *in vitro*. For example, Fernandez-Fuente et al. proposed that resistance to sunitinib induced receptor tyrosine kinase (RTK) inhibition is mediated by interactions specific to a 3D microenvironment [158]. Using a number of different GSC, NGSC, and established GBM cell lines, the authors determined that GSCs were comparatively insensitive to RTK inhibition in 3D collagen gels versus standard 2D conditions and 2D collagen coated polyacrylamide. The observed resistance was abrogated via chemical inhibition of the PI3K/Akt and MEK/ERK signaling pathways leading the authors to hypothesize that focal adhesions in 3D were responsible for promoting RTK resistance. Notably, changes in collagen content, stiffness (2D and 3D), and soluble HA inclusion in 3D collagen gels did not produce a measurable effect on drug sensitivity.

The biochemical response to matrix bound HA has also been identified as a regulator of GSC resistance to chemotherapy in 3D culture. In a recent study by Pedron et al., the EGFR inhibitor erlotinib produced little GSC cytotoxicity in gelatin hydrogels, and its effects were predictably dependent on basal EGFR status ($EGFR^{wt}$, $EGFR^{+}$, and the GBM specific constitutively active form $EGFR^{VIII}$) [122]. In addition, incorporation of HA within the gelatin hydrogels increased erlotinib resistance in $EGFR^{VIII}$ cells, while inhibition of EGFR and CD44 increased cytotoxic effects in $EGFR^{wt}$ and $EGFR^{+}$ cells. This study provides evidence for EGFR-CD44 signaling interactions that promote GSC resistance to RTK inhibition dependent on the microenvironment and molecular profile of the GBM cells. Considering the clinical importance of EGFR in GBM, this mechanism may be highly relevant designing novel inhibition strategies for GSCs. Moreover,

measuring divergent responses as a function of EGFR signaling provides an example of how tumor heterogeneity may negatively impact treatment.

The development of tumor heterogeneity diminishes sensitivity to treatment as a result of divergent phenotypes (proliferative vs. quiescent, invasive vs. stationary, protein expression, etc.). Hubert et al. modeled this process by culturing GSCs in Matrigel coupled with continuous mechanical agitation [159]. This model generated large GBM organoids with hypoxic cores that were composed of populations of GSCs and NGSCs. GSCs were primarily located at the organoid rim, but were also sporadically identified in regions of hypoxia. Moreover, the GSC populations within the organoids displayed resistance to apoptosis following radiation treatment, while NGSCs were observed to be sensitive to treatment. This test demonstrates a prevailing GSC theory that conventional modes of treatment may effectively target NGSCs but leave GSCs relatively unharmed. Finally, organoid cultures were orthotopically implanted and formed tumor architecture and single-cell invasive patterns that were a better representation of the parent tumor than matched cells in neurosphere culture [159]. Thus, developing models that can recapitulate tumor heterogeneity may provide avenues for determining patient-specific drug responses via personalized medicine.

1.8. Overview and Specific Aims

Although GBM is aggressively treated, recurrence is nearly inevitable. Radiation provides the most effective post-surgical treatment method, but is characteristically resisted by the GSC subpopulation. This opens opportunities for GSCs to drive tumor recurrence and mediate disease progression. The GBM microenvironment is broadly protective to a variety of tumor and tumor associated cells, and specialized niches therein provide critical functions for maintaining GSCs. Furthermore, there is a growing body of evidence that suggests that these microenvironments directly support treatment

resistance and induction of stem plasticity through a diverse set of dynamic interactions. This is evidenced, for example, by the clinical failure of bevacizumab, which successfully inhibited GBM vasculogenesis but produced hypoxic microenvironments that promote compensatory malignant responses. Therefore, better understanding of the regulatory mechanisms that govern GSCs in the microenvironment may precede new methods of niche disruption.

In vitro studies utilizing three-dimensional (3D) scaffolds are powerful for identifying and isolating microenvironmental regulatory mechanisms of malignant behaviors. In this work, we aim to develop models of the GBM microenvironment that facilitate understanding of niche regulation of key GSC phenotypes. Our central hypothesis is that GSC phenotypes are sensitive to regulation by model niche microenvironments, and that this regulation will enable analysis of stem maintenance and radioresistance. We addressed this hypothesis through testing these specific aims:

1.8.1. Specific Aim 1

Design a tunable 3D biomaterial model of the GBM tumor microenvironment that enables recollection of live cells under mild conditions.

1.8.2. Specific Aim 2

Identify microenvironmental conditions that support and enrich GSC phenotypes *in vitro*.

1.8.3. Specific Aim 3

Define the regulatory capacity of *in vitro* GSC niche models, and determine biological mechanisms that support GSC maintenance and radioresistance.

1.9. Figures and Tables

Table 1.1: Review of biomaterial models of the GBM tumor microenvironment.

Scaffold Components	**References**
Hyaluronic Acid	[120–124,160,116,27,115,25,117,24,118,161,139,149, 141,158,126,114,162,163]
Collagen	[20,27,28,32,114–116,120–124,126,139,146,151,156, 158,160,162,164–167]
Matrigel	[32,54,114,126,151,157,159,161,168]
Poly(ethylene glycol)	[27,28,116,120,124,147,163,169]
Chitosan	[139–142,149,170]
Alginate	[140,141,147]
Poly(N-isopropylacrylamide)	[1,2,32,148]
Polyacrylamide	[23,26,32,118,152,156–158]
Polycaprolactone	[115,114,140,141]
Polystyrene	[113,140]
Bioactive Peptide/Protein	[1,20,23–26,32,113,117,118,124,156,162,163,168]
Complex 3D Models	[26,114,115,117,121,126,151,169,171,172]
Biophysical Properties	
Stiffness	[1,2,23–28,114,115,117,118,120,121,123,124,126,139, 156–158,160,163–165,167]
Porosity	[24,26,28,113–115,126,139–141,146,149,160,163,164, 167,169]
Microchannels	[26,121,151,169]
Fibers/Alignment	[113–115,126,160,164,165,167]
GBM Cell Lines	
U87	[24,25,27,28,116,118,120,121,124,140,141,158,161,163, 166,167,169]
U118	[1,27,139,140]
U251	[20,113,123,161]
U373	[23–26,117,118,156,161,165]
U138	[166,168]
U178	[20]
T98	[158]
LN229	[166,168]
LN18	[168]
A172	[158,166,168]
Genetically Modified GBM	[25,27,120,121]
Co-culture	[32,124,141,151]
Murine Model	[116,151,159,162,164]
Patient-Derived	[2,32,114–116,122,126,146,147,149,156–160,166]
Biological Behaviors	
2D Migration	[24–26,32,114,118,151,156–158,161,166,167]
3D Invasion	[20,24,25,27,32,54,115,118,123,126,139,151,156,157, 160–162,164–168]

Proliferation	[1,23,24,27,28,32,113,115,116,120–123,139–141,146, 149,156,159,162–164,166]
Malignancy Markers	[2,20,23,25,28,32,54,113–117,120–123,126,139–141, 146,149,151,156,158,159,161,163,166–168]
Stem Phenotypes	[2,32,54,113,115,122,126,139–141,146,149,151,156–159]
In Vivo Characteristics	[32,54,116,122,140,146,156,159]

Treatment Response	
Chemotherapy	[23,26,115,116,118,122,139,146,149,158,166,167,169]
Radiation	[2,116,159,166,168]

CHAPTER 2

Temperature Responsive Hydrogels Enable Transient Three-Dimensional Tumor Cultures via Rapid Cell Recovery

2.1. Abstract

Recovery of live cells from three-dimensional (3D) culture would improve analysis of cell behaviors in tissue engineered microenvironments. In this work, we developed a temperature responsive hydrogel to enable transient 3D culture of human glioblastoma (GBM) cells. N-isopropylacrylamide was copolymerized with hydrophilic grafts and functionalized with the cell adhesion peptide RGD to yield the novel copolymer poly(N-isopropylacrylamide-co-Jeffamine® M-1000 acrylamide-co-hydroxyethylmethacrylate-RGD), or PNJ-RGD. This copolymer reversibly gels in aqueous solutions when heated under normal cell culture conditions (37°C). Moreover, these gels redissolve within 70 seconds when cooled to room temperature without the addition of any agents to degrade the synthetic scaffold, thereby enabling rapid recollection of viable cells after 3D culture. We tested the efficiency of cell recovery following extended 3D culture and were able to recover more than 50% of viable GBM cells after up to 7 days in culture. These data demonstrate the utility of physically crosslinked PNJ-RGD hydrogels as a platform for culture and recollection of cells in 3D.

2.2. Introduction

In vitro cell culture is a key component of biomedical research. Standard cell culture methods utilize plastic surfaces that facilitate cell adhesion and growth across a single, two-dimensional (2D) plane. However, 2D conditions do not fully recapitulate the mechanical and biophysical features of the three-dimensional (3D) microenvironment to which cells are exposed *in vivo* [173–175]. This is of particular concern in cancer research, where interactions between neoplastic cells and the 3D tumor

microenvironment drive tumor expansion and malignancy [33,176,177]. As a result, 3D biomaterial scaffolds and extracellular matrix (ECM) mimics (for example, Matrigel® [178], collagen [177], hyaluronic acid [24], and polyethylene glycol (PEG) [163]) have become popular tools for developing more relevant cancer cell culture methods. However, one key limitation of many biomaterials commonly used in these applications is that recovery of viable cells for post-culture analysis can be challenging. These insoluble hydrogel networks may require prohibitive environmental alterations (pH, temperature), the addition of harsh chemical or enzymatic agents, and/or long time periods to dissolve.

The goal of this work was to develop a physically crosslinked scaffold that would enable transient 3D cell culture via rapid recollection of cells under mild conditions. Poly(N-isopropylacrylamide) (PNIPAAm) exhibits a lower critical solution temperature (LCST) near 30°C in aqueous solution, which enables reversible physical crosslinking where the polymer is soluble at room temperature and gels at 37°C [179]. In the gelled state, PNIPAAm gels undergo notable phase separation and shrinking due to hydrophobic interactions between polymer chains. The equilibrium polymer concentration in a PNIPAAm hydrogel is approximately 50 wt% for gels initially formed at 5-20 wt% [179,180]. This low equilibrium water content prevents fast dissolution when gels are cooled below the LCST and would also inhibit any recovery of live cells cultured therein. We have reported that the phase separation of PNIPAAm is decreased by the incorporation of Jeffamine® M-1000 acrylamide (JAAm) as a graft comonomer [180,181], which opens the possibility of developing a fast-dissolving PNIPAAm copolymer scaffold for cell culture.

Other groups have demonstrated the ability to functionalize PNIPAAm with cell adhesion peptides such as RGD for the purpose facilitating 3D cell culture [182–187].

PNIPAAm has also been used to facilitate the formation and subsequent detachment of cellular monolayers and sheets primarily for the purpose of tissue engineering [188–192]. However, to our knowledge, none have developed a fast-dissolving PNIPAAm-RGD hydrogel and demonstrated recovery of live cells grown in a 3D scaffold. To this end, we describe the development of the novel temperature responsive graft copolymer poly(*N*-isopropylacrylamide-co-Jeffamine® M-1000 acrylamide-co-hydroxyethylmethacrylate-RGD), or PNJ-RGD, that we characterized in transient 3D cell culture. This platform was applied to studying *in vitro* cultures of human glioblastoma (GBM) brain tumor cells. GBM is the most malignant and aggressive primary brain tumor and is associated with poor median survival (12-15 months) and substantial morbidities [193]. Previously, we reported that PNIPAAm-hydroxyethylmethacrylate copolymers (PNIPAAm-co-HEMA) can be made thiol-reactive following post-polymerization acrylation of hydroxyls [194]. We utilized this approach along with methods reported by Shu et al. [195] to graft a cysteine containing RGD peptide to acrylated poly(NIPAAm-co-JAAm-co-HEMA) via Michael addition. The resulting PNJ-RGD copolymer formed a physically crosslinked hydrogel that was rapidly reversible when cooled below the LCST. These hydrogels supported physiological behaviors and recollection of viable GBM cells maintained in an adherent 3D culture.

2.3. Methods

2.3.1. Materials.

All chemicals were reagent grade and purchased from Sigma-Aldrich unless otherwise stated. N-isopropylacrylamide (NIPAAm; Tokyo Chemical Industry Co., Portland, OR, USA) was recrystallized from hexane, and 2,2′-Azobisisobutyronitrile (AIBN) was recrystallized from methanol. Tetrahydrofuran (THF) used in polymer synthesis and gel permeation chromatography was HPLC grade. Jeffamine® M-1000

was generously donated by Huntsman Corporation (Salt Lake City, UT, USA). The CGRGDS peptide (63.5% purity, 954 Da MW) was purchased from American Peptide Company (Sunnyvale, CA, USA). All cell culture reagents were purchased from Invitrogen (Carlsbad, CA, USA) or Fisher Scientific (Anthem, AZ, USA) unless otherwise stated.

2.3.2. Synthesis of Temperature Responsive PNIPAAm Copolymers.

Jeffamine® M-1000 acrylamide (JAAm) was synthesized from Jeffamine® M-1000 and acryloyl chloride as described previously [181]. PNIPAAm copolymers were synthesized by free radical polymerization of NIPAAm, JAAm, and hydroxyethylmethacrylate (HEMA) monomers to yield poly(NIPAAm-co-JAAm-co-HEMA), or PNJH. NIPAAm (9 g), JAAm (1 g), and HEMA (200 mg) were dissolved in 100 mL of anhydrous benzene in a dried flask and heated to 65°C. After bubbling with nitrogen for 20 minutes, AIBN (95 mg) was added to initiate polymerization, and the reaction proceeded under positive nitrogen pressure for 18 hr. PNJH polymer precipitated during the reaction and was redissolved in an equal volume of acetone, precipitated in cold diethyl ether, collected by filtration, and vacuum dried overnight. For the purpose of evaluating the effect of JAAm content on polymer properties, poly(NIPAAm-co-JAAm) copolymers were synthesized through the same method with a 100:0, 95:5, or 90:10 ratio of NIPAAm: JAAm by weight in the feed [180]. These copolymers are abbreviated as PNIPAAm, PNJ5, and PNJ10, respectively.

Poly(NIPAAm-co-JAAm-co-HEMA-acrylate), or PNJHAc, was synthesized by reacting PNJH with acryloyl chloride to convert hydroxyl groups to pendent acrylates [194]. The polymer was dried by heating to 60°C overnight under vacuum and dissolved at 15 wt% in THF with 5 molar equivalents of triethylamine relative to HEMA repeat units. Acryloyl chloride predissolved in THF was added dropwise to the stirring solution

on ice and under nitrogen to achieve a final polymer concentration of 10 wt%. After 6 hr, TEA-HCl salts were removed by filtration and the copolymer was precipitated in ether, filtered, and vacuum dried. The product was purified by dialysis against deionized water at 4°C with a 3500 MWCO membrane for 3 days. Polymer was lyophilized for storage at -20°C.

2.3.3. Conjugation of Integrin Adhesion Peptide.

Poly(NIPAAm-co-JAAm-co-HEMA-RGD), or PNJ-RGD, was formed by Michael addition of an RGD peptide containing a terminal cysteine residue onto the acrylates of the polymer. PNJHAc was dissolved at 3 wt% in chilled PBS and Cys-Gly-Arg-Gly-Asp-Ser (CGRGDS) TFA salt was added in a 3-fold molar excess of the available acrylate groups. The solution was titrated to pH 8 and stirred for 24-48 hr at 4°C. The polymer was then purified by dialysis (3,500 Da MWCO) against deionized water at 4°C for 1 week and lyophilized to obtain PNJ-RGD. Dry polymers were sterilized by ethylene oxide gas.

2.3.4. ^{1}H NMR Characterization.

^{1}H NMR spectroscopy (Varian Inova, 400 MHz) was used to determine the chemical composition of all polymers following each synthesis. All polymer samples were prepared at a concentration of 10 mg/mL in D_2O. NIPAAm repeat units were calculated by integration of the peak associated with the lone isopropyl proton [δ = 3.84, 1H, $(CH_3)_2$-C*H*-NHCO] in reference to peaks associated with oxyethylene protons in JAAm [δ = 3.63, 76H, CH_2CH_2O], methylene protons in HEMA [δ = 4.09, 4H, HO-C*H2*C*H2*-OCO], and methylene protons in HEMA-acrylate [δ = 4.09, δ = 4.38, 4H, CH_2=CH-COO-CH_2CH_2-OCO].[180,194] Peaks corresponding to the terminal olefin protons in HEMA-acrylate, [δ = 5.97, δ = 6.18, δ = 6.41, 3H, OCO-C*H*=CH_2], were integrated in respect to the other monomer peaks to determine the degree of acrylation to be ~88% of the HEMA

groups (^{1}H NMR spectrum provided in Figure 2.6). Addition of the CGRGDS peptide to the PNJHAc polymer by Michael addition was confirmed by characteristic shifts from the methylene protons in aspartic acid [δ = 2.58, 2H, OHCO-C*H*$_2$-CH], methylene protons in serine [δ = 3.86, 2H, OH-C*H*$_2$-CH], and methylene protons in arginine [δ = 3.09, 2H, NH_2CNHNH-C*H*$_2$-CH_2] [196]. Peptide concentration was calculated to be approximately 140 μmoles of RGD per gram of PNJ-RGD copolymer (^{1}H NMR spectra provided in Figure 2.7).

2.3.5. Molecular Weight and Polydispersity Determination.

The molecular weight and polydispersity of the PNIPAAm copolymers were determined by gel permeation chromatography (GPC) using refractive index detection (Shimadzu) in conjunction with static light scattering (MiniDawn, Wyatt Tech. Corp.). Samples were run through two columns in series (Waters Styragel HR 4 and 6) to separate polymer chains by size exclusion. Measurements were made using HPLC grade THF as the mobile phase running at a flow rate of 1 mL per minute.

2.3.6. LCST Determination.

The LCST was evaluated by cloud point measurement and rheometry. For cloud point assays, PNIPAAm copolymers (n = 3) were dissolved at 0.1 wt% in PBS at pH 7.4 in cuvettes and heated in a water bath from 20 to 40°C in 1°C increments and 40 to 55°C in 5°C increments. Samples remained at each temperature for at least 120 s prior to each measurement. Absorbance readings in the visible range (450 nm) were recorded with a UV/Vis spectrometer (Pharmacia Biotech Ultrospec 3000). The maximum absorbance was defined as the highest absorbance prior to polymer precipitation (determined by first measurement at which absorbance decreased). The LCST was defined as the temperature at which 50% of the relative maximum absorbance was recorded during the assay. For rheometry, PNIPAAm copolymer solutions were prepared at 16.7 wt% in 150

mM PBS (pH 7.4) and placed on a parallel plate rheometer (MCR-101, Anton-Paar) that provided real-time temperature control over the measurement stage. In all tests, an oscillatory 0.5% shear strain deformation was applied at 1 Hz frequency without normal force control to measure the sample storage (G') and loss modulus (G"). Polymer solutions were allowed to equilibrate to 4°C on the rheometer and were then measured during controlled heating (0.5°C/min) to 37°C to induce gelation transition.

2.3.7. Viscoelastic Characterization.

Rheometry was performed to measure the viscoelastic properties of the PNJ-RGD copolymer over a range of concentrations during heating and cooling. Solutions were prepared by dissolving PNJ-RGD at 4.2, 8.3, or 16.7 wt% in PBS. Concentrations were selected starting at the maximum concentration that permitted solution flow and decreasing by a factor of 2 until the solution did not gel. The storage and loss modulus in the solution and gel states were assessed by a multistep temperature controlled protocol. In all tests, an oscillatory 0.5% shear strain deformation was applied at 1 Hz frequency, and normal force control was used at temperatures above the LCST to maintain consistent contact between the gel and rotating head. Polymer solutions were allowed to equilibrate to 4°C on the rheometer and were measured during controlled (0.5°C/min) and sustained heating (37°C for 1 hr) followed by rapid and sustained cooling (4°C for 1 hr).

2.3.8. Cell and Tumor Spheroid Culture.

The human GBM cell line U118 and U118 cells expressing green fluorescent protein (U118-GFP) were generously gifted by colleagues at the Translational Genomics Institute (TGen, Phoenix, AZ, USA). Cells were cultured in antibiotic free DMEM + 10% FBS. Multicellular GBM spheroids (5000 cells/spheroid) were formed in 4 days by a hanging drop culture [104].

2.3.9. Cytocompatibility of PNJ-RGD Hydrogels.

PNJ-RGD was dissolved in culture media at 8.3 wt% with U118 cells dispersed uniformly throughout the mixture (400,000 cells per mL polymer solution). Samples were plated in approximately 70 μL aliquots (n = 6 per time point) in a 96 well plate. After incubating overnight at 37°C, an equal volume of cell culture media was added to each sample and exchanged for fresh media every 2-3 days. Cells were stained with fluorescent calcein AM (2 μM; 488 nm excitation / 535 nm emission) and ethidium homodimer-1 (4 μM; 528 nm excitation / 617 nm emission) using a Live/Dead assay kit (Invitrogen) at 1, 3, and 14 days. Live and dead cells were quantified through fluorescence detection via fluorescence confocal microscopy. 3D stacks of images were collected through 300 μm with a step size of 10 μm. Cells within the images were quantified using an automated cell counting algorithm described in our previous work [27].

2.3.10. Three Dimensional (3D) Cell Culture.

PNJ10 and PNJ-RGD were dissolved at 16.7 wt% in cell culture media overnight at 4°C. The elastic strength of gels at this concentration is similar to hydrogels that we have previously observed to promote proliferation and invasion of this cell line [27]. The polymer solution was transferred in approximately 70 μL aliquots (n = 6) to a 96-well tissue culture plate and incubated at 37°C to form hydrogels. A single multicellular U118-GFP spheroid was seeded on top of the gel in each well and incubated overnight to allow for attachment. An equal volume of cell culture media was added to each well and exchanged with fresh media every 2-3 days. Cellular behavior was analyzed using 3D fluorescence confocal microscopy (Leica SPE II) of live cells. Prior to imaging, samples were cooled to room temperature (making the gels transparent), and images were captured through a depth of 500 μm with a step size of 10 μm. Each individual spheroid

was tracked separately to allow for analysis of behaviors observed over the culture period.

2.3.11. Recollection of 3D Cultured Cells.

PNJ-RGD samples were prepared as for the Live/Dead assay and seeded uniformly with U118-GFP cells at low (86,000 cells/mL), medium (186,000 cells/mL), or high (357,000 cells/mL) densities. The experiment was replicated in 3 separate assays. Samples were transferred in 70 μL aliquots (n = 6 per time point) into a 96-well tissue culture plate and incubated at 37°C. Cells were recollected from the hydrogels after 1, 2, 3, and 7 days of 3D culture. Only cells seeded at the medium density were collected at 7 days. To recollect cells, the plate was first cooled to room temperature to liquefy the hydrogels and allow removal from the well plate. The samples were diluted in 2 mL of media, mixed with a micropipette, and centrifuged at 1,100 RPM for 5 minutes at 4°C. The pellet was resuspended in 2 mL of 0.25% trypsin-EDTA. This solution was cycled between the gel (37°C) and soluble (4°C) states for 5 minutes to improve activity and penetration of the enzyme into the copolymer network. The solution was diluted in media and passed through a 100 μm cell strainer (Fisher Scientific). Cell viability was quantified in the liquid media fraction for the recollected cells and in the gel fraction for the gel encapsulated cells using CellTiter-Glo (Promega) with luminescence measured in a microplate reader (Tecan).

2.4. Results

2.4.1. Polymer Synthesis and Characterization.

PNIPAAm copolymers with varying amounts of JAAm, HEMA, and RGD were synthesized as outlined in Figure 2.1. Characterization data is summarized in Table 1 and described in detail below. The incorporation of the constituent monomers and the RGD peptide was confirmed by ^{1}H NMR analysis (spectra provided in Supplementary Figures

2.1 and 2.2). Quantification of peaks corresponding to the amino acid sequence indicated that PNDJ-RGD was functionalized with 140 μmoles RGD per gram of polymer. Molecular weight determination indicated that all copolymers exhibited M_W greater than 500,000 Da. The molecular weight of PNJ-RGD was not measured by GPC due to poor solubility in THF.

From cloud point data (Figure 2.2A), PNIPAAm homopolymer displayed the lowest LCST (26.5°C), and the addition of JAAm increased the LCST in PNJ5 (27°C) and PNJ10 (28.5°C) proportional to the incorporation of the hydrophilic monomer. Conversely, the addition of hydrophobic pendant acrylate groups in PNJHAc resulted in a slight decrease in LCST (27.5°C). PNJ-RGD exhibited the highest LCST (31.3°C), which is attributed to increased hydrophilicity of the copolymer imparted by the RGD peptide. The phase transition was also studied by measuring the shear storage (G') and loss moduli (G") of PNIPAAm copolymer gels at high concentration (16.7 wt%) during temperature ramp (Figure 2.2B). The LCST was determined to be the temperature at which the storage and loss moduli exponentially increase and invert, i.e. G' > G". This inversion was observed as expected in the PNJ5, PNJ10, and PNJ-RGD formulations. However, G' remained greater than G" for PNIPAAm homopolymer and PNJHAc even below the LCST, indicating that these solutions behaved like viscous gels at all temperatures. Therefore, the LCST was defined for these samples as the temperature of at least two-fold increase in the shear storage modulus. The copolymers showed the same trend in LCST transition as measured by cloud point, with PNIPAAm having the lowest LCST (22.6°C) and LCST increasing with JAAm content for PNJ5 (23.6°C) and PNJ10 (28.1°C). PNJHAc again had a lower LCST (26.6°C) than PNJ10, and PNJ-RGD displayed the highest transition point (29.1°C).

Dissolution kinetics were evaluated by rheology while rapidly cooling hydrogels below the LCST (samples were maintained at 37°C for one hour and then rapidly brought to 4°C) (Figure 2.3A). In general, copolymers with greater hydrophilic content re-dissolved more quickly upon cooling. However, PNIPAAm, PNJ5, PNJHAc, and PNJ10 showed poor dissolution, maintaining viscoelastic solid behavior (G' > G") and exhibiting shear storage moduli that exceeded 900 Pa for 30 minutes after cooling. This indicates that water was unable to effectively penetrate the gel structure and solvate the polymer. PNIPAAm gels did not return to solution when cooled and, interestingly, exhibited signs of stiffening, as evidenced by a brief increase in storage modulus (Figure 2.3A). Conversely, PNJ-RGD showed much improved dissolution kinetics, returning to a predominantly liquid state (G" > G') within 70 seconds of cooling below the LCST. Collectively, these data demonstrate that increasing the hydrophilic content of NIPAAm copolymers enables complete phase reversal and rapid dissolution upon cooling below the LCST.

To further evaluate the mechanical changes induced during the phase transition, PNJ-RGD gels were subjected to multi-stage rheological measurements at various concentrations with controlled heating and cooling cycles (Figure 2.3B). Data were collected for 4.1, 8.3, and 16.7 wt% samples heated from 4°C to 37°C (0.5°C/min) to estimate LCST and gel strength. Samples were then maintained at 37°C to allow the gel to equilibrate, and then cooled rapidly to 4°C to estimate dissolution time. The LCST was consistent between the samples and viscoelastic strength, measured by the storage and loss modulus, increased with concentration. At 37°C, the hydrogels formed viscoelastic solids with storage moduli (G') ranging from 40 Pa (4.1 wt%) to 3 kPa (16.7 wt%). Most importantly however, all PNJ-RGD gels were capable of rapid (~70 seconds) phase reversal to a soluble state when cooled below the LCST following prolonged (1 hr)

gelation. Thus, unlike PNIPAAm homopolymer, PNJ-RGD exhibits tunable mechanical properties through a rapidly reversible phase transition. These data motivated us to further evaluate PNJ-RGD as a platform for recollection of live cells cultured in 3D.

2.4.2. 3D Scaffolds for Transient Cell Culture.

The primary goal of these experiments was to evaluate if PNJ-RGD hydrogels could promote cell viability and physiological behavior while also enabling the recovery viable cells from the culture. To examine material cytocompatibility, U118 GBM cells were dispersed uniformly in PNJ-RGD hydrogels. A fluorescent live/dead assay was performed within the gel to analyze cell viability through 3D space with fluorescence confocal microscopy. 3D stacks of live/dead confocal images were collected after 1, 3, and 14 days of culture (Figure 2.4A). These images were analyzed by a previously developed automated image processing method to identify and count the number of live and dead cells [27]. Over 14 days in culture, the hydrogels were found to consistently support a viable fraction of cells that was greater than 85% of the total number of cells counted (Figure 2.5A). Elongated cell morphologies were observed in PNJ-RGD, confirming that pendent RGD sites on the polymer allowed for cell attachment (Figure 2.4A).

Proliferative and invasive behaviors of GFP-expressing GBM cells within PNJ10 and PNJ-RGD hydrogels were assayed by 3D fluorescence confocal microscopy. Multicellular spheroids tracked during culture showed markedly different behaviors on gels with RGD versus gels without RGD (Figure 2.4B). Cultures on PNJ-RGD showed increased cellular invasion, altered morphologies, and increasing spheroid size at successive time points. In contrast, spheroids in the PNJ10 hydrogels exhibited minimal changes in size and morphology and also did not produce invasive cells over the times measured here.

Recollection of live cells from PNJ-RGD cultures was enabled by the rapid gel dissolution after cooling. In preliminary experiments (results not shown), we attempted to remove live cells from hydrogels by simply cooling gels below the LCST with no further treatment. However, we observed that cells cultured for any extended period of time (> 18 hrs) secreted extracellular matrix proteins that prevented their complete release from the gel. To improve cellular detachment from the matrix, the hydrogels were treated with trypsin. Recovered cells and those that remained attached to the gel were quantified with a luminescence viability assay to determine the recollection efficiency (Figure 2.5B). Using this method, live cells were successfully recovered from the hydrogels after 1 to 7 days in culture. Recollected cells maintained normal proliferation and morphology when reintroduced to standard 2D culture (results not shown). Cells cultured for 1 day in PNJ-RGD were recollected with the highest efficiency, with approximately 79% of the live cells composing the recollected fraction. As culture times increased, the combined collection efficiency declined but remained above 50% after up to 7 days in culture. High initial cell seeding densities were also observed to have a slight negative effect on recollection efficiency compared to the lower initial cell numbers (Figure 2.8).

2.5. Discussion

Standard 2D tissue culture plastic provides reproducible, simplistic conditions for growing cells *in vitro*. However, 2D cultures limit important biological behaviors such as matrix remodeling and invasion, which can be observed in even the most basic 3D substrates such as Matrigel® and collagen [197]. Yet the majority of 3D cultures are designed as endpoint assays that do not allow for cells to be cultured transiently in the scaffold and then recollected. To this end, we aimed to develop a temperature responsive biomaterial that would enable recollection of live cells and improve investigation of GBM

cancer cell biology in a controlled microenvironment. PNIPAAm hydrogels are both cytocompatible and temperature responsive, but their slow gel-sol transition and lack of cell adhesion sites limits their utility in this application. To overcome these limitations, we copolymerized NIPAAm with hydrophilic JAAm at a relatively low molar fraction (<0.9 mol%) of the copolymer to increase the equilibrium water content of the hydrogels while maintaining the LCST within the physiological range [198–201]. HEMA was also incorporated as a comonomer to provide an active site for functionalizing the polymer with the cell adhesion peptide RGD. Our characterization and analysis of the resulting PNJ-RGD copolymer indicates that PNJ-RGD forms a robust temperature responsive scaffold that is well suited as a platform for transient 3D cell culture.

All of the synthesized polymers exhibited a favorable LCST for 3D culture in that polymers were soluble at room temperature and gelled at body temperature. However, the transition temperature measured by cloud point (Figure 2.2A) was consistently higher than when measured by rheology (Figure 2.2B) for each material. Cloud point measurements were taken at low concentrations (0.1 wt%) to observe the phase transition (i.e., collapse of polymer chains) that produces precipitation. Rheology measurements were made at higher concentrations (16.7 wt%) in parallel to observe subtle changes in mechanical properties during physical crosslinking (i.e., increase in gel strength) that do not require complete phase transition. Thus, these data highlight that increased strength precedes complete polymer precipitation, as expected. Ultimately, both measures demonstrate that hydrophobic HEMA-acrylate decreased the LCST and hydrophilic JAAm had a small increasing effect on LCST, which is consistent with our previous reports [180,194]. The inclusion of both monomers along with the hydrophilic RGD peptide caused a modest LCST increase over PNIPAAm homopolymer. Therefore,

the measured LCST was consistently a function of the hydrophobic versus hydrophilic content of NIPAAm copolymers.

One of the primary obstacles with using PNIPAAm hydrogels for transient cell culture is the extended time required to solubilize the gel when cooled below the LCST. This is primarily caused by the phase separation of the precipitated polymer and can be mitigated by the addition of hydrophilic comonomers. This is supported by rheological measurements of hydrogel dissolution (Figure 2.3A) which indicate that PNJ-RGD is capable of rapid and complete phase reversal following physical crosslinking. The remaining formulations displayed incomplete phase reversal that was proportional to hydrophilic monomer content. Moreover, measurements of the mechanical properties of PNJ-RGD (Figure 2.3B) showed that the physical gelation was tunable over almost two orders of magnitude (40 Pa – 3 kPa) by simply varying polymer-solution concentration.

Hydrogels formed with PNJ10 and PNJ-RGD copolymers displayed suitable properties for 3D cell culture, including LCST between room and body temperature, high equilibrium water content, and high gel-state viscoelasticity. We compared these two gels as scaffolds for transiently culturing a GBM cell line (U118) that spreads and proliferates rapidly in adherent conditions [27,94]. In 3D cultures, PNJ-RGD hydrogels facilitated U118 cell viability, attachment, and invasion (Figure 2.4) which are all behaviors that are responsible for the overwhelming morbidity associated with GBM. More importantly however, PNJ-RGD enabled rapid recovery of live cells from 3D culture under mild conditions (Figure 2.5B). From 1 to 7 days in culture, a high fraction (> 50%) of viable cells were extracted from the hydrogel scaffolds with the potential to be used in subsequent assays.

Many conventional biomaterials available for 3D cell culture (e.g. Matrigel®, collagen, hyaluronic acid) may require may require harsh conditions, such as prolonged

enzymatic digestion, to dissolve the substrate. One of the primary goals of this work was to engineer a synthetic cell culture scaffold that presented a bioactive ligand and could be dissolved without the use of enzymes; i.e., by a mild drop in temperature. The developed PNJ-RGD material is thermally reversible and liquefies completely in response to reduced temperature (Figure 2.3). However, in cell culture we observed that dissolution of the synthetic hydrogel did not enable complete release of cells from PNJ-RGD scaffolds. Additionally, longer cultures and increased cell densities correlated negatively with cell recollection efficiency (Figure 2.3). We hypothesized that this incomplete recollection was due to cellular attachment to RGD binding sites and protein deposition. This hypothesis was supported by the observation that brief (5 min.) treatment of PNJ-RGD gels with trypsin enabled release of the cells albeit incomplete during extended cultures. Importantly, this enzymatic treatment does not affect the synthetic hydrogel, and was used only to release cells from RGD binding sites and to degrade proteins deposited by cells within the gel.

To our knowledge, this is the first report of a 3D PNIPAAm-RGD based platform that enables transient 3D culture through rapid recovery of live cells under mild conditions. This material offers several distinct advantages as a cell culture biomaterial. First, the 3D format allows for observation and measurement of interactions between cells and their surrounding microenvironment, an approach that is becoming increasingly valuable in the fields of cancer biology and regenerative medicine. Second, by engineering the scaffold to enable easy recovery of live cells, this platform could be used to study a variety of relevant cell behaviors and to perform analysis of transient biomarkers (e.g., measurement of protein expression in live cells via fluorescence activated cell sorting (FACS)) that could not be studied using other scaffolds. Finally, the thiol-reactivity of the PNJHAc copolymer intermediate allows allowing for other thiol-

containing molecules of interest to be interchangeably immobilized to the scaffold. In summary, this work shows that PNJ-RGD is a suitable material for maintaining and passaging malignant cells in 3D culture, and it presents an opportunity for studying long-term, progressive responses of cells to their microenvironment in future studies.

2.6. Conclusions

Temperature responsive PNIPAAm copolymers were successfully synthesized with and without RGD for cell adhesion as a platform for transient 3D culture. PNJ-RGD solutions formed a mechanically tunable viscoelastic gel when heated above 29°C and displayed rapid phase reversal when cooled. In cell culture assays, the hydrophilicity of the hydrogel structure and presence of the RGD peptide promoted viability of an adherent cancer cell line over 14 days in culture. Additionally, invasive phenotypes were observed in 3D cultures, indicating that PNJ-RGD gels were capable of elucidating physiological phenotypes important to cancer research. Finally, recollection of live cells was achieved from the hydrogels from 1 to 7 days in culture. In all, these findings indicate that this hydrogel is an effective *in vitro* biomaterial platform for maintaining and affecting the biology of adherent tumor cells in a transient 3D culture.

2.7. Tables and Figures

Table 2.1: Characterization of PNIPAAm copolymers.

Polymer	Monomer Ratios NIPAAm : JAAm : HEMA (wt%)		Peptide Content (μmol / g polymer)	Molecular Weight Determination		LCST Determination(°C)	
	Feed	Composition	CGRGDS	M_W (10^6 Da)	Dispersity (M_W / M_n)	Cloudpoint	Rheology
PNIPAAm	100 : 0 : 0	100 : 0 : 0	-	1.127	1.382	26.5	22.6
PNJ5	95 : 5 : 0	97.3 : 2.7 : 0	-	1.257	1.223	27.0	23.6
PNJ10	90 : 10 : 0	92.1 : 7.9 : 0	-	1.303	1.351	28.5	28.1
PNJHAc	88.2 : 9.8 : 2.0	90.7 : 8.2 : 1.1	-	0.5488	1.411	27.5	26.6
PNJRGD	88.2 : 9.8 : 2.0	90.7 : 8.2 : 1.1	140	0.5944		31.3	29.1

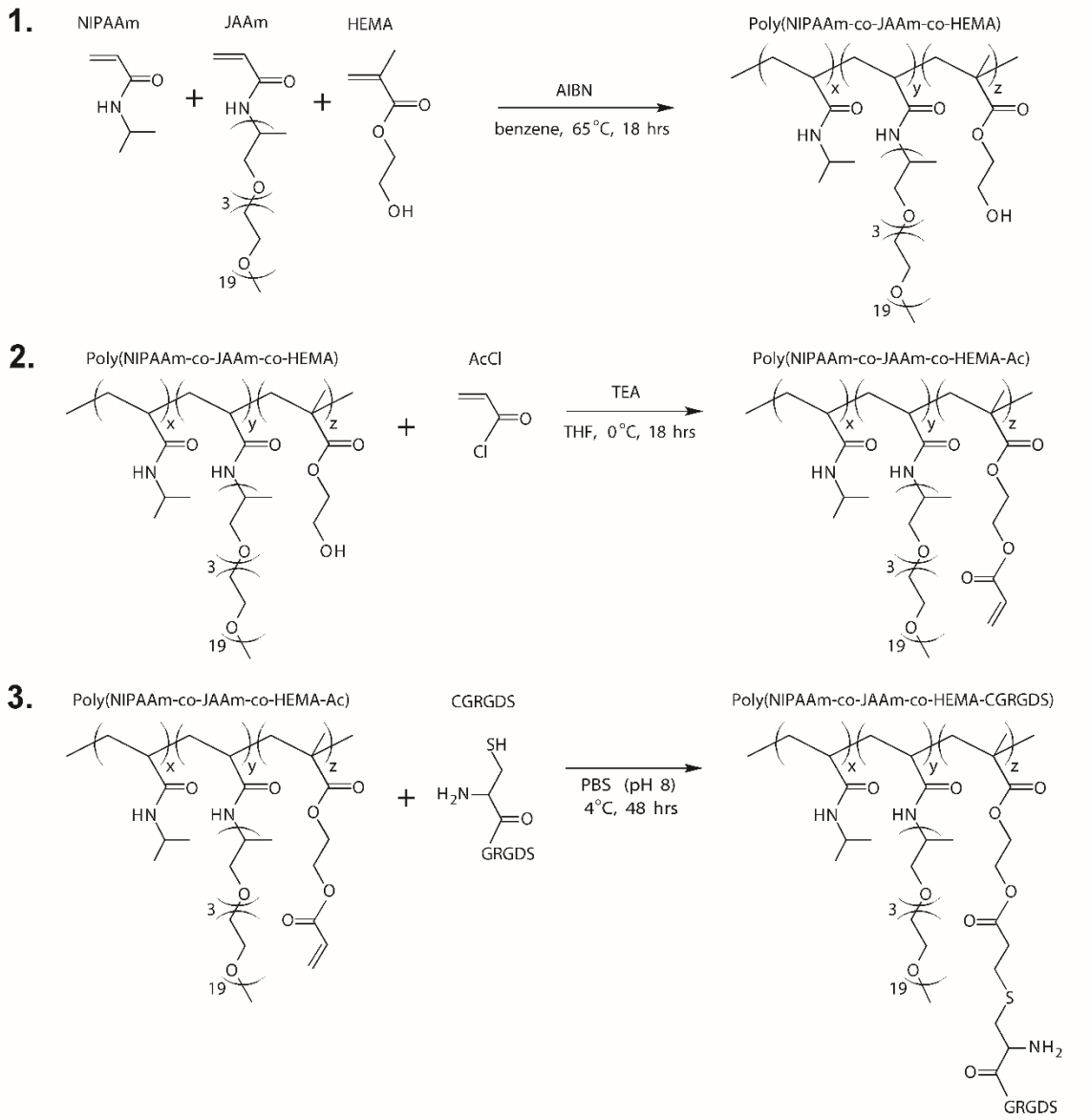

Figure 2.1: Three step synthesis of PNJ-RGD. (1) PNJH is synthesized through free radical polymerization. (2) Acrylation of the HEMA side chain to form PNJHAc. (3) Conjugation of the CGRGDS peptide through Michael addition of the thiol-containing cysteine residue to form PNJ-RGD.

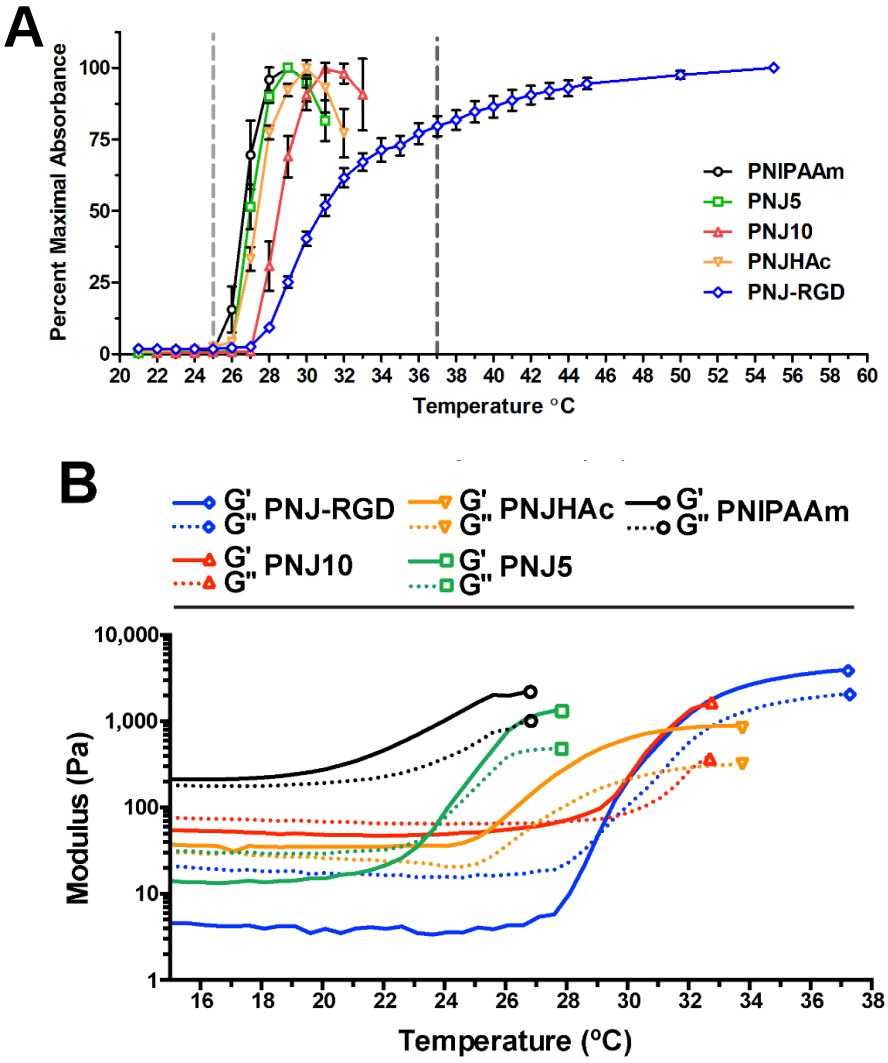

Figure 2.2: LCST determination for PNIPAAm copolymers by (A) cloudpoint and (B) rheology. (A) Cloudpoint measurements are reported as the absorbance at 450 nm relative to the maximal absorbance for 0.1 wt% polymer solutions at increasing temperatures. Room temperature is marked at 25°C and body temperature is marked at 37°C. The LCST is defined as 50% relative absorbance. Error bars represent standard deviation. (B) Rheology measurements of the storage (G') and loss modulus (G") were collected for 16.7 wt% polymer solutions under controlled heating (0.5°C/min). The LCST is defined at the point of G' and G" inversion or exponential increase.

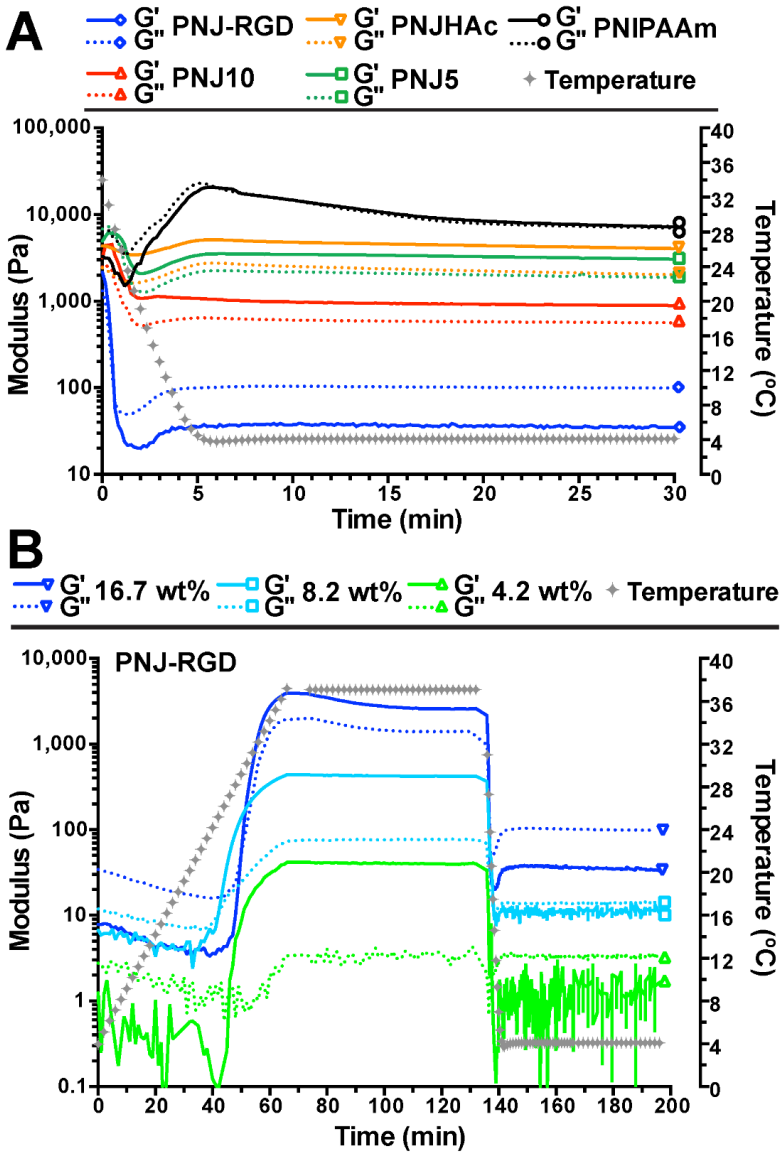

Figure 2.3: Viscoelastic characterization of PNIPAAm copolymers by temperature controlled rheology. (A) Storage (G') and loss modulus (G") measurements were made on 16.7 wt% polymer samples heated to 37°C for 1 hr and rapidly cooled to 4°C. The degree of hydrogel dissolution is measured by the decay in G' and G". (B) Mechanical properties of PNJ-RGD hydrogels at 3 concentrations during controlled heating and rapid cooling. Hydrogel viscoelasticity is dependent on polymer concentration, but all samples displayed reversible gelation kinetics at the LCST. Temperature is displayed on the right axis.

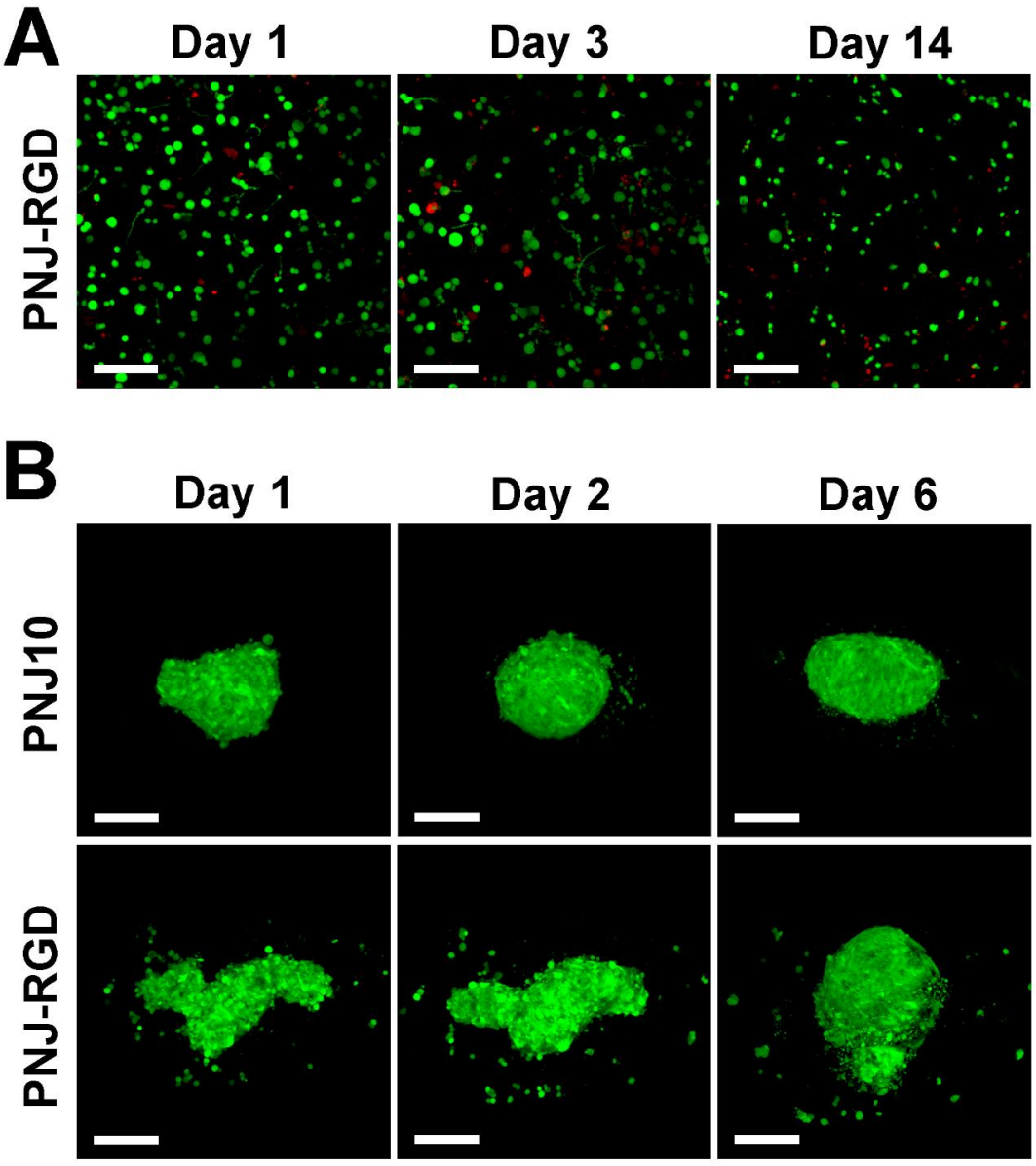

Figure 2.4: Cell viability and behavior assays. (A) Live/Dead assay results showing that U118 cells maintain a high viable fraction (green to red) over 14 days in culture. (B) U118-GFP proliferation and invasion was imaged over 6 days in PNJ10 and PNJ-RGD hydrogels. The presence of the RGD peptide allowed for cells to both proliferate and invade into the matrix, while cells in PNJ10 did not appreciably exhibit these behaviors. Images of cells are 2D maximum intensity projections of 3D stacks of images (Scale bars = 200 μm).

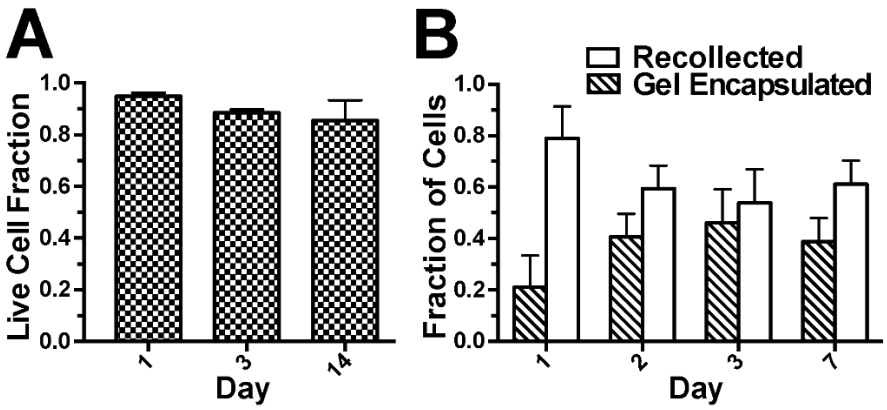

Figure 2.5: Quantification of results from 3D cell culture assays. (A) Fraction of live cells compared to total cells counted via automated image processing. (B) Quantification of cell recollection efficiency. Fraction of cells recollected out of PNJ-RGD hydrogels compared to the fraction remaining encapsulated in the gel after 1 to 7 days in culture. Error bars represent standard deviation.

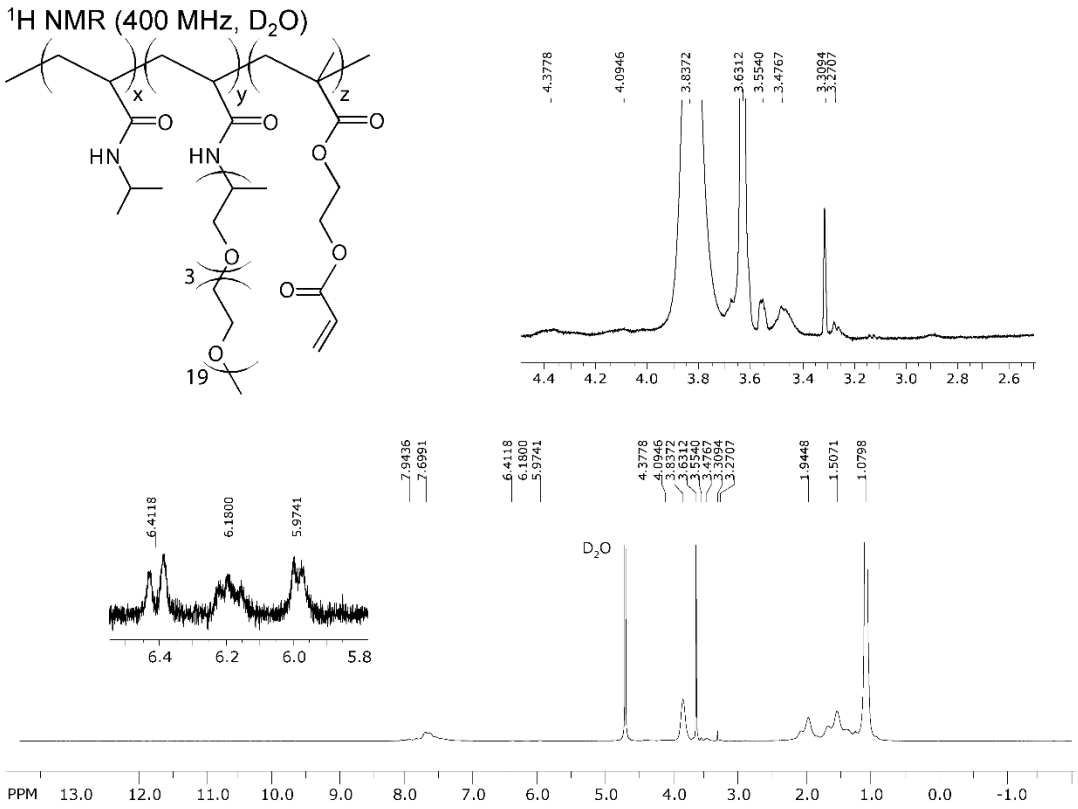

Figure 2.6: [1]H NMR spectra collected for PNJHAc. Chemical shifts for NIPAAm [δ = 3.84, 1H, $(CH_3)_2$-C*H*-NHCO], JAAm [δ = 3.63, 76H, CH_2CH_2O], HEMA [δ = 4.09-4.38, 4H, CH_2=CH-COO-CH_2CH_2-OCO], Acrylates [δ = 5.97, δ = 6.18, δ = 6.41, 3H, OCO-C*H*=CH_2].

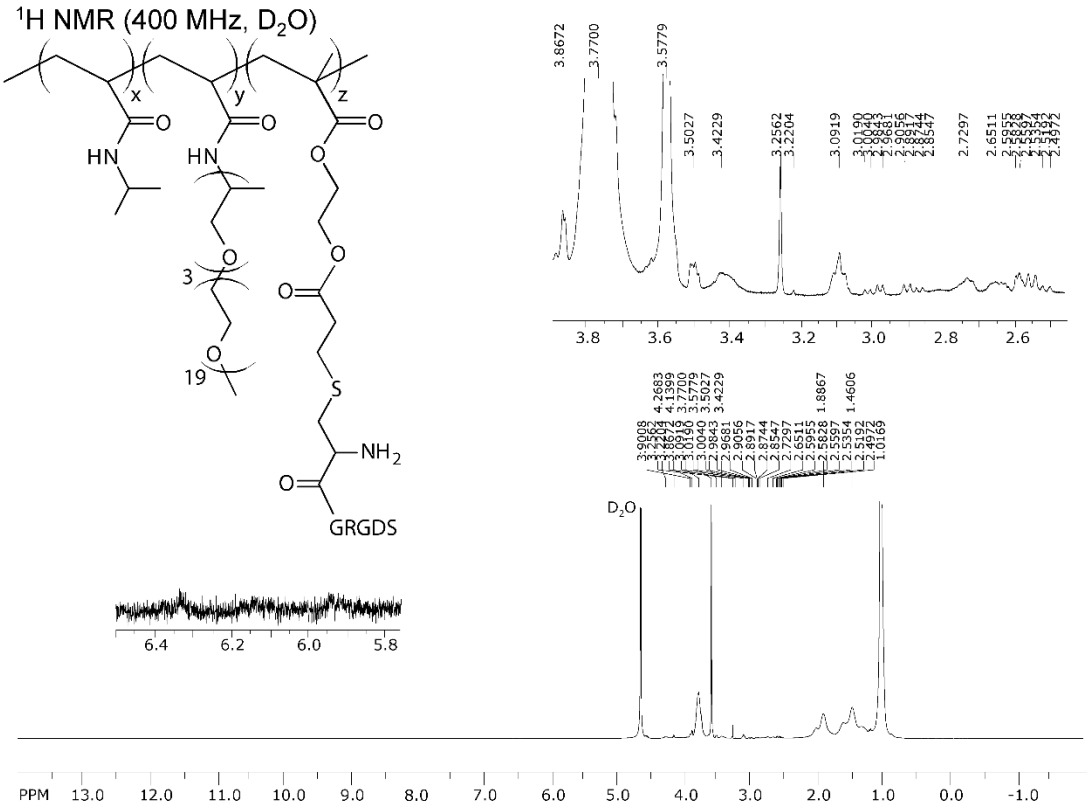

Figure 2.7: ^{1}H NMR spectra collected for PNJ-RGD. Chemical shifts for NIPAAm [δ = 3.77, 1H, $(CH_3)_2$-C*H*-NHCO], JAAm [δ = 3.58, 76H, CH_2CH_2O], HEMA [δ = 3.87, 2H, CH2=CH-COO-CH_2-CH_2OCO], Aspartic acid [δ = 2.58, 2H, OHCO-CH_2-CH], Serine [δ = 3.87, 2H, OH-CH_2-CH], Arginine [δ = 3.09, 2H, NH_2CNHNH-CH_2-CH_2].

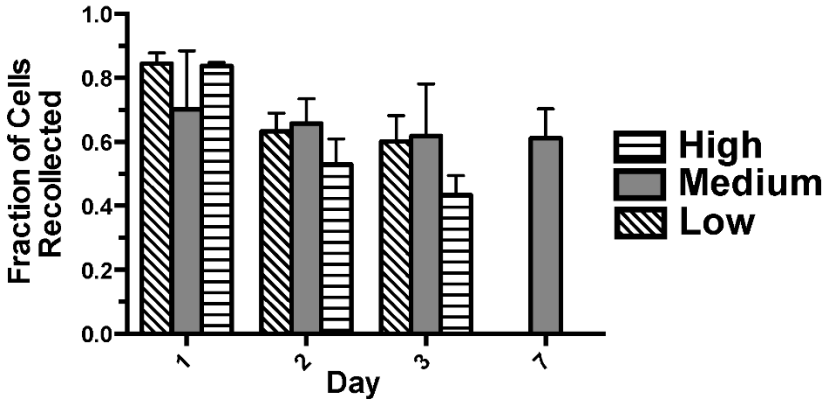

Figure 2.8: Fraction of cells recollected from PNJ-RGD hydrogels stratified by initial seeding density (high, medium, and low). Increasing density has a slight negative effect on recollection efficiency. Error bars represent standard deviation.

CHAPTER 3

PNIPAAm-co-Jeffamine® (PNJ) Scaffolds as In Vitro Models for Niche Enrichment of Glioblastoma Stem-Like Cells

3.1. Abstract

Glioblastoma (GBM) is the most common adult primary brain tumor, and the 5-year survival rate is less than 5%. GBM malignancy is driven in part by a population of GBM stem-like cells (GSCs) that exhibit indefinite self-renewal capacity, multipotent differentiation, expression of neural stem cell markers, and resistance to conventional treatments. GSCs are enriched in specialized niche microenvironments that regulate stem phenotypes and support GSC radioresistance. Therefore, identifying GSC-niche interactions that regulate stem phenotypes may present a unique target for disrupting the maintenance and persistence of this treatment resistant population. In this work, we engineered 3D scaffolds from temperature responsive poly(N-isopropylacrylamide-co-Jeffamine M-1000® acrylamide), or PNJ copolymers, as a platform for enriching stem-specific phenotypes in two molecularly distinct human patient-derived GSC cell lines. Notably, we observed that, compared to conventional neurosphere cultures, PNJ cultured GSCs maintained multipotency and exhibited enhanced self-renewal capacity. Concurrent increases in expression of proteins known to regulate self-renewal, invasion, and stem maintenance in GSCs (NESTIN, EGFR, CD44) suggest that PNJ scaffolds effectively enrich the GSC population. We further observed that PNJ cultured GSCs exhibited increased resistance to radiation treatment compared to GSCs cultured in standard neurosphere conditions. GSC radioresistance is supported in vivo by niche microenvironments, and this remains a significant barrier to effectively treating these highly tumorigenic cells. Taken in sum, these data indicate that the microenvironment created by synthetic PNJ scaffolds models niche enrichment of GSCs in patient-derived

GBM cell lines, and presents tissue engineering opportunities for studying clinically important behaviors such as radioresistance in vitro.

3.2. Introduction

Glioblastoma (GBM), the most common primary brain tumor in adults, has a devastatingly low 4.7% 5-year survival rate with a median survival of only 15 months [4,5]. Standard treatments, including surgical tumor resection, radiation, and chemotherapy, provide little long-term benefit, and relapse is nearly universal. GBMs are heterogeneous tumors composed of neoplastic cells that exhibit a hierarchy of tumorigenic potential. In accordance with the cancer stem cell hypothesis, this hierarchy is directed by a small population of cancer stem cells that exhibit the greatest capacity for tumor formation [41]. These GBM stem-like cells (GSCs) display many similarities to normal adult neural stem cells (NSCs), including a capacity for indefinite self-renewal, multipotent differentiation, and expression of NSC marker proteins [37,38,40,43]. GSCs are also highly tumorigenic [39], invasive [54], and resistant to both radiation [56] and chemotherapy [202,203]. GSCs that evade and survive treatment are hypothesized to play a prominent role in tumor recurrence [41].

In vivo, GSCs are concentrated in specialized niches that regulate stem phenotypes [51,60]. In the absence of essential niche regulation *in vitro*, GSCs can be maintained and propagated in NSC culture conditions as multicellular neurospheres [44]. However, neurosphere cultures can hinder effective enrichment of GSCs. Diffusion of nutrients and signaling factors that are essential for stem maintenance is limited by the size and number of cells within multicellular neurospheres [95]. The resulting intra-sphere nutrient gradients lead to growth of a poorly controlled population of stem, non-stem, apoptotic, and necrotic cells [97,144,145]. GSCs are commonly enriched and purified from these cultures by fluorescence activated cell sorting (FACS) for cell-surface

biomarkers (including CD133 [38,39], SSEA-1/CD15 [46], Integrin α6 [29]), which is typically paired with functional analysis of stem cell behaviors [100]. However, the use of cell-surface markers alone contributes to high false positive rates of GSC identification [47]. Therefore, it is essential to analyze GSC populations at the functional level, to identify stem cell behaviors such as multipotency and self-renewal.

Although neurosphere culture conditions provide a pseudo three-dimensional (3D) context for cell growth, this format present limited opportunities for controlling and studying microenvironmental influences on stem cell behavior. Microenvironmental regulation of stem-specific behaviors has been investigated extensively in regenerative medicine by utilizing 3D biomaterials, but comparably few examples exist in GSC research. Acquisition of selected stem characteristics has been reported for U87 and U251 GBM cell lines cultured in 3D scaffolds [113,139–141]. However, serum cultured long-term established GBM cell lines like U87 and U251 do not maintain the functional stem characteristics of primary GSCs, nor do they provide an accurate representation of GBM biology [43,40,44,101]. This severely limits the relevance of using immortalized cells to study either GBM or GSC biology. Recently, Li et al. reported that multipotent patient-derived GBM cells could be maintained in Mebiol® Gel (Cosmo Bio USA), a temperature responsive poly(N-isopropylacrylamide) (PNIPAAm) based hydrogel scaffold [148]. In addition, Hubert et al. described the development of large heterogeneous GBM organoids from patient-derived GSCs cultured in Matrigel® [159]. These prior works emphasize the significance of using biomaterials to study GSCs, but 3D culture conditions that actively enrich the full complement of GSC functional phenotypes (e.g., multipotency, self-renewal, treatment resistance) have not been defined *in vitro*.

In this study, we engineered poly(N-isopropylacrylamide-co-Jeffamine® M-1000 acrylamide) (PNJ) copolymers as tunable scaffolds for 3D GSC culture. PNJ copolymers exhibit a lower critical solution temperature (LCST) phase transition when heated in aqueous solution [1,180,181]. As a result, these materials encapsulate cells in physically crosslinked viscoelastic scaffolds at body temperature and easily release the cells by cooling to room temperature. We have previously reported the utility of this platform for enabling serial expansion of immortalized GBM cell lines in 3D [1]. Here, we describe conditions under which two patient-derived GBM lines are cultured in PNJ scaffolds to actively enrich GSC phenotypes, as measured by the full diversity of stem cell behaviors expected to drive tumor malignancy; this analysis includes multipotency, self-renewal capacity, expression of stem cell markers, and radiation resistance. For the purpose of these studies, we focus on self-renewal capacity, as measured by the *in vitro* limiting dilution assay, as the most direct approach for evaluation of relative GSC fractions under distinct culture conditions. We postulate that PNJ scaffolds may function similar to the native niche by serving as a depot for growth factors that maintain the GSC population [60]. The broader significance of these findings is that radioresistance, which is hallmark feature of GSC biology, is supported *in vivo* by microenvironmental factors that may be deficient or completely absent from standard cultures. Therefore, by defining microenvironmental mechanisms that drive GSC enrichment and radioresistance, 3D PNJ cultures may improve the accuracy and understanding of GSC responses to radiation *in vitro*.

3.3. Methods

3.3.1. Materials

All chemicals were reagent grade and purchased from Sigma Aldrich (St. Louis, MO, USA) unless otherwise stated. All cell culture reagents were purchased from Thermo

Fisher Scientific (Waltham, MA, USA) unless otherwise stated. N-isopropylacrylamide (NIPAAm) purchased from Tokyo Chemical Company (Portland, OR, USA) was purified by recrystallization from hexane. 2,2'-Azobisisobutyronitrile (AIBN) was purified by recrystallization from methanol. Jeffamine® M-1000 was generously donated by the Huntsman Corporation (Salt Lake City, UT, USA). Jeffamine® M-1000 acrylamide (JAAm) was synthesized as previously reported [180,181].

3.3.2. Polymer Synthesis

Poly(N-isopropylacrylamide-co-Jeffamine® M-1000 acrylamide) or PNJ copolymers were synthesized as previously described [1,180]. Briefly, radical polymerization of NIPAAm and JAAm monomers was initiated with AIBN (7 mmol AIBN/mol monomer) in anhydrous benzene. Copolymer feed ratios of NIPAAm:JAAm by mass were 90:10 (PNJ10), 85:15 (PNJ15), or 80:20 (PNJ20). All PNJ copolymers were purified by dialysis (3,500 MWCO) against diH_2O at 4°C and sterilized with ethylene oxide. Chemical compositions were analyzed by ^1H NMR in D_2O (400 MHz Varian Inova, Agilent Technologies, Santa Clara, CA, USA).

3.3.3. Rheology

The mechanical properties of PNJ scaffolds were measured at various concentrations by rheology. PNJ solutions were prepared at 5, 7.5, and 10 wt% in PBS at room temperature and placed on a parallel plate rheometer with a temperature controlled stage (MCR-101, Anton Paar, Ashland, VA, USA). Samples were rapidly heated to 37°C and subjected to a frequency sweep (0.1 - 10 Hz) with 0.5% shear strain deformation and normal force control (50 mN) to determine the storage (G') and loss (G") modulus.

3.3.4. Patient-Derived Primary GSC Culture

Patient tissue samples were acquired from the Biobank Core Facility at St. Joseph's Hospital and Medical Center and Barrow Neurological Institute (BNI) (Phoenix, AZ, USA). All samples were collected and transmitted according to the Biobank Institutional Review Board's approved protocol. In our previous work, two patient-derived GSC cell lines, GB3 [204,205] and GB7 [204], were established from primary GBM tumors surgically resected at BNI and characterized as human GSC models. GB3, classified as a proneural GBM subtype, was characterized through *in vitro* testing of stem behaviors, and *in vivo* via orthotopic transplantation. GB7 was classified as a classical GBM subtype through *in vitro* characterization of stem behaviors. GSCs were propagated in cell culture as non-adherent neurospheres grown in GSC media (DMEM/F12 media supplemented with B27, N2 and penicillin/streptomycin) in low-attachment poly(hydroxyethylmethacrylate) (polyHEMA) coated plates. Cultures were supplemented with 20 ng/mL of epidermal growth factor (EGF) and basic fibroblast growth factor (bFGF) (Merk Millipore, Billerica, MA, USA) every 2-3 days.

3.3.5. GSC Culture in PNJ Scaffolds

PNJ copolymers were dissolved at 5 wt% in GSC media overnight at 4°C. GSCs were dissociated with Accutase to a single cell suspension, counted (Cellometer Mini, Nexcelom, Lawrence, MA, USA), and resuspended in PNJ-media solution at room temperature (350k cells/mL). Cultures were then incubated at 37° C to crosslink PNJ scaffolds and encapsulate cells in 3D culture. After 48 hours, an equal volume of warm culture media was added above the scaffold. Every 2-3 days, scaffolds were supplemented with EGF and FGF (20 ng/mL) after being solubilized at room temperature to allow for distribution of nutrients. Upon warming the cultures back to 37°C, the scaffolds were reformed and encapsulated the freshly added growth factors. At

confluence (7 - 14 days for GB7; 14 - 21 days for GB3), PNJ scaffolds were cooled to room temperature, diluted in PBS, and centrifuged to recover live cells. In all experiments, PNJ cultures were compared with neurosphere cultures described in section 2.4.

3.3.6. Analysis of Neurosphere Area

GSCs cultured in PNJ scaffolds and in standard neurosphere conditions were imaged using brightfield microscopy (Zeiss Axio Observer A1) over the duration of the culture period. The area of GSC spheres (n > 225 spheres per condition per day) was measured using ImageJ (NIH) and compared across culture conditions.

3.3.7. GSC Multipotent Differentiation

GSC spheres were dissociated with Accutase to a single cell suspension. Cells were differentiated by culturing GSCs in serum supplemented media (DMEM + 10% FBS + 1% penicillin/streptomycin) on glass coverslips coated with poly-d-lysine. Media was replaced every 2-3 days for 14 days, after which cells were immunostained for markers of differentiation into astrocytes (GFAP), oligodendrocytes (GALC), and neurons (TUBULIN βIII). Cells were fixed with 4% PFA for 10 minutes, permeabilized and blocked for 30-60 minutes in PBST + 5% goat serum, and incubated in primary antibodies (Table 3.1) diluted in blocking buffer at 4°C overnight. Cells were stained with fluorescent secondary antibodies (Table 3.1) diluted in blocking buffer at 37°C for 30 minutes, counterstained with DAPI (3 ng/mL) for 10 minutes, and mounted on slides prior imaging with an inverted fluorescence confocal microscope (Zeiss LSM 710 Axio Observer Z1).

3.3.8. Limiting Dilution Assay

GSCs were dissociated with Accutase and cultured at low initial densities (1 – 50 cells) in polyHEMA coated 96 well plates. After 7 days, wells were imaged with brightfield microscopy (Zeiss Axio Observer A1) to determine sphere formation at each

initial density. Wells negative for sphere formation (% nonresponsive) were counted. This experiment was replicated 4 times with at least n = 12 samples for each initial cell density.

3.3.9. Western Blot Analysis

To prepare protein lysates, GSCs were lysed in ice cold RIPA buffer supplemented with fresh protease and phosphatase inhibitors. Protein concentration was measured using a standard Bradford assay. Western blots were run with 40 μg samples separated by gel electrophoresis on a 10% bisacrylamide gel (Bio-Rad, Hercules, CA, USA). Proteins were transferred to a polyvinylidene difluoride (PVDF) membrane at 4°C (Bio-Rad, USA). Membranes were blocked in 5% milk TBST and incubated with primary antibodies diluted in blocking solution shaking overnight at 4°C. Membranes were then incubated with fluorescent secondary antibodies diluted in blocking solution at room temperature. Blots were analyzed using a fluorescence reader (LiCor Odyssey CLx). Protein expression data is represented as the mean of n = 4 independent experiments.

3.3.10. Radiation Sensitivity

GSCs were irradiated (RAD Source 2000, RAD Source) in PNJ scaffolds or in neurosphere conditions with 2, or 10 Gy ionizing radiation. Immediately following treatment, cells were recovered from cultures, counted, and re-plated as single cells at equivalent densities in neurosphere growth conditions. Cell viability was measured with Cell Titer Glo (Promega) in comparison to a matched non-treated control 48 hours after radiation.

3.3.11. Statistical Testing

Statistical tests for neurosphere size data (Section 2.6) were performed in Prism 5 (GraphPad). Neurosphere size data was analyzed using a one-way ANOVA test with Bonferroni post-test. Statistical testing for limiting dilution data (Section 2.8) was

performed using a chisquare test through the extreme limiting dilution analysis (ELDA) software previously published by Hu and Smyth [206]. Statistical significance is reported for $p < 0.05$.

3.4. Results

3.4.1. PNJ Scaffolds

Three formulations of PNJ copolymers (Figure 3.1A) were synthesized by varying the concentration of JAAm (10%, 15%, and 20%) during polymerization with NIPAAm. JAAm incorporation was measured by ^{1}H NMR and the resulting formulations are distinguished by their JAAm content: PNJ10, PNJ15, and PNJ20 (Table 3.2). Similar to our previous reports, the LCST for each copolymer was measured by rheology between 29 and 31°C (data not shown). This characteristic allows for PNJ copolymer solutions to remain soluble when handled at room temperature (~25°C) and to form physically crosslinked scaffolds when heated to body temperature (~37°C) [1,180,181]. We observed that the three PNJ formulations formed viscoelastic scaffolds with storage and loss moduli that decreased in response to decreasing total polymer concentration (Figure 3.1B). JAAm incorporation also affected scaffold stiffness; for 7.5 wt% and 5 wt%, higher JAAm content produced less stiff gels, whereas we observed that PNJ15 scaffolds exhibited increased stiffness compared to PNJ10 scaffolds when formed at 10 wt%. This observation, although unexpected, was repeatable across independent polymer batches. We also observed that the PNJ10 scaffolds were slower to dissolve when formed at 10 wt% than the PNJ15 and PNJ20 scaffolds; it is thus possible that, at 10 wt%, a higher concentration of polymer facilitated additional hydrophobic interactions to promote phase separation, thus generating mild syneresis and a plateau in the PNJ10 modulus. Taken in sum, these data demonstrate the ability to produce a library of PNJ materials with scaffold stiffness (i.e., G') tunable between 153 and 1240 Pa.

3.4.2. GSCs in PNJ Scaffolds

Patient-derived primary GSCs (GB3 and GB7) were cultured in soft 5 wt% PNJ scaffolds, which possess brain-mimetic stiffness (153 Pa - 325 Pa). We compared the growth of GSCs in these conditions to standard neurosphere culture conditions as a control. In neurosphere culture, GSCs displayed as expected, high variability in sphere sizes. Conversely, we observed that GSCs cultured in 3D grew as individual spheres that remained smaller and more uniform in size due to decreased cell-cell contact within the scaffold (Figure 3.2a). These qualitative observations were quantified by measuring the area of neurospheres in both neurosphere and 3D culture (Figure 3.2b). Both GB3 and GB7 grew as significantly smaller spheres with a higher degree of uniformity in 3D compared to controls. These data indicate that PNJ scaffolds segregate cells to prevent sphere aggregation, a key drawback of neurosphere culture.

3.4.3. GSC Multipotency and Self-Renewal

Live GSCs were recovered from PNJ scaffolds by cooling the cultures to room temperature to induce scaffold phase transition [1]. The multipotency of the recovered cells was determined by differentiating GSCs in serum supplemented media. After two weeks, the differentiated cells were stained for markers of neuronal lineage (βIII-tubulin), oligodendrocyte lineage (GalC), and astrocytic lineage (GFAP). GB3 and GB7 cells grown in all PNJ and control cultures were observed to differentiate into each of the assayed neural subtypes (Figure 3.3) indicating that multipotency was maintained in control and PNJ culture conditions.

We also measured the self-renewal capacity of the recovered cells in an *in vitro* limiting dilution assay (Figure 3.4). Given the initial cell density and resulting probability of neurosphere formation, we determined the concentration of clonal cells in populations taken from each culture condition using extreme limiting dilution analysis

[206]. The stem cell frequency of GB3 cells cultured in neurosphere conditions was 1 in 6.7 (95% CI: [5.68, 7.97]) compared to 1 in 4.3 (95% CI: [3.68, 7.97]), 4.0 (95% CI: [3.39, 4.63]), and 3.8 (95% CI: [2.05, 4.03]) for PNJ10, PNJ15, and PNJ20 respectively. For GB7 cells, the stem cell frequency in neurosphere conditions was 1 in 14.0 (95% CI: [11.41, 17.22]) compared to 1 in 6.9 (95% CI: [5.72, 8.45]), 8.0 (95% CI: [6.57, 9.75]), and 6.4 (95% CI: [5.29, 7.80]) for PNJ10, PNJ15, and PNJ20 respectively. For both GB3 and GB7, all three PNJ scaffold formulations resulted in a significant ($p < 0.01$) increase in stem cell frequency compared to neurosphere culture; GSC enrichment in scaffolds was highest for the GB7 cell line.

3.4.4. Stem Marker Expression in PNJ Scaffolds

For comprehensive characterization of the GSC phenotype, we measured the expression of proteins important to both GBM and GSC biology in PNJ cultured cells. In these assays, we measured expression of NESTIN along with the transcription factors SOX2 and OLIG2 as markers of GBM stemness [47]. We also measured expression of the receptor tyrosine kinases (RTKs) for epidermal growth factor (EGFR) and platelet derived growth factor alpha (PDGFRα) along with the hyaluronic acid receptor CD44, all of which are associated with malignant GBM phenotypes, GSC maintenance, and interactions with the GSC niche [16,47,71]. In both cell lines, we observed an increase in NESTIN and EGFR expression in all scaffold conditions compared to neurosphere controls (Figure 3.5). CD44 expression was also increased in PNJ cultured GB3 cells compared to neurosphere controls. In GB7, CD44 was increased in PNJ10 and PNJ20 scaffolds but not in PNJ15. All other proteins tested did not display notable differences between scaffold and control cultures. The increases in expression of these proteins provides further evidence of GSC maintenance and enrichment in PNJ scaffolds.

3.4.5. Radiation Sensitivity in PNJ Scaffolds

Radiation resistance is a hallmark feature of GSCs *in vivo* and is actively supported by the GSC niche microenvironment. Here, we compared the viability of neurosphere and PNJ cultured GSCs following radiation treatment at a clinically relevant dose (2 Gy) and a high dose (10 Gy). Both GB3 and GB7 cells displayed a dose response to treatment in neurosphere conditions with GB3 cells exhibiting a more resistant baseline phenotype. Interestingly, 3D culture in PNJ scaffolds, regardless of composition, significantly increased resistant behavior in both GB3 and GB7 cells at all levels of treatment (Figure 3.6). This provides further evidence for the positive regulatory effect that the 3D PNJ microenvironment exerts on GSCs in culture.

3.5. Discussion

GSCs are distinguished within the broader population of GBM tumor cells by their multipotency, self-renewal capacity, NSC marker expression, and radioresistance [37,38,40,43].Together, these phenotypic features lead GSCs to be highly tumorigenic and likely drivers of tumor recurrence following conventional treatments such as radiation therapy. GSCs, similar to NSCs, are enriched in distinct niche microenvironments comprised of both cellular (e.g. immune cells) and non-cellular (e.g. extracellular matrix) components that provide critical regulatory signaling cues. In addition, niche inputs are also implicated in actively supporting treatment resistance in these cells [50,51,60,65,66]. Therefore, identifying mechanisms of GSC regulation contributed by the physical microenvironment may lead to options for targeting the niche with therapeutics that disrupt their regulatory capacity and sensitize otherwise resistant cells to treatment.

The complexity and anisotropy of the GSC microenvironments complicates analyzing specific regulatory contributions *in vivo*. As a result, three-dimensional

scaffolds have been routinely used to measure various interactions between GBM cell lines or GSCs and their local microenvironment by us [1,27] and others [24,32,115,116,120,126,139,148,156–159]. Although immortalized cell lines are proven tools in GBM research, they are poor biological models of the clinical condition and do not maintain functional GSCs [43,40,44,101]. In addition, 3D culture conditions that enrich GSCs, as measured by their functional phenotype, and concurrently support radioresistance have not been reported. Thus, there remains a significant need to engineer physical microenvironments to study GSC-niche interactions and their contribution to therapeutic response. Here, we designed a synthetic polymeric biomaterial platform composed of poly(N-isopropylacrylamide-co-Jeffamine® M-1000 acrylamide) (PNJ copolymers [1,180,181]) as a scaffold for expanding and enriching GSCs in 3D culture. To identify conditions under which the GSC phenotype was enriched, we performed a complete functional characterization (multipotency, self-renewal capacity, and radioresistance) of GSC behaviors alongside analysis of relevant GSC markers. In this study, we utilized two molecularly distinct GSC lines, GB3 (proneural) and GB7 (classical), primarily to illustrate the robustness of effects from the PNJ culture system. Evaluation of subtype-specific responses would be an interesting avenue for future work. In all, we utilized this approach to identify conditions within an engineered *in vitro* 3D microenvironment that positively regulate the GSC phenotype and contribute to radioresistant behaviors.

PNIPAAm is a temperature responsive polymer that exhibits a lower critical solution temperature (LCST) phase transition near 30°C in aqueous solution [179]. The LCST enables reversible physical crosslinking where the polymer is soluble at room temperature and precipitates to form a non-water soluble scaffold at 37°C. In the gel state, PNIPAAm scaffolds experience significant phase separation due to hydrophobic

chain interactions which limits their utility in 3D culture. The phase separation of PNIPAAm is reduced considerably by copolymerization with Jeffamine M-1000® acrylamide (JAAm) [180], which generates PNJ copolymers that exhibit fast dissolution to enable transient 3D cell culture [1]. In this study, the biochemical properties of PNJ scaffolds were tuned by modulating JAAm incorporation to form the three different PNJ formulations (PNJ10, PNJ15, PNJ20). Increasing JAAm concentration effects a corresponding increase in equilibrium water content in the scaffold [180]. The physical properties of PNJ scaffolds can also be easily tuned by altering the dissolved copolymer concentration. At the concentrations tested, PNJ copolymers formed viscoelastic (G' > G") scaffolds with stiffness (G') ranging from 153 and 1240 Pa (Figure 3.1) which directly coincides with the stiffness of healthy brain tissue [154]. We also observed that JAAm content affected PNJ scaffold stiffness, and that this effect was amplified in the higher concentration constructs. Overall, the tunable nature of the PNJ platform enables analysis of cell responses to variations in both microenvironmental chemistry and stiffness. For these studies, we chose to utilize soft scaffolds (153 – 325 Pa) to model the microenvironment. Stable cell culture scaffolds in this stiffness range are currently underreported as they may be difficult to create with chemical crosslinking strategies due to a low incipient density of crosslinks.

One initial observation of PNJ cultured GSCs was that cells did not cluster into large aggregates that are common in standard neurosphere cultures. During gelation, the physically crosslinked scaffolds form a polymeric network that segregates and suspends the cells in their location. Over the course of the culture, the cells grow as individual spheres that do not contact neighboring spheres as they inevitably do during free flotation in culture media. This caused GSCs to grow in significantly smaller and more uniform spheres in PNJ scaffolds compared to neurosphere conditions (Figure 3.2). This

phenomena has also been reported in other 3D scaffold systems [147,148]. One of the primary drawbacks of neurosphere culture is that nutrient gradients develop quickly in relation to sphere size and have an adverse effect on stem enrichment [144,145]. To this end, viscoelastic PNJ scaffolds prevent sphere aggregation and thus provide microenvironmental conditions that are fundamentally distinct from neurosphere or large organoid cultures. These conditions may positively contribute to enrichment of the GSC phenotype; it would be interesting, in future work, to consider hanging drop culture or culture within micro-patterned wells as methods to further define and control neurosphere size [207].

We measured functional GSC characteristics of GB3 and GB7 cells cultured in PNJ scaffolds to determine how stem phenotypes may be altered in comparison to neurosphere conditions. GSCs cannot be identified by a single feature but instead require multifaceted characterization. Multipotency, is a direct driver of GBM tumor heterogeneity as GSCs are capable of generating a diverse hierarchy of neoplastic cells that work to support tumor maintenance and growth [40,43,44]. Here, we observed that cells propagated in neurosphere culture as well in PNJ scaffold cultures were capable of multipotent differentiation (Figure 3.3) as measured by expression of proteins associated with three neural subtypes (neurons, oligodendrocytes, astrocytes). Importantly, differentiating GSCs will often promiscuously express differentiation markers of multiple neuronal lineages in ways that are not observed in healthy neural stem cells [37,40,44]. Thus, positive staining indicating overlapping expression of these antigens is possible under the described conditions. This phenomenon is generally ascribed to aberrant activation of differentiation machinery as a result of the malignant transformation that affects these tumor cells.

Self-renewal is another essential GSC characteristic that is a primary driver of tumorigenicity and recurrence *in vivo* [38–40]. We assayed the self-renewal capacity of GB3 and GB7 cells using an *in vitro* limiting dilution assay. *In vivo* limiting dilution is one of the gold standard methods for GSC identification. However, given that the control (neurosphere) cultures were previously characterized as containing GSCs [204,205], the *in vitro* limiting dilution and subsequent ELDA analysis were employed to measure quantitative differences in stem cell frequency [39,206]. Using this method, the stem cell frequency of PNJ cultured GB3 and GB7 cells was measured to be significantly increased ($p < 0.01$) for all scaffold formulations compared to neurosphere cultured controls (Figure 3.4). To our knowledge, this is the first report of a 3D biomaterial that increases self-renewal capacity in patient-derived GSC cultures. Mebiol® gel scaffolds have been shown to be useful for maintaining multipotent patient-derived GBM cells, but functional stem enrichment was not directly measured [148]. While Mebiol® gel and PNJ are chemically similar, the reported scaffold stiffness (1,000 Pa) is more than three times greater than the stiffest PNJ scaffold (325 Pa) and may play a role in this dichotomy. Alternatively, Matrigel® cultured GSCs reportedly develop GBM tumor organoids that reduce self-renewal capacity of the original stem population [159]. In contrast to Matrigel®, which contains both serum and extracellular matrix proteins, synthetic PNJ scaffolds do not provide any bioactive or native niche cues. Yet, the biochemical and biophysical properties of these scaffolds provide permissive conditions for non-adherent neurosphere growth that maintain GSCs in an undifferentiated state and increase self-renewal capacity. The interplay of effects imparted by the biochemical and biophysical properties of the scaffold is an important and likely complex relationship that warrants future study.

PNJ cultures also altered the expression of proteins that are attributed to the GSC phenotype. Specifically, NESTIN and EGFR expression were increased in both cell lines across all scaffold conditions (Figure 3.5). NESTIN is an established NSC marker and has been shown to regulate self-renewal capacity [208,209]. The EGFR pathway is one of the most studied in GBM biology as it is frequently amplified and/or mutated in the disease state [11]. Moreover, EGFR signaling in GSCs has been shown to help maintain the molecular characteristics of the original tumor sample [44] and also regulate their self-renewal capacity *in vitro* [210]. Thus, increases in NESTIN and EGFR expression are consistent with the measured increase in GB3 and GB7 self-renewal. Additionally, expression of the hyaluronic acid receptor CD44 was also increased in PNJ cultured GB3 cells as well as PNJ10 and PNJ20 cultured GB7 cells. CD44 expression has been proposed as a GSC marker and is commonly associated with an invasive phenotype [16,204]. Taken together, these data suggest that PNJ scaffolds promote expression of proteins that are known to regulate key GSC phenotypes such as self-renewal and invasion.

In vivo, GSCs are concentrated in specific niches (hypoxic, invasive, and perivascular), each of which may regulate cellular phenotype via distinct mechanisms [51]. Culturing GSCs as neurospheres or organoids is expected to drive cellular evolution primarily as a result of the gradients of oxygen and nutrient deprivation, which develop as cells proliferate [144,145]. In contrast, the PNJ microenvironment is expected to be relatively nutrient and oxygen rich. This expectation is based on the relatively small size of neurospheres grown within the gel (which prevents formation of a necrotic core), as well as our previous work showing that PNJ scaffolds retain encapsulated protein [180]. It is possible that proteins secreted by GSCs in PNJ scaffolds are effectively sequestered near cells, leading to increased autocrine signaling. The increased expression of EGFR

we observed in these studies supports this hypothesis, and the small size of clonogenic cell aggregates produced by culture within PNJ draws further parallel to the *in vivo* circumstance, where GSCs are found in small clusters near blood vessels. We thus propose that the PNJ microenvironment may be a relevant model for GSC interactions with the perivascular niche [60,65].

From a clinical perspective, total surgical resection of GBM tumors is often impossible due to tumor location and the potential for damage to healthy brain tissue. As a result, radiation offers the best treatment modality for remaining tumorigenic cells due to its ability to directly penetrate the target tissue. However, radiotherapy is resisted by GSCs that respond with increased activation of DNA damage repair pathways [56]. This behavior, similar to self-renewal capacity, enables GSCs to mediate tumor recurrence and disease progression. Moreover, support from the GSC niche is believed to be significant driver of radioresistance [50,51,60,65,66]. Hubert et al. investigated this by irradiating GSC derived 3D GBM organoids and found that GSC marker expression was inversely correlated with apoptotic marker expression [159]. In our work, populations of PNJ cultured GSCs displayed significantly increased radioresistance in an experimental model that directly assayed cell viability in response to treatment (Figure 3.6). Additionally, EGFR activity has been studied as a driver of GBM radioresistance [211,212] and may in this context be a contributing factor to the behavior we observed. These data suggest that 3D cultures, and specifically PNJ scaffolds, are valuable tools for studying microenvironmental support of radioresistance *in vitro*; we propose that these microenvironments are an effective GSC niche model, which are implicated in driving treatment resistance and tumor recurrence *in vivo* [65].

3.6. Conclusion

This work describes 3D culture conditions that were implemented using fully synthetic PNJ scaffolds to expand and enrich GSCs in culture. Using these scaffolds, we measured enrichment of functional GSC characteristics, including radioresistance, as well as corresponding protein expression in two molecularly distinct patient-derived models of GBM. The tunable nature of the PNJ platform is a substantial advantage as it enables control over the chemical and physical properties of the scaffold to study niche regulation of GSCs in a variety of conditions. PNJ chemistry also presents the opportunity for additional engineering; for example, by inclusion of bioactive peptides such as RGD to study cell adhesion related GSC-TME interactions [1]. In conclusion, we propose that the PNJ platform offers significant opportunities for studying microenvironmental regulation of clinically relevant models of GBM *in vitro*. Although current methods of GBM treatment have proven minimally effective, future therapeutic strategies may achieve a higher degree of success by focusing on disruption of GSC regulatory mechanisms within the microenvironment.

3.7. Tables and Figures

Table 3.1: List of primary and secondary antibodies used in this study

Primary Antibodies	Company	Product #	Host	Dilution	Application
NESTIN	Novus Biologicals	NB300-266	Mouse	1:2000	WB
EGFR	Abcam	AB52894	Rabbit	1:10000	WB
CD44	Cell Signaling	3570S	Mouse	1:2000	WB
SOX2	Cell Signaling	3579S	Rabbit	1:2000	WB
OLIG2	[213]	DF308	Rabbit	1:1000	WB
PDGFRα	Santa Cruz	SC-338	Rabbit	1:1000	WB
VINCULIN	Abcam	SPM227	Mouse	1:10000	WB
GFAP	Merck Millipore	AB9598	Rabbit	1:200	IF
GALC	Merck Millipore	MAB342	Mouse	1:250	IF
TUBULIN βIII	Merck Millipore	MAB1637	Mouse	1:200	IF

Secondary Antibodies	Company	Product #	Host / Isotype	Dilution	Application
Alexa Fluor 488	Thermo Fisher	A21121	Goat anti-Mouse IgG1	1:1000	IF
Alexa Fluor 488	Thermo Fisher	A21151	Goat anti-Mouse IgG3	1:1000	IF
Alexa Fluor 488 and 568	Thermo Fisher	A11008/A11011	Goat anti-Rabbit IgG	1:1000	IF
DyLight 680	Thermo Fisher	PI35519	Goat anti-Mouse IgG	1:10000	WB
DyLight 800	Thermo Fisher	PISA510036	Goat anti-Rabbit IgG	1:10000	WB

Table 3.2: Properties of PNJ copolymers. Monomer incorporation was measured by ^{1}H NMR in D_2O, and molecular weight was determined by GPC with THF as the mobile phase.

	NIPAAm wt% (x) : JAAm wt% (y)		Molecular Weight	
Polymer	Feed	Composition	M_W (x 10^6 Da)	P_D
PNJ10	90 : 10	92.4 : 7.6	1.671	1.047
PNJ15	85 : 15	89.3 : 10.7	1.649	1.133
PNJ20	80 : 20	85.2 : 14.8	1.182	1.076

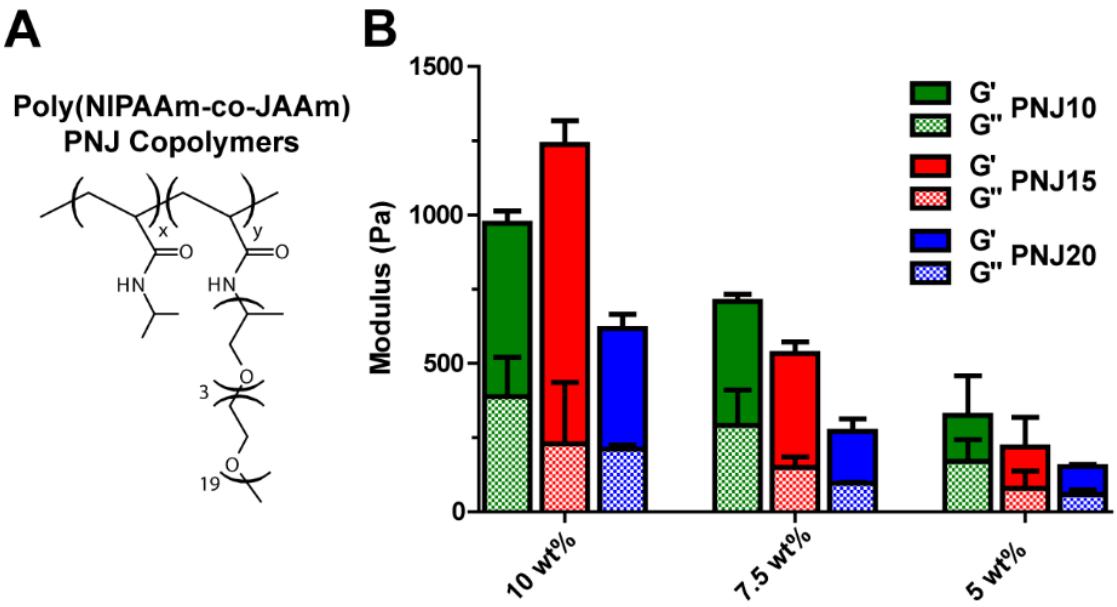

Figure 3.1: (A) Chemical structure of PNJ copolymers. (B) Complex modulus of PNJ scaffolds formed at 10 wt%, 7.5 wt% and 5 wt% measured by rheology. Rheological measurements (n = 2) were made with samples heated to 37°C.

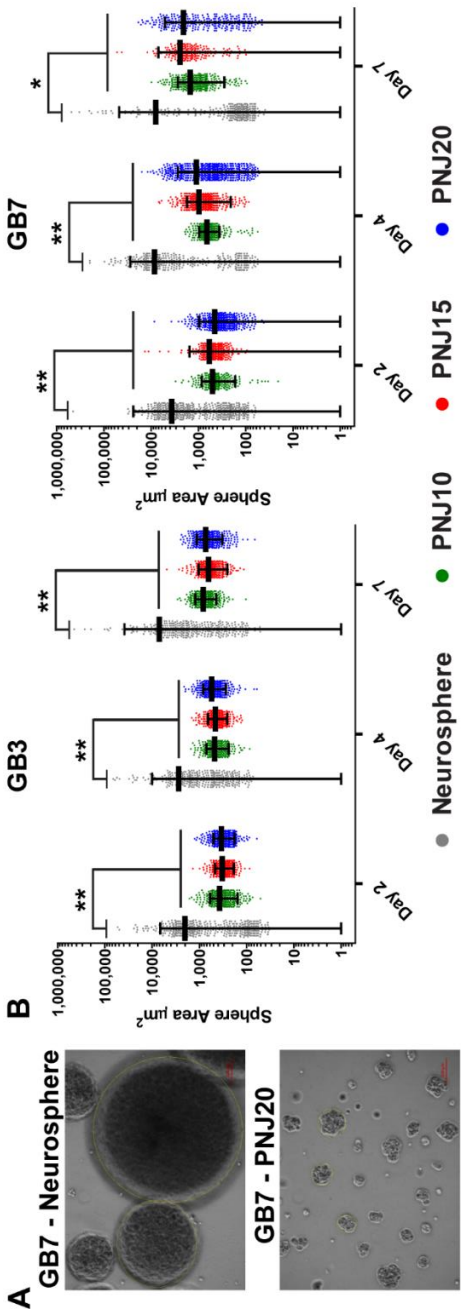

Figure 3.2: (A) Brightfield images of GB7 spheres in neurosphere conditions and PNJ20 scaffolds after 7 days of culture. (B) Quantification of 2D GSC sphere area during culture in neurosphere or PNJ scaffold conditions. Spheres were significantly smaller in all PNJ scaffolds at all time points compared to neurosphere cultures (* $p < 0.05$ and ** $p < 0.01$; 1-way ANOVA with Tukey post-test; $n > 225$ for each data set).

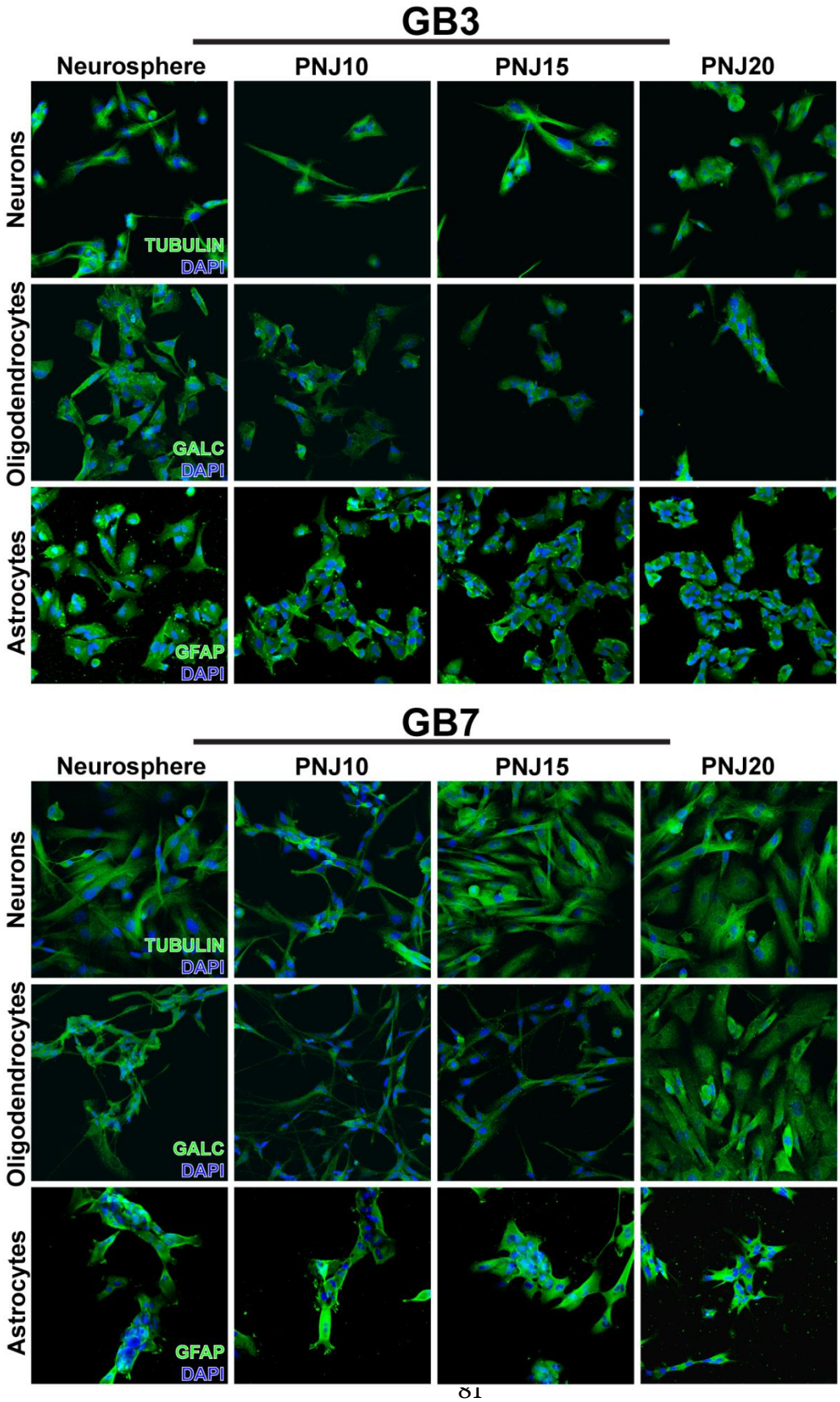
GB3
Neurosphere
PNJ10
PNJ15
PNJ20
Neurons
TUBULIN
DAPI
Oligodendrocytes
GALC
DAPI
Astrocytes
GFAP
DAPI
GB7
Neurosphere
PNJ10
PNJ15
PNJ20
Neurons
TUBULIN
DAPI
Oligodendrocytes
GALC
DAPI
Astrocytes
GFAP
DAPI

Figure 3.3: Multipotency of GB7 and GB3 GSCs measured by immunofluorescence staining for differentiation markers (green) along with DAPI nuclei counterstaining (blue). Cells cultured in both neurosphere and PNJ scaffold conditions were capable of differentiating into Neuronal (Tubulin), Oligodendrocyte (GalC), and Astrocytic (GFAP) lineages (nonlinear adjustments were made to some images for visual clarity).

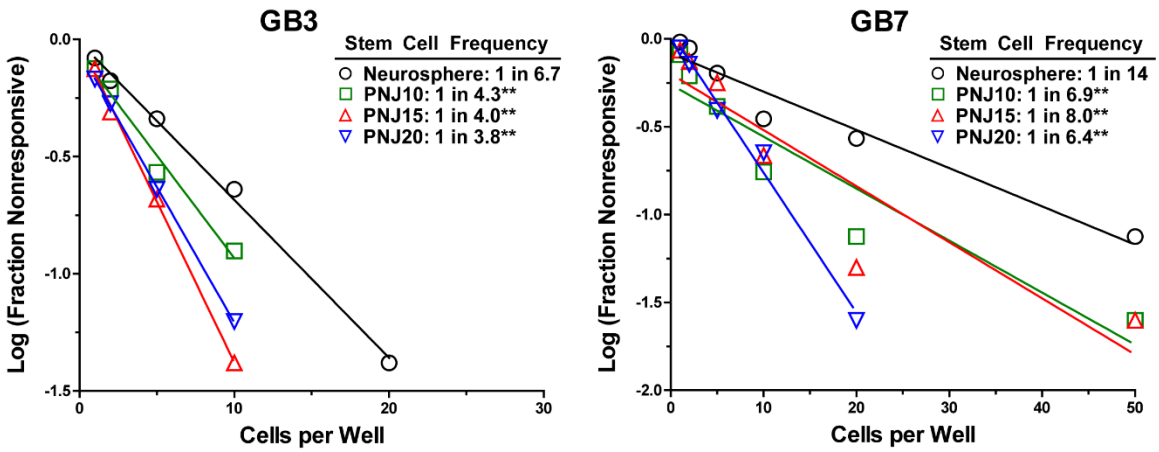

Figure 3.4: Self-renewal and stem cell frequency of GB7 and GB3 cells measured in a limiting dilution assay. Stem cell frequency was significantly increased in all PNJ cultures compared to control (** $p < 0.01$; chi-squared test for pairwise differences).

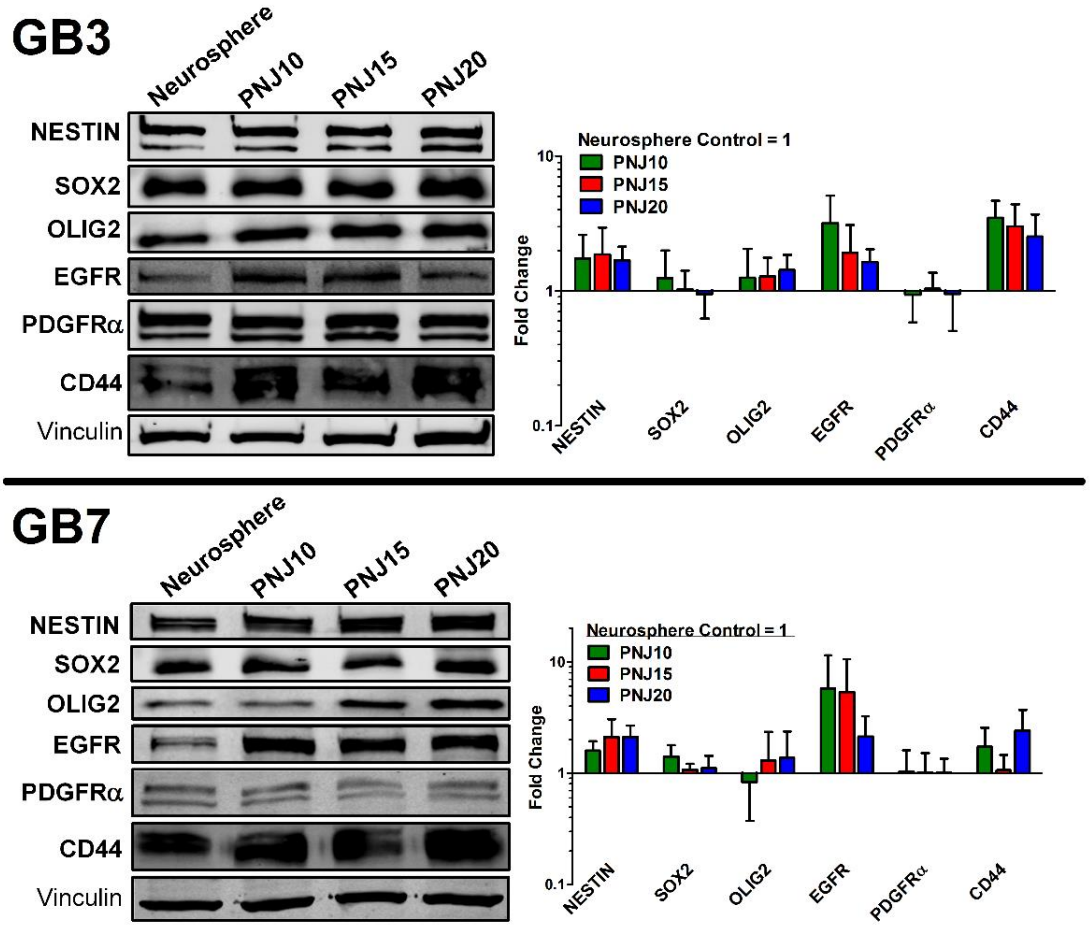

Figure 3.5: Expression of GSC marker proteins in PNJ scaffolds compared to neurosphere control cultures measured by Western Blot. In GB3 (n = 4), NESTIN, EGFR, and CD44 expression were increased in PNJ scaffolds compared to controls. In GB7 (n = 4), expression of NESTIN and EGFR were again increased in all scaffold conditions, while CD44 was increased in PNJ10 and PNJ20 scaffolds. Nonlinear adjustments were made to some images for visual clarity.

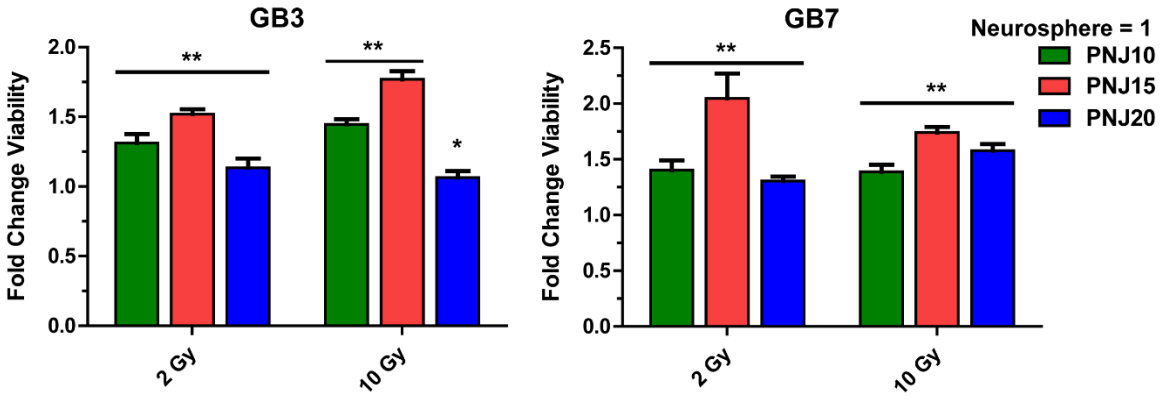

Figure 3.6: Viability of GSCs following low dose (2 Gy) and high dose (10 Gy) radiation is significantly higher in PNJ scaffolds compared to neurosphere cultures (fold change calculated in comparison to neurosphere controls; mean values are reported with SD; n = 12 replicates; * $p < 0.05$ and ** $p < 0.01$; 2-way ANOVA with Bonferonni post-test).

CHAPTER 4

PNIPAAm-co-Jeffamine® (PNJ) Scaffolds Regulate Glioblastoma Stem-Like Cell (GSC) Self-Renewal and Model Niche Support for Radioresistance

4.1. Abstract

Glioblastoma (GBM) is the most deadly malignant primary brain tumor. Within GBM exists a subpopulation of glioblastoma stem-like cells (GSCs), which are maintained in niche microenvironments within the brain and are believed to be a primary source of tumor recurrence. Niche regulation supports the GSC population primarily through maintenance of self-renewal, multipotency, and expression of stem-associated genes. However, these specialized microenvironments also provide protection from radiation and sustain the stem cell pool by promoting stem-plasticity in differentiated GBM cells. Previously, we described the design and development of temperature responsive poly(N-isopropylacrylamide-co-Jeffamine® M100 acrylamide) (PNJ) copolymer scaffolds as microenvironmental models that enriched patient-derived GSCs. Building on this prior work here, we investigated the capacity for PNJ scaffolds to regulate self-renewal and radioresistance in response to alterations in the physical microenvironment. We cultured two distinct patient-derived GSC models in four different PNJ scaffold formulations for comparison to conventional neurosphere culture. We identified dynamic microenvironmental regulation of GSC self-renewal that was a function of both the physical scaffold properties and cell-type. In conditions where self-renewal was enriched, the GSC marker NESTIN was ubiquitously expressed; in conditions that were detrimental to self-renewal, NESTIN expression was decreased. Importantly, we observed that PNJ scaffolds produced *de novo* expression of the transcription factor HIF2α, which has well-documented functional roles in GSC tumorigenicity and stem-plasticity. In contrast, HIF2α was not expressed in neurosphere

culture conditions. We also observed that PNJ scaffolds were radio-protective, with the strongest protection provided in conditions that also promoted GSC self-renewal. Importantly, we also observed increased NESTIN expression in select PNJ scaffold conditions in response to radiation. The relative maintenance of HIF2α in both treated and untreated scaffold conditions provides mechanistic evidence for stem plasticity and enrichment in response to radiation in 3D culture. Therefore, PNJ scaffolds provide unique opportunities for understanding GSC-specific microenvironmental regulation in response to radiation.

4.2. Introduction

The brain microenvironment provides broad support for the development and growth of glioblastoma (GBM). Specialized niches within the tumor and healthy tissue harbor small populations of glioblastoma stem-like cells (GSCs) that exhibit neural stem cell (NSC) phenotypes, including self-renewal, a capacity for multipotent differentiation, and expression of NSC marker proteins [38,39,51]. GSC niche microenvironments have been described in multiple distinct anatomical locations with GSCs concentrated near blood vessels in perivascular niches, on the edge of necrotic tissue in hypoxic niches, and also at the invasive edge of the tumor [51,65,72,81]. Accordingly, these microenvironments provide a diverse set of regulatory functions that support GSC phenotypes, and have been implicated in contributing to tumor recurrence via development of resistance to chemotherapy and radiation [62–64,85,90,214,215]. Thus, identifying and disrupting GSC-niche interactions may provide an avenue for sensitizing this population of cells to treatment.

Radiation is the most effective post-surgical treatment for GBM, although not all cells will be susceptible. GSCs are characteristically described as radioresistant, and radiation exposure has been observed to enrich GSC-specific markers *in vitro*

[56,61,138,216]. Importantly, GSCs are more radioresistant *in vivo* than *in vitro*, indicating that cellular microenvironment plays a critical role in supporting this behavior [63,64]. In situations where GSCs are depleted, the niche may induce dedifferentiation of remaining GBM cells to maintain the stem fraction. This bidirectional differentiation (interconversion) indicates that the GSC state is plastic and may be induced as a result of microenvironmental, epigenetic, or treatment responses [74,79,137,217]. Thus, through the functional treatment resistance and stem-plasticity provided by the microenvironment GSCs are unimpeded to maintain the hierarchical structure of GBM.

Designing reliable assays to measure microenvironmental regulation of stem phenotypes and radioresistance is challenging in standard *in vitro* cultures, particularly when comparing stem and non-stem tumor cell populations, which requires divergent growth conditions (serum vs. serum free; growth factor addition; attached vs. suspension culture) [62]. Importantly, standard conditions for culturing GSCs do not permit selective manipulation of the microenvironment. To address some of the challenges in traditional cell culture approaches, we recently developed scaffolds composed of poly(N-isopropylacrylamide-co-Jeffamine M-1000 acrylamide) (PNJ) as an *in vitro* model of the GSC microenvironment [2]. We observed that patient derived GBM cultured within the scaffolds demonstrated enriched self-renewal, stem marker expression, and decreased radiation sensitivity compared to neurosphere cultures [2].

Here, using two patient-derived models of GBM, our goal was to define the capacity for PNJ microenvironments to regulate GSC-phenotypes, including self-renewal, expression of stem markers, and radioresistance. We hypothesized that cell behaviors within PNJ scaffolds would be dynamically regulated as a function of the biophysical scaffold environment as well as cell type. This enabled identification of molecular mechanisms, specifically HIF2α, that are activated in PNJ scaffolds and model

in vivo niche regulation of GSCs. Furthermore, we provide evidence for radioresistance and stem plasticity in PNJ scaffolds, which indicates that this platform is relevant for studying treatment resistance in GBM, and may facilitate our long-term goal of identifying targets for disrupting niche regulation of GSCs.

4.3. Methods

4.3.1. Materials

Chemicals were reagent grade and purchased from Sigma Aldrich (St. Louis, MO, USA) unless otherwise stated. Cell culture reagents were purchased from Thermo Fisher Scientific (Waltham, MA, USA) unless otherwise stated. N-isopropylacrylamide (NIPAAm) purchased from Tokyo Chemical Company (Portland, OR, USA) was purified by recrystallization from hexane, while 2,2'-Azobisisobutyronitrile (AIBN) was purified by recrystallization from methanol. Jeffamine® M-1000 was generously donated by the Huntsman Corporation (Salt Lake City, UT, USA). Jeffamine® M-1000 acrylamide (JAAm) was synthesized as previously described [180,181].

4.3.2. Polymer Synthesis

Poly(N-isopropylacrylamide-co-Jeffamine® M-1000 acrylamide) or PNJ copolymers were synthesized as previously described [1,2,180] with copolymer mass feed ratios of NIPAAm:JAAm 90:10 (PNJ10) or 80:20 (PNJ20). PNJ copolymers were purified by dialysis (3,500 MWCO) against diH_2O at 4°C and sterilized with ethylene oxide. Syntheses were confirmed by ^{1}H NMR in D_2O (400 MHz Varian Inova, Agilent Technologies, Santa Clara, CA, USA).

4.3.3. Patient Derived GSC Cultures

Patient tissue samples were acquired from the Biobank Core Facility at St. Joseph's Hospital and Medical Center and Barrow Neurological Institute (BNI) (Phoenix, AZ, USA). All samples were collected and transmitted according to the

Biobank Institutional Review Board's approved protocol. Two low-passage patient-derived GSC cell lines, GB3 and GB7, were established from primary GBM tumors surgically resected at BNI. Both lines were characterized as human GSC models with GB3, classified as a proneural GBM subtype, and GB7 was classified as a classical GBM subtype (detailed characterization is provided in prior publications; GB3: [2,204,205]; GB7: [2,204]). GSCs were propagated in standard neurosphere conditions for less than 20 passages. Briefly cells were cultured in DMEM/F12 media supplemented with B27, N2 and penicillin/streptomycin in poly(hydroxyethylmethacrylate) (polyHEMA) coated plates. Cultures were supplemented with 20 ng/mL of epidermal growth factor (EGF) and basic fibroblast growth factor (bFGF) (Merk Millipore, Billerica, MA, USA) every 2-3 days.

4.3.4. PNJ Scaffold Cultures

PNJ copolymer was dissolved at low (5 wt/v%) and high (10 wt/v%) concentrations in GSC media overnight at 4°C generating 4 separate PNJ solutions: $PNJ10_{Low}$, $PNJ10_{High}$, $PNJ20_{Low}$, $PNJ20_{High}$. GSC neurosphere cultures were dissociated with Accutase to a single cell suspension, counted (Cellometer Mini, Nexcelom, Lawrence, MA, USA), and diluted in PNJ-media solution at room temperature (GB3: 500k cells/mL; GB7: 250k cells/mL). Cultures were incubated at 37° C to crosslink PNJ scaffolds and encapsulate cells in 3D culture. After 48 hours, an equal volume of warm neurosphere media (no PNJ) was added above the scaffold. Every 2-3 days, scaffolds were supplemented with EGF and bFGF (20 ng/mL) after being solubilized at room temperature to allow for nutrient distribution. At confluence (7 - 14 days), PNJ scaffolds were diluted in cold PBS, and centrifuged to recover live cells. Neurosphere cultures were utilized as controls for all comparisons of scaffold growth characteristics.

4.3.5. EGF Diffusion

Low and high concentration PNJ solutions were added in 10 μL aliquots to a sample chamber on a 3D gel chemotaxis slide (μ-Slide Chemotaxis ^{3D}, IBIDI, Martinsried, Germany) and heated to 37°C to form scaffolds. PBS + 1% BSA was added to empty channels on either side of the newly formed scaffold and the slides were equilibrated at 37°C overnight. One channel was replaced with EGF in PBS + 1% BSA to set up a growth factor gradient such that $C_{source}(0)$ = 4 ng/mL and $C_{sink}(0)$ = 0 ng/mL . Both the source and sink channels were collected at 48, 96, or 120 hrs. EGF concentration was measured using a sandwich ELISA (DuoSet, R&D Systems, Minneapolis, MN, USA) in comparison to EGF controls. The diffusion coefficient was calculated using the following relationship for diffusion across a diaphragm [218]:

$$D = \frac{1}{\beta t}\ln\left(\frac{C_{source}(0) - C_{sink}(0)}{C_{source}(t) - C_{sink}(t)}\right)$$

Where C_{source} and C_{sink} are the EGF concentrations in the source and sink chambers at a given time t; A_s is the scaffold cross-sectional area; W_s is the scaffold width; V_{source} and V_{sink} are the volume of the source and sink chambers; t is the time at measurement; and

$$\beta = \frac{A_S}{W_S}\left(\frac{1}{V_{source}} + \frac{1}{V_{sink}}\right)$$

4.3.6. Stem Cell Frequency

Stem cell frequency was determined using a limiting dilution assay as previously described [2]. GSCs were collected from low and high concentration PNJ scaffolds as well as neurosphere conditions, dissociated with Accutase, and cultured at low initial densities (1 – 100 cells/well) in polyHEMA coated 96 well plates. Plates were analyzed with brightfield microscopy (Zeiss Axio Observer A1) at 7 days to determine sphere formation at each initial density; wells negative for sphere formation (% nonresponsive)

were counted. This experiment was replicated 3 times with n = 24 samples for each initial cell density. Data was analyzed using the Extreme Limiting Dilution Analysis (ELDA) software to quantify differences in stem cell frequency across culture conditions using a chi-squared test for pairwise differences [206]. Statistical significance is reported for $p < 0.05$.

4.3.7. Radiosensitivity

GSCs in PNJ scaffolds and neurosphere conditions were cultured for 7-8 days and were treated with 2 Gy ionizing radiation (RS 2000, RAD Source, Suwanee, GA, USA). Cells were collected as described in section 4.3.4 for TUNEL and immunostaining staining 48 hrs after radiation.

4.3.8. Immunofluorescence Staining

GSCs were collected from neurosphere or PNJ scaffold conditions and processed for immunofluorescence staining using an established protocol [219]. Briefly, cells were incubated in 4% paraformaldehyde for 3 hrs at 4°C, dehydrated in 30% sucrose for 30 min at 25°C, resuspended in OCT, and frozen at -80°C. Samples were sectioned at 5 μm, collected on gelatin coated slides, and stored at -80°C until staining. Slides were defrosted at room temperature (5-10 min) and samples were fixed to the gelatin coating with 4% paraformaldehyde (5 min). Antigen retrieval was performed by heating samples in 10 mM Sodium Citrate buffer (pH 6.0) for 30 minutes at 80°C. Samples were blocked for 30 min (10% Normal Goat Serum, 0.1 M glycine, 0.3% Triton-X 100 in PBS). Primary antibodies were incubated overnight at 4°C (Table 4.1; 10% Normal Goat Serum, 0.3% Triton-X 100 in PBS), and secondary antibodies were incubated for 45 minutes at 25°C (Table 4.1; 10% Normal Goat Serum, 0.3% Triton-X 100 in PBS). Cells were counterstained with DAPI. Samples were imaged with an inverted fluorescence confocal

microscope (Zeiss LSM 710 Axio Observer Z1) with imaging settings applied uniformly across conditions to enable direct comparison of staining results.

4.3.9. TUNEL Assay

Irradiated GSCs were processed in the same manner as for immunofluorescence staining. Fragmented DNA was labeled via TUNEL staining (DeadEnd Fluormetric TUNEL System, Promega, Fitchburg, WI, USA) to label apoptotic cells 48 hrs after radiation. Cells were counterstained with DAPI.

4.3.10. Image Analysis

Image analysis of immunostaining and TUNEL staining was performed in ImageJ (NIH). For each image, the area of positive staining was measured and normalized to DAPI area, which enabled quantitative comparison across different culture conditions. Statistical testing was performed in Prism 5 (GraphPad) using a one-way ANOVA with Bonferroni multiple comparisons post-test. Statistical significance is reported for $p < 0.05$.

4.4. Results

4.4.1. Biophysical Characterization

EGF diffusion was measured across PNJ scaffolds in a diaphragm diffusion cell, and compared to diffusion through water, which was measured at D = 3.0E-6 cm^2/s using this experimental setup. For the tested scaffolds, both JAAm content and total polymer concentration altered the diffusion coefficient (Figure 4.1). The JAAm content of PNJ20 scaffolds led to an increase in the diffusion coefficient compared to PNJ10 scaffolds as a result of greater equilibrium water content enabling better penetration and transfer of the growth factor [180]. In the low concentration scaffolds the diffusion coefficients were measured at D = 1.28E-6 cm^2/s in $PNJ10_{Low}$ and D = 2.70E-6 cm^2/s in $PNJ20_{Low}$. High concentration scaffolds predictably effected a decrease in EGF diffusion,

presumably as a result of the increased polymer content and decreased equilibrium water content. These scaffolds yielded diffusion coefficients of D = 6.43E-7 cm^2/s in $PNJ10_{High}$ and D = 1.67E-6 cm^2/s in $PNJ20_{High}$. These values are within range of the diffusion of EGF through brain tissue, which has been reported at D = 5.18 ± 0.16 E-7 cm^2/s [220]. These results indicate that all tested scaffold conditions retarded the rate of diffusion of a model growth factor relative to diffusion through water, such that scaffold cultures are likely to maintain higher concentrations of cell-derived and exogenous biomolecules. Along with these distinct diffusion profiles, PNJ scaffolds possessed composition dependent stiffness that was described in our previous work ($PNJ10_{Low}$ G' = 325 Pa; $PNJ10_{High}$ G' = 972 Pa; $PNJ20_{Low}$ G' = 153 Pa; $PNJ20_{High}$ G' = 617 Pa) [2]. The relationship between composition, stiffness and diffusion is described in Figure 4.2. From this, we can qualitatively describe scaffold PNJ concentration (low vs. high) in terms of the scaffold stiffness (low vs. high), and JAAm concentration (10 vs. 20) in terms of diffusion (low vs. high).

4.4.2. Stem Cell Frequency

An *in vitro* limiting dilution assay was used to measure self-renewal capacity, and we identified significant differences in self-renewal based on scaffold conditions and cell-type in these assays (Figure 4.3). We have previously reported that GB3 and GB7 cells exhibited a significant increase in stem cell frequency when cultured in low stiffness PNJ10 and PNJ20 scaffolds [2]. Here, we observed that culture in high stiffness PNJ scaffolds significantly decreased GB3 self-renewal compared to neurosphere conditions ($p < 0.01$, Figure 4.3A, B). JAAm content did not produce a measurable effect in either high or low stiffness conditions. Thus, total polymer content was the primary biophysical factor in regulating GB3 self-renewal. GB7 cells produced an opposing response to changing scaffold conditions. In this cell line, both high and low stiffness scaffolds

produced a significant increase in self-renewal compared to neurosphere conditions ($p < 0.01$, Figure 4.3C, D). Furthermore, $PNJ20_{High}$ scaffolds elicited a significant increase in self-renewal compared to all other scaffold conditions ($p < 0.01$). Therefore, the combination of high PNJ and JAAm content were significant factors in promoting GB7 self-renewal. Altogether, these data suggest that GSC self-renewal is affected by both PNJ and JAAm content through mechanisms that may be differentially regulated according to cell type.

4.4.3. Functional Radiation Response

Following irradiation, scaffold and neurosphere grown GSCs were analyzed for specific functional responses. First, a TUNEL assay was used to label cells in late-stage apoptosis (Figs. 4.4A, 4.5A). GB3 apoptosis was significantly reduced ($p < 0.05$) in $PNJ10_{Low}$ and $PNJ20_{Low}$ scaffolds compared to neurosphere conditions (Figure 4.4B). However, GSCs cultured in $PNJ10_{High}$ and $PNJ20_{High}$ scaffolds did not produce a significant change in apoptosis compared to controls. PNJ scaffolds also altered the apoptotic fraction of GB7 cells following radiation. Here, we observed a significant decrease ($p < 0.01$) in apoptotic cells in $PNJ10_{High}$, $PNJ20_{Low}$, and $PNJ20_{High}$ scaffolds compared to neurosphere conditions (Figure 4.5B). Although GSCs cultured in $PNJ10_{Low}$ scaffolds showed fewer apoptotic cells than neurosphere culture, differences were not significant.

In parallel to apoptosis, we also measured functional markers of DNA damage (γH2AX) and proliferation (Ki67). Both GB3 (Figure 4.4A, C) and GB7 (Figure 4.5A, C) showed relatively little activation of DNA damage repair as identified by γH2AX intranuclear foci. The one exception to this was GB3 cells cultured in $PNJ20_{High}$ scaffolds which showed an increase in γH2AX, though it was not significantly different from

neurosphere cultures. All other scaffold conditions tended to show decreased γH2AX activity in both cell lines, however, these differences were not statistically significant.

GSC proliferation, as identified by the intranuclear marker Ki67, did not significantly change following radiation in either GB3 (Figure 4.4A, D) or GB7 (Figure 4.5A, D) PNJ scaffold cultured cells compared to controls. GB3 cells in high concentration scaffolds show greater proliferation than neurosphere and low concentration scaffold conditions. Conversely, GB7 cells in low concentration scaffolds, particularly $PNJ20_{Low}$, showed greater proliferation than both neurosphere and high concentration scaffolds. While overall, GB7 cells showed lower overall Ki67 activity following radiation compared to GB3.

The results of these functional assays following radiation indicate that scaffold conditions provide radioprotection for GSCs *in vitro*. Conditions that enriched the self-renewing population also limited radiation-induced cell death. Additionally, there was minimal evidence of DNA damage and no significant differences in proliferation across the culture conditions at 48 hrs post-treatment.

4.4.4. GSC Marker Expression

Based on the impact PNJ cultures have on GSC self-renewal and functional radiation response, we investigated the expression of GSC markers (NESTIN, HIF2α) to further probe for potential changes in stem regulation. First, in untreated cultures, GB3 cells in $PNJ10_{Low}$, $PNJ20_{Low}$ and neurosphere conditions all showed high expression of NESTIN (Figure 4.6A). However, $PNJ10_{High}$ and $PNJ20_{High}$ cultures, which maintained the fewest self-renewing cells, elicited a significant decrease in NESTIN (Figure 4.6C) with few spheres showing expression. After radiation treatment, $PNJ10_{Low}$ and $PNJ20_{Low}$ cultures maintained NESTIN expression. In contrast, NESTIN expression decreased in neurosphere cultures with few cells showing strong expression. Notably, NESTIN

expression increased in radiated $PNJ10_{High,}$ and significantly increased ($p < 0.01$) in $PNJ20_{High}$ conditions compared to untreated conditions (Figure 4.6C). Moreover, all radiated scaffold conditions produced increased NESTIN expression compared to radiated neurosphere cultures, but these differences were not significant.

Expression of the transcription factor HIF2α was not observed in neurosphere conditions. However, HIF2a was stabilized in untreated PNJ scaffold GB3 cultures (Figure 4.6B). Expression was significantly increased ($p < 0.01$) in $PNJ10_{High}$ cultures compared to neurosphere, while $PNJ10_{Low}$ cultures also exhibited relatively high expression (Figure 4.6D). Moreover, strong HIF2α expression was identified in a subset of cells in each of the 3D culture conditions (Figure 4.6B). In response to radiation, $PNJ20_{High}$ scaffolds produced higher expression of HIF2α, while expression significantly decreased ($p < 0.05$) in $PNJ10_{High}$ cultures, and also decreased in $PNJ10_{Low}$ and $PNJ20_{Low}$ though not significantly. Importantly, HIF2α remained stabilized and strongly expressed in a subset of GSCs in all PNJ culture conditions following radiation. Neurosphere cultures exhibited a slight increase in expression following radiation that was not statistically significant. Moreover, HIF2α expression in neurosphere conditions was never comparable to the high levels of expression observed in scaffold conditions.

In untreated GB7 cultures, NESTIN expression was ubiquitous across all tested conditions (Figure 4.7A). Therefore, unlike GB3, NESTIN expression was not directly reflective of the self-renewal enrichment provided by PNJ scaffolds. Radiation treatment elucidated a significant increase in NESTIN expression in both $PNJ10_{Low}$ ($p < 0.05$) and $PNJ10_{High}$ ($p < 0.01$) compared to radiated neurosphere cultures; $PNJ10_{High}$ NESTIN expression was also significantly increased ($p < 0.05$) compared to untreated $PNJ10_{High}$ culture (Figure 4.7C). NESTIN expression increased in radiated $PNJ20_{Low}$ and $PNJ20_{High}$ scaffolds, and decreased in matched neurosphere cultures compared to untreated

conditions but differences were not significant. Similar to GB3, NESTIN expression following radiation was lowest in neurosphere conditions.

Strong and consistent expression of HIF2α was again observed for PNJ scaffold cultured GB7 cells, while neurosphere cultures produced sporadic HIF2α stabilization (Figure 4.7B). $PNJ20_{High}$ scaffolds elicited significantly increased HIF2α expression compared to neurosphere culture, while other scaffold conditions producing comparable expression levels. Similar to GB3, a subset of GB7 cells in PNJ scaffolds consistently exhibited strong expression of this transcription factor. Here, HIF2α expression was reflective of GB7 self-renewal. Radiation treatment produced an increase in HIF2α in $PNJ10_{Low}$ cultures, and a decrease in both $PNJ10_{High}$, $PNJ20_{Low}$, and $PNJ20_{High}$ scaffolds, although differences were not significant. Neurosphere cultures showed a slight increase in HIF2α in response to radiation, but again, was not significant or strongly expressed in any cells. Radiation thus did not eradicate the HIF2α positive population of GSCs.

A complete summary showing quantitative comparisons of GB3 and GB7 self-renewal capacity, expression of NESTIN and HIF2α, along with their response to radiation is provided in Tables 4.2 and 4.3.

4.5. Discussion

The GSC population consists of highly tumorigenic, self-renewing cells [39] residing in niche microenvironments [51] that are resistant to conventional chemotherapy [57] and radiation [56]. GSC niche microenvironments are dynamic regulatory structures that provide integral support for both self-renewal and radioresistance [51,62–64,74,85,214]. In addition, these structures also enable stem-plasticity by directing the dedifferentiation of neoplastic cells to acquire the GSC phenotype [74]. Following standard of care treatments, recurrent GBM tumors have been shown by histology to be enriched with GSCs compared to matched primary tumor

samples [57]. As a result, these defining features collectively suggest GSCs play a prominent role in driving near universal rates of tumor recurrence and a correspondingly low median patient survival.

GSC niches may contribute to radioresistance through mechanisms that include interactions with the ECM [168,221], soluble signaling factors [56,62,214,222–224], and hypoxia [36,72,74,76,77,88,225,226]. Of these components, hypoxia may provide the strongest direct and indirect protection against radiation [87]. Mechanistically, radiation generates free radicals such as reactive oxygen species (ROS) which subsequently induce double strand break DNA damage. In oxygen restricted conditions, the capacity for ROS generation is reduced thereby protecting cells from DNA damage. In addition, GSCs respond to decreases in oxygen through activation of hypoxia inducible transcription factors 1α (HIF1α) and 2α (HIF2α). HIF1α is stabilized under conditions of chronic hypoxia, while HIF2α acts in an early response to hypoxia and can be stabilized in normoxic conditions, as well [36,72]. Clinically, expression of HIF2α, but not HIF1α, is correlated with poor prognosis in GBM [78], and, experimentally, HIF2a has been shown to promote stem plasticity [74,79]. Furthermore, activation of these transcription factors may decrease GBM radiation sensitivity through downstream activation of HIF target genes that include both stem and survival pathways [72,74,88,89].

Isolating the contribution of individual GSC-niche interactions *in vivo* is generally not feasible, given the complex landscape of the brain. Therefore, modeling the three-dimensional (3D) GSC microenvironment *in vitro* provides opportunities for separating specific components of stem maintenance. Recently, we developed PNJ copolymer scaffolds as 3D models of the GSC microenvironment that are capable of enriching stem phenotypes *in vitro* [2]. This platform is advantageous for a number of reasons, including that it is thermally reversible, mechanically tunable, and biologically

inert. These feature enable facile recollection of cells under mild temperature stimulus, and manipulation of microenvironmental parameters to study cell behaviors. Additionally, we demonstrated that these materials actively enrich GSCs compared to conventional neurosphere conditions, and proposed that this enrichment could present a model of stem maintenance in the nutrient rich perivascular niche [1].

Here, we expand on our prior work, designing PNJ microenvironments to study mechanisms that govern GSC response to radiation in 3D. Despite the functional importance of the microenvironment to treatment response, relatively few studies have investigated GSC contributions to radiation resistance using a 3D culture paradigm. Recently, Hubert et al. reported the development of large heterogeneous GBM organoids from GSCs cultured in Matrigel scaffolds with constant mechanical agitation. While these constructs decreased self-renewal overall, GSCs identified within the organoids exhibited little sensitivity to radiation induced apoptosis [159]. In our prior work, we determined that cells irradiated within PNJ microenvironments showed greater viability than neurosphere cultured cells, after the cells were replated; these assays did not allow us to probe cell behavior *during* recovery in a 3D environment [2].

In vivo, the tumor microenvironment ECM sequesters soluble signaling factors and serves as a depot for GSCs [34,62]. Mitogenic growth factors, such as EGF and FGF, are potent regulators of GSC phenotypes and requisite for stem maintenance *in vitro* [44]. Additionally, soluble factors may promote GBM radioresistance via growth factor (EGF/bFGF [56,62], EGFR [211,212], TGFβ/TGFβR1 [214], IGF-1/IGF1R [222]) and cytokine signaling (SDF-1/CXCR4 [223,224]). We previously observed that PNJ scaffolds increased expression of EGFR in both GB3 and GB7 cells [2], and in separate studies, retained ovalbumin protein in sink diffusion conditions [180]. Biomolecules encapsulated within PNIPAAm homopolymer are poorly retained due to water expulsion

in the gel state. However, incorporation of the hydrophilic comonomer Jeffamine limits water expulsion; we thus predicted that the movement of biomolecules through PNJ scaffolds would be hindered relative to pure water, enabling PNJ microenvironments to effectively sequester signaling molecules to stimulate autocrine/paracrine signaling ([180] Figure 7). To test this hypothesis, we measured the diffusion of EGF (6.6 kDa) as a model for growth factor diffusion. Our measurement of EGF diffusion through water (D = 3.0E-6 cm^2/s) was comparable to reported values, and is nearly an order of magnitude greater than the reported diffusion coefficient through brain tissue (D = 5.18E-7 cm^2/s) [220]. Predictably, each of the PNJ scaffold formulations retarded growth factor diffusion compared to diffusion through water, which was used to effectively model growth factor mobility in neurosphere conditions (Figure 4.1). PNJ concentration and JAAm content independently produce a measureable effect on both EGF diffusion and scaffold stiffness (measured by the storage modulus (G'); Figure 4.2). Increasing JAAm content effected an increase in diffusion and a decrease in G', while increasing PNJ concentration decreased diffusion and increased G'. This characterization indicates that these 4 PNJ scaffold formulations cover the reported stiffness of brain tissue (100-1,000 Pa [129,154,155]), and slow growth factor diffusion toward more physiological levels compared to standard culture conditions [220].

Having generated scaffolds to present distinct microenvironments, we next sought to study how these microenvironments would impact GSC behaviors. Microenvironmental stiffness and chemistry have been shown to regulate the migration and invasive capacity of GSCs *in vitro* [32,115,126,156,157], while growth factor accessibility is known, particularly in neurosphere cultures, to be critical in maintaining the stem fraction [144,145]. Furthermore, self-renewing NSCs were reported by Saha et al. to be preferentially enriched on substrates with stiffness ≥ 100 Pa [129]. Therefore,

these different microenvironmental characteristics may each independently regulate GSC behaviors *in vitro*, and to our knowledge, GSC self-renewal capacity has not been investigated as a function of the biophysical microenvironment. Our prior work indicated that both GB3 and GB7 exhibited significantly increased populations of self-renewing cells in low stiffness PNJ10 and PNJ20 scaffolds [2]. Here, we expanded the number of scaffold conditions tested and observed that GB3 cells cultured in high stiffness scaffolds showed a significant decrease in the self-renewing population (Figure 4.3B). In contrast, GB7 demonstrated a significant increase in self-renewing cells in both low and high stiffness scaffolds, with a further significant increase in the high stiffness/high diffusion scaffolds ($PNJ20_{High}$) compared to neurosphere culture (Figure 4.3D). Comparison of GB3 and GB7 data suggest that regulation of self-renewal by the physical microenvironmental is dependent on cell-type. Grundy et al. described subtype-specific regulation of GSC migration where neural subtype GSCs migrated efficiently on soft substrates where mesenchymal GSCs were poorly motile [157]. In the present study, GB3 cells belong to the proneural classification, which phenotypically best represent an oligodendrocyte lineage [11]; accordingly, Jagielska et al. reported that oligodendrocyte precursors are better maintained on soft (100 Pa) substrates but show increased differentiation on substrates with greater stiffness [227]. This may provide a possible mechanism for the decline in GB3 self-renewal in high concentration scaffolds. GB7 cells, on the other hand, are characterized as classical subtype, and self-renewing cells showed affinity for each of the tested scaffold conditions. The classical subtype most directly corresponds to an astrocytic lineage [11] which prefer stiff (> 1 kPa) substrates [129,228]. However, both soft and stiff microenvironments enriched GB7 self-renewal, and this behavior showed dependence on a balance of microenvironmental stiffness and diffusion properties that was not observed in GB3. Thus, our data are suggestive that the

observed behaviors may be related to subtype characteristics of their originating tumor, although additional work will be needed to fully define these subtype differences. Importantly, this highlights the critical need to utilize multiple patient-derived models for identifying mechanisms of microenvironmental regulation.

Since treatment resistance is considered a characteristic of self-renewing GSCs and is actively supported by features of the *in vivo* tumor microenvironment [51,62–64,74,214], we investigated PNJ scaffolds for their ability to model radio-protection *in vitro*. Here, we observed decreased radiation induced apoptosis in GB3 and GB7 cells cultured in scaffolds that enriched the self-renewal capacity (Tables 4.2, 4.3). For GB3, we also observed that high stiffness PNJ20 scaffolds produced a slight increase in apoptotic cells compared neurosphere conditions, while high stiffness PNJ10 scaffolds tended to show a slight decrease in apoptosis, although these differences were not statistically significant. Interestingly, these conditions appear to provide a level of radio-protection that extended beyond the pool of self-renewing cells. Neurosphere conditions maintain approximately twice as many self-renewing cells compared to these scaffolds, but did not provide a measurable benefit to cell viability. Thus, one significant observation from this work is that radiation resistance exhibited by cells was not exclusively a function of the self-renewing fraction; these data demonstrate that other microenvironmental variables must play a role.

In considering cellular responses to radiation, we also examined expression of γH2AX which marks DNA double strand breaks and leads to activation of DNA repair machinery [229]. Phosphorylation of this protein occurs within minutes of DNA damage, is dephosphorylated following repair, and prolonged activation (>24 hrs) is a precursor to cell death [64,230]. Although we did not observe statistically significant activation of γH2AX in any of the tested culture conditions for either cell line following irradiation,

this was not necessarily surprising given the 48 hr recovery period following treatment. Importantly, γH2AX activation tended to be higher in cultures retaining the least clonal populations (GB3: neurosphere, $PNJ10_{High}$, $PNJ20_{High}$; GB7: neurosphere). As a final functional marker, we measured proliferation via presence of intranuclear Ki67. In GB3, high stiffness PNJ scaffolds tended to produce more proliferative cells than neurosphere conditions, while in GB7, low stiffness PNJ scaffolds tended to maintain the most proliferative cells. Mildly proliferative behaviors following treatment may be indicative of selection toward a more malignant phenotype, and suggest that these conditions may provide a model for investigating tumorigenicity following radiation.

Expression of GSC marker proteins NESTIN and HIF2α was measured using immunofluorescence to identify molecular level changes in stem regulation that may contribute to radio-response. Immunofluorescence was chosen for the ability to detect differences in intra-sphere protein spatial distribution (a concern in large neurospheres [144,219]), and to better identify expression patterns in small cell fractions. NESTIN marks the self-renewing population of NSCs [209]; expression in GBM identifies the stem fraction [38,39] is strongly correlated to poor clinical prognosis, and is observed in invasive cells *in vivo* [58]. HIF2α has been reported as a GSC selective biomarker, and is instrumental to tumor angiogenesis via downstream production of VEGF [72]. Although stabilization of this transcription factor is associated with hypoxia, expression has been observed in GSCs residing in perivascular niches, acidic microenvironments, and also importantly, in normoxic *in vitro* culture conditions [36,72,79]. Furthermore, Li et al. reported that orthotopic GBM tumors initiated by GSCs with genetic knockdown of HIF2α exhibited histological expression of the transcription factor [72]. This indicates that the *in vivo* microenvironment selected GSCs that were not efficiently targeted by HIF2α knockdown. Indeed, when GSCs were purified for HIF2α knockdown, they were

unable to form tumors thus suggesting a requisite function for *in vivo* tumorigenesis [72]. Therefore, HIF2α expression has significant implications beyond hypoxia, and appears to be a key factor that is dynamically regulated the tumor microenvironment. Outside of functions in tumorigenicity and angiogenesis, HIF2α also has a documented role in promoting GBM stem-plasticity [74,79]. Downstream target genes of HIF2α include Oct4, c-Myc, and Nanog all of which are critical to the development of induced pluripotent stem cells (iPSCs) [231].

GB3 cells exhibited NESTIN expression that closely mirrored the population of self-renewing cells (Table 4.2). Similar patterns of near ubiquitous NESTIN expression were observed in low stiffness scaffolds, as well as in neurosphere cultures, while expression was abrogated in high stiffness scaffolds (Figure 4.6a). Following radiation, the NESTIN expression profile was significantly altered. While low stiffness scaffolds maintained high expression, neurosphere conditions exhibited decreased NESTIN, and notably, high stiffness scaffolds increased NESTIN expression (Figure 4.6C). The high stiffness conditions are particularly intriguing as these conditions were detrimental to self-renewal. Therefore, increased NESTIN in these conditions provides evidence that the PNJ microenvironment may promote stem plasticity in response to radiation. Expression of HIF2α was not predictive of GB3 self-renewal, as high stiffness PNJ10 scaffolds exhibited the highest expression and low self-renewal (Table 4.2). However, HIF2α did appear to decrease the radiosensitivity of cells in high stiffness PNJ10 scaffolds, particularly compared to high stiffness PNJ20 scaffolds, which maintained the lowest HIF2α expression in untreated cultures, and provided the least protection from radiation induced apoptosis. Moreover, high stiffness PNJ20 scaffolds showed the strongest increase in HIF2α expression in response to radiation again providing evidence that mechanistically suggests stem plasticity in these conditions.

In contrast to GB3, GB7 cultures showed ubiquitous expression of NESTIN in all culture conditions, and NESTIN was not directly predictive of self-renewal status (Table 4.3). In response to radiation, scaffold cultured cells maintained ($PNJ20_{Low}$, $PNJ20_{High}$) or were enriched ($PNJ10_{Low}$, $PNJ10_{High}$) in NESTIN expressing cells, while neurosphere cultures exhibited a slight decrease in expression. The increase in NESTIN expression may again be indicative of further enrichment of the stem population as a component of the radiation response. Unlike NESTIN, HIF2α expression in GB7 was a better predictor of self-renewal with high stiffness PNJ20 cultures showing the strongest expression in untreated conditions. Similarly, high expression of HIF2α correlated with decreased radiation induced apoptosis. Moreover, low stiffness PNJ10 cultures, which were the most radiosensitive scaffold conditions, also exhibited the lowest expression of HIF2α in untreated cultures. Yet in response to radiation, these conditions exhibited the strongest increase of the transcription factor, again possibly suggesting a plastic response (Table 4.3). We also examined expression of EGFR, FAK, AKT, and pAKT in both GB3 and GB7 cells; while variations in expression were observed between scaffold and neurosphere cultures, the data did not directly correlate to GSC self-renewal or radiosensitivity (results not shown).

GSC plasticity is a critically important mechanism for maintenance of the stem cell pool and development of tumor heterogeneity *in vivo* [137]. Stem plasticity or enrichment of the stem fraction has been described both as a response to radiation [56,138,216], and separately as a function of HIF2α signaling induced by the tumor microenvironment [75,79]. Here, we described that PNJ microenvironments consistently maintained a population of HIF2α expressing cells even in conditions where the fraction of self-renewing cells was depleted. Increased expression of NESTIN following radiation provides evidence for dynamic regulation of stem phenotypes in PNJ cultures. Given the

role of HIF2α in maintaining the stem fraction, we hypothesize that this response is mediated by the activity of this transcription factor. To our knowledge, the contribution of HIF2α to promoting GSC radioresistance and stem plasticity has not been described in any 3D models of the GSC microenvironment. The critical importance of HIF2α in GSC tumorigenicity and stem maintenance indicates that PNJ scaffolds provide a unique opportunity for studying microenvironmental regulation of this transcription factor *in vitro*.

4.6. Conclusions

In conclusion, we developed PNJ scaffolds as a tunable biomaterial platform for identification of microenvironmental regulation of stem phenotypes in patient-derived GBM. We observed PNJ scaffolds provide microenvironmental regulation of self-renewal that was dependent on the physical properties of the scaffold and the cell-type. Enhancement of paracrine/autocrine signaling or activation of mechanosensation pathways are possible mechanisms supporting this behavior and will require further study. Scaffold cultures were also radio-protective as they decreased radiation induced cell death in two distinct GSC models. Additionally, in response to radiation, all scaffold conditions maintained increased expression of NESTIN and HIF2α compared to neurosphere cultures, with selected conditions providing evidence of stem-plasticity. Finally, HIF2α expression was almost exclusively observed in scaffold conditions with only rare and sporadic activation in any neurosphere culture. Overall, these data suggest that GSC maintenance is fundamentally unique in PNJ scaffolds, thus enabling further analysis of the microenvironmental regulation of HIF2α, stem-plasticity, and radioresistance.

4.7. Figures and Tables

Table 4.1: List of primary and secondary antibodies used in this study

Primary Antibodies	Company	Product #	Host	Dilution
NESTIN	Novus Biologicals	NB300-266	Mouse	1:200
HIF2α	Millipore	MAB3472	Mouse	1:200
Ki67	Cell Signaling	9449S	Mouse	1:400
γH2AX	Cell Signaling	2577S	Rabbit	1:400
FAK	Novus Biologicals	NBP1-47494	Mouse	1:200
pAKT	Cell Signaling	4060S	Rabbit	1:25
EGFR	Abcam	AB52894	Rabbit	1:200

Secondary Antibodies	Company	Product #	Host / Isotype	Dilution
Alexa Fluor 488	Thermo Fisher	A21121	Goat anti-Mouse IgG1	1:500
Alexa Fluor 488	Thermo Fisher	A21151	Goat anti-Mouse IgG3	1:500
Alexa Fluor 568	Thermo Fisher	A11011	Goat anti-Rabbit IgG	1:500

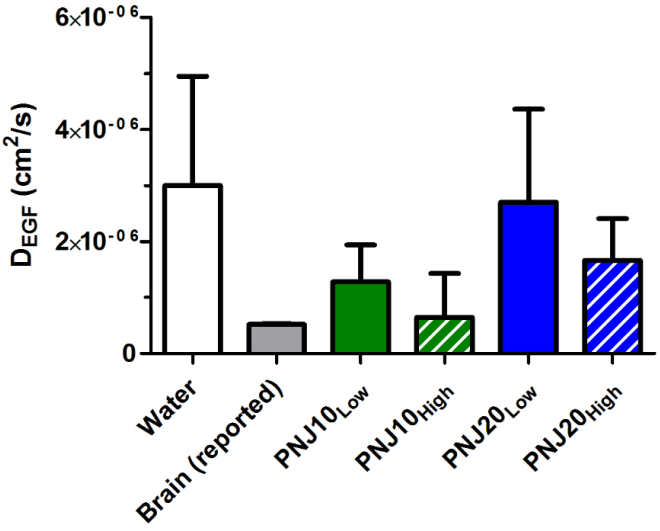

Figure 4.1: Diffusion coefficient of EGF in various conditions. EGF diffusion was measured across a diaphragm diffusion cell with PNJ scaffolds or water separating the source and sink chambers [218]. The diffusion of EGF in brain was reported by Thorne et al [220].

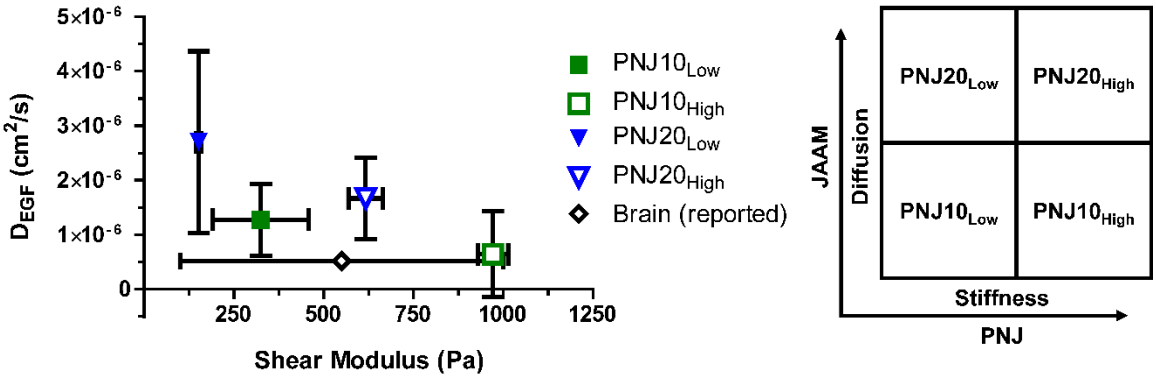

Figure 4.2: The relationship between EGF diffusion, shear modulus (stiffness), and the composition of PNJ scaffolds. (Left) These PNJ scaffold formulations effectively represent the shear modulus range reported for brain tissue [129,154,155], while also slowing EGF diffusion toward more physiological levels compared to fully liquid culture. (Right) Increasing JAAm leads to increased rates of diffusion, and increasing the total polymer content effects an increase in scaffold stiffness (shear modulus).

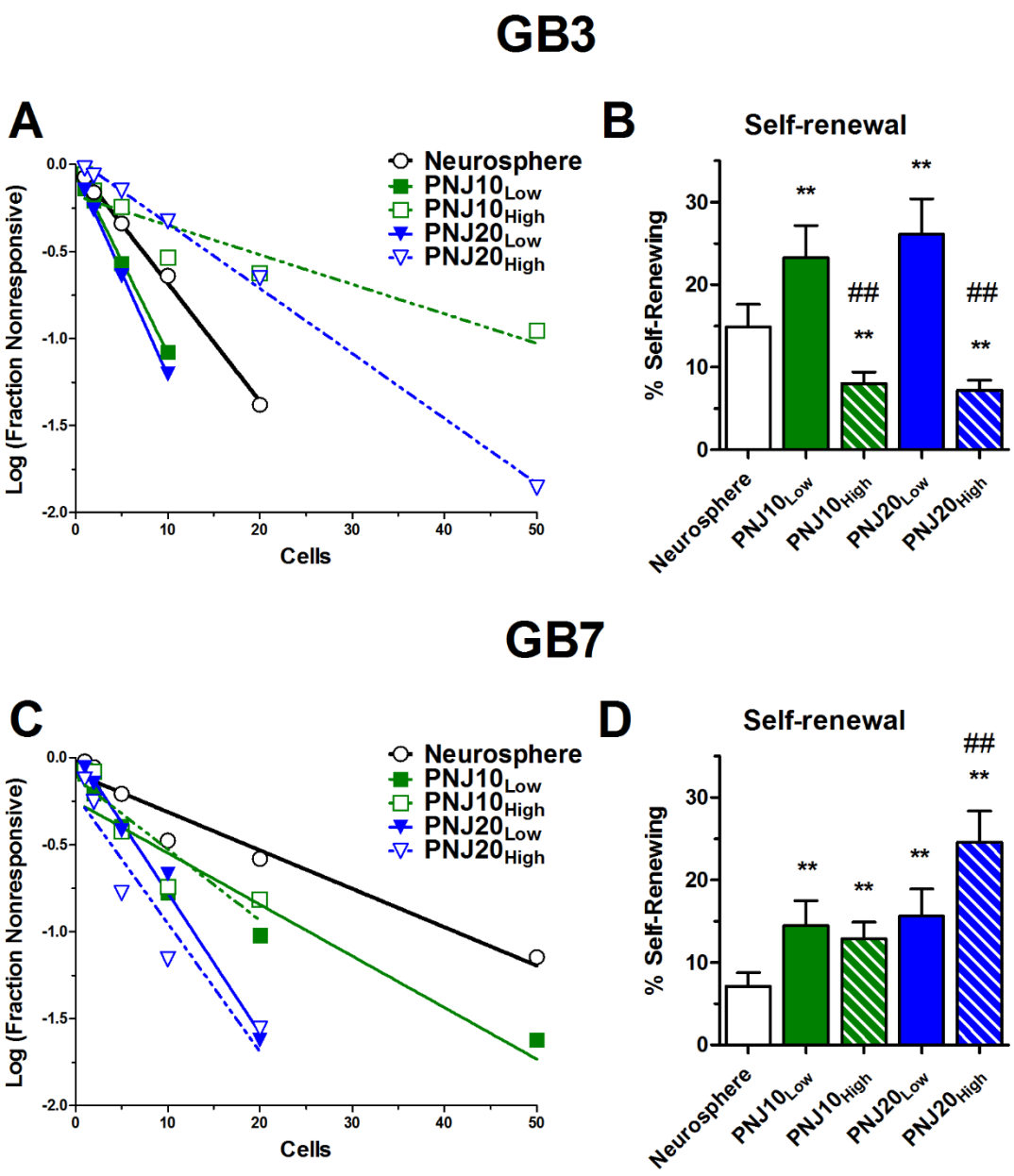

Figure 4.3: GSC self-renewal measured in response to Neurosphere or PNJ scaffold culture conditions. (A,B) Using an *in vitro* limiting dilution assay, GB3 cells exhibited a significant increase in self-renewing cells in low stiffness PNJ scaffolds (** $p < 0.01$ compared to neurosphere), and a corresponding significant decrease in self-renewing cells in high stiffness PNJ scaffolds (** $p < 0.01$ compared to neurosphere; ## $p < 0.01$ compared to low stiffness scaffold conditions). (C,D) Self-renewing GB7 cells were

observed to be significantly increased in all low and high stiffness scaffold conditions with $PNJ20_{High}$ scaffolds maintaining significantly higher self-renewal capacity than all other conditions (** $p < 0.01$ compared to neurosphere; ## $p < 0.01$ compared to other scaffold conditions). Percentages of self-renewing cells were calculated and tested for statistical differences using the Extreme Limiting Dilution Analysis software [206].

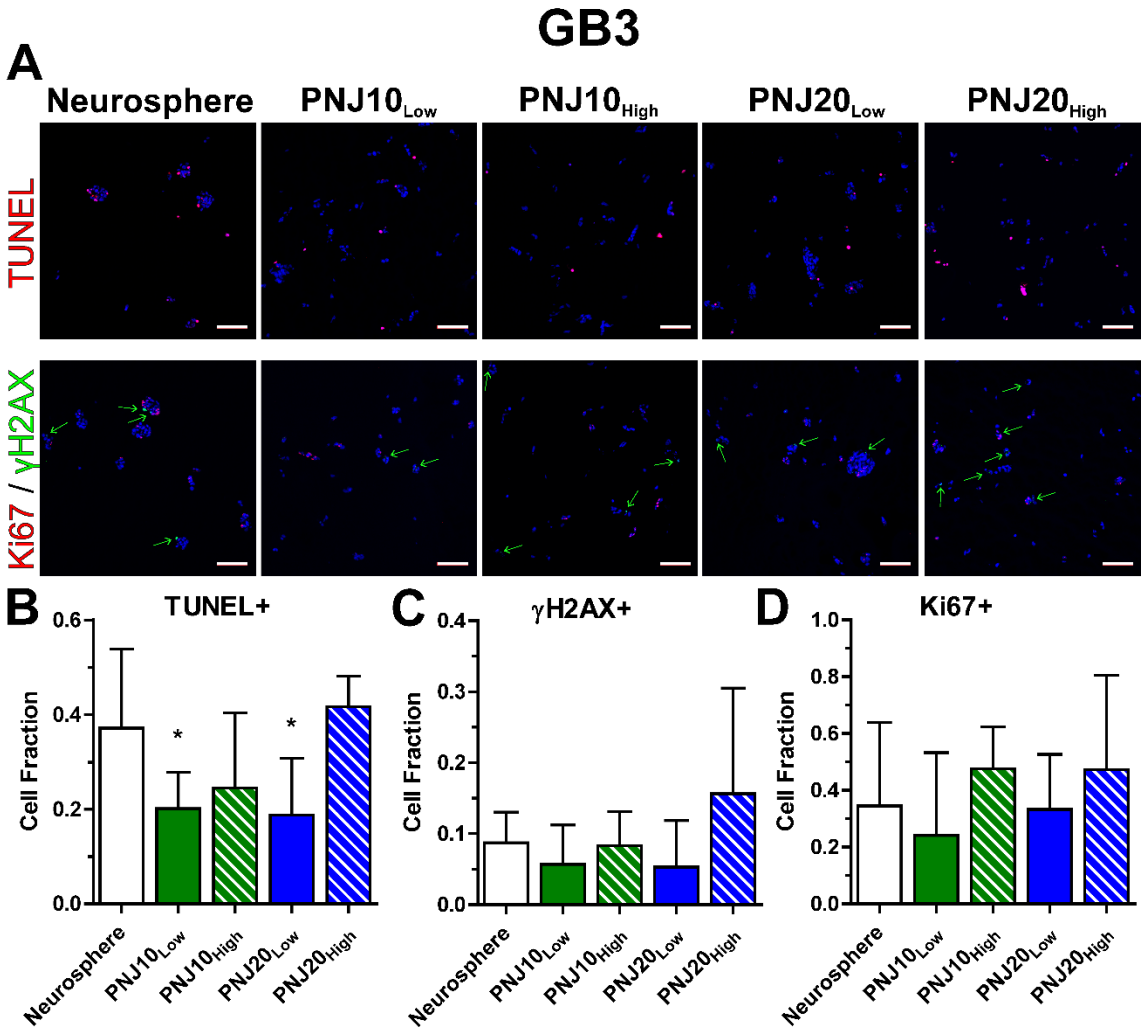

Figure 4.4: Functional response of GB3 GSCs to radiation treatment. Cultures were treated (2 Gy) and given 48 hrs to recover prior to analysis. (A – TUNEL) Apoptotic cells were identified via TUNEL staining (red). (B) Low stiffness scaffolds significantly reduced radiation induced cellular apoptosis compared to neurosphere culture (* $p <$

0.05). (A – γH2AX) Unrepaired DNA damage was assessed via γH2AX staining (green). (C) High stiffness PNJ20 scaffolds showed the highest fraction of cells with DNA damage, but differences between conditions were not statistically significant. (A – Ki67) Proliferation was measured via Ki67 staining. (D) High stiffness scaffolds produced the highest proliferative index, but differences among groups were not statistically significant. Quantification (Cell Fraction) is presented as number of staining events normalized to the number of cells estimated from nuclear counterstaining (DAPI, scale bars = 100 μm).

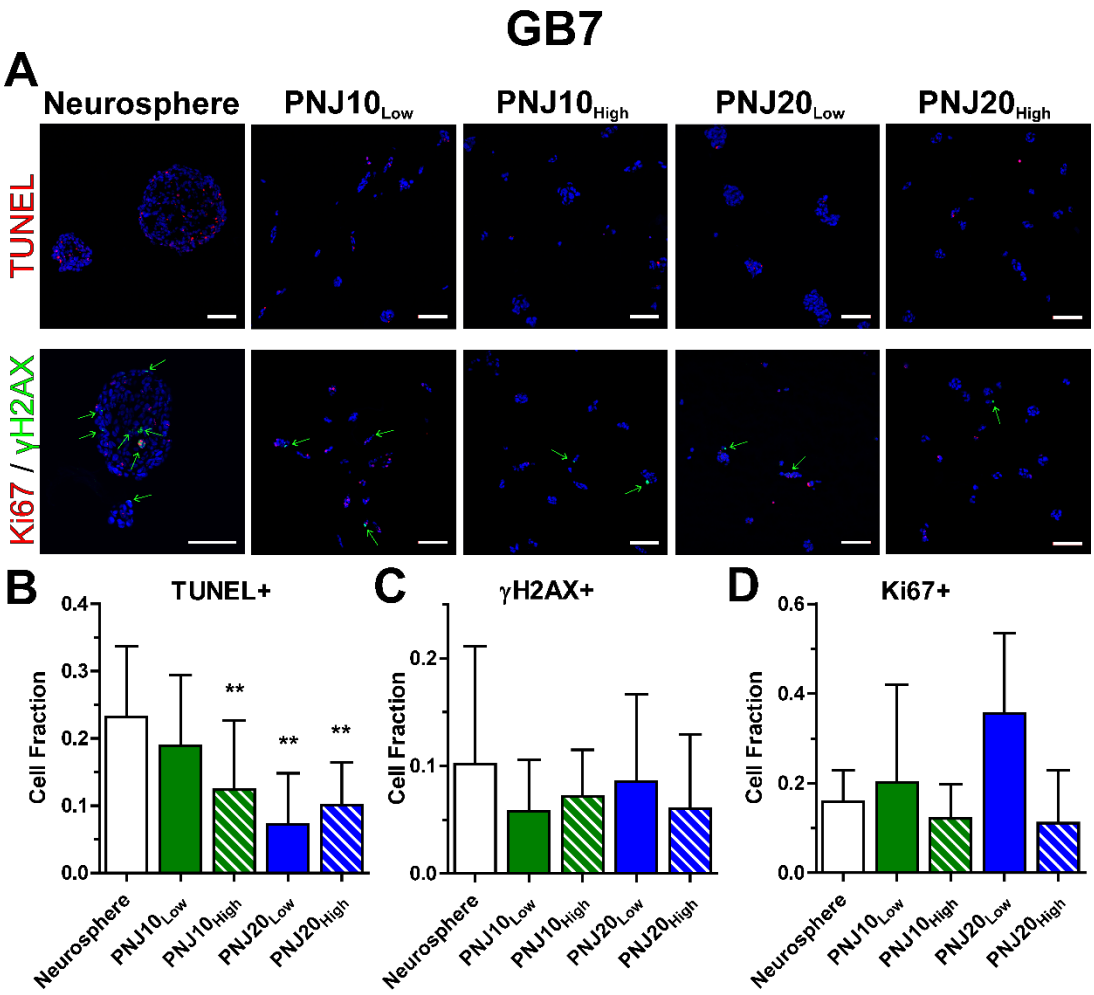

Figure 4.5: GB7 functional response to radiation treatment. Cultures were treated (2 Gy) and given 48 hrs to recover prior to analysis. (A – TUNEL) Apoptotic cells were

identified via TUNEL staining (red). (B) Radiation induced cellular apoptosis was reduced in PNJ scaffolds, significantly so in $PNJ10_{High}$, $PNJ20_{Low}$, and $PNJ20_{High}$ conditions compared to neurosphere culture (** $p < 0.01$). (A – γH2AX) Unrepaired DNA damage was assessed via γH2AX staining (green). (C) PNJ scaffolds reduced DNA damage, but differences between conditions were not statistically significant. (A – Ki67) Proliferation was measured via Ki67 staining. (D) Low stiffness scaffolds produced the highest proliferative index, but differences among groups were not statistically significant. Quantification (Cell Fraction) is presented as number of staining events normalized to the number of cells estimated from nuclear counterstaining (DAPI, scale bars = 100 μm).

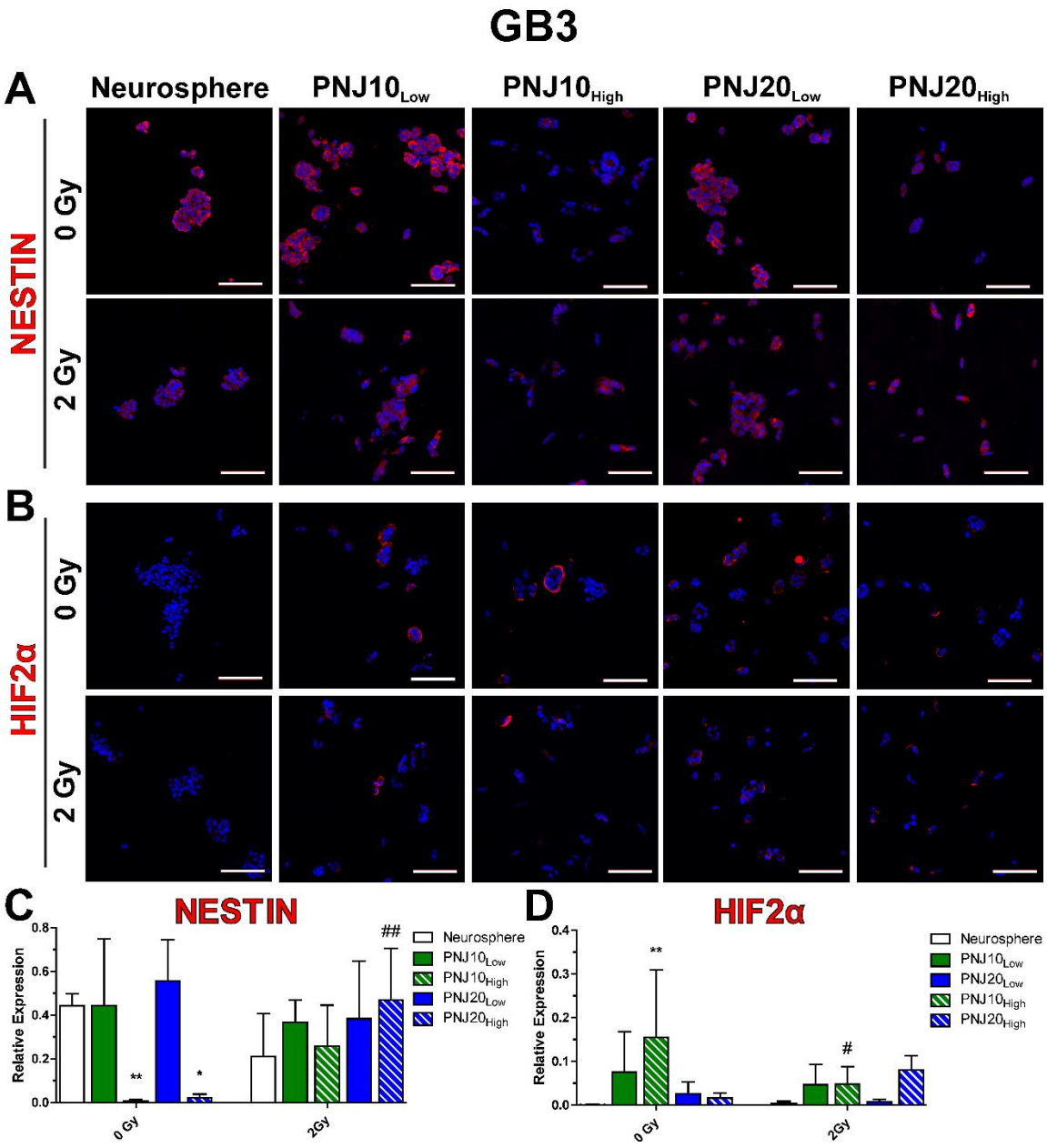

Figure 4.6: GB3 molecular response to radiation in PNJ scaffolds and neurosphere conditions. (A) Expression of NESTIN (red) and (B) HIF2α (red) was measured in untreated (0 Gy) and radiated (2 Gy) conditions with a 48 hr recovery period following treatment. (C) Untreated (0 Gy) high stiffness scaffolds produced significantly decreased NESTIN expression compared to neurosphere conditions (* $p < 0.05$, ** $p < 0.01$). Irradiated (2 Gy) high stiffness scaffolds exhibited increased NESTIN that was

statistically significant compared to untreated conditions for $PNJ20_{High}$. Irradiated (2 Gy) neurosphere cultures produced the lowest expression of NESTIN, but was not significantly different from scaffold conditions. (D) Untreated (0 Gy) PNJ10 scaffolds produced the highest expression of HIF2α with $PNJ10_{High}$ scaffold having significantly higher expression compared to neurosphere cultures (** $p < 0.01$). No HIF2α expression was identified in untreated neurosphere cultures. In response to radiation treatment (2 Gy), all PNJ scaffold conditions maintained a subset of HIF2α expressing cells that was increased over neurosphere cultures, but $PNJ10_{High}$ cultures exhibited a significant decrease in HIF2α expression (* $p < 0.05$). Quantification (Relative Expression) is presented as area of staining (NESTIN or HIF2α) normalized to area of nuclear counterstain (DAPI, scale bars = 100 μm).

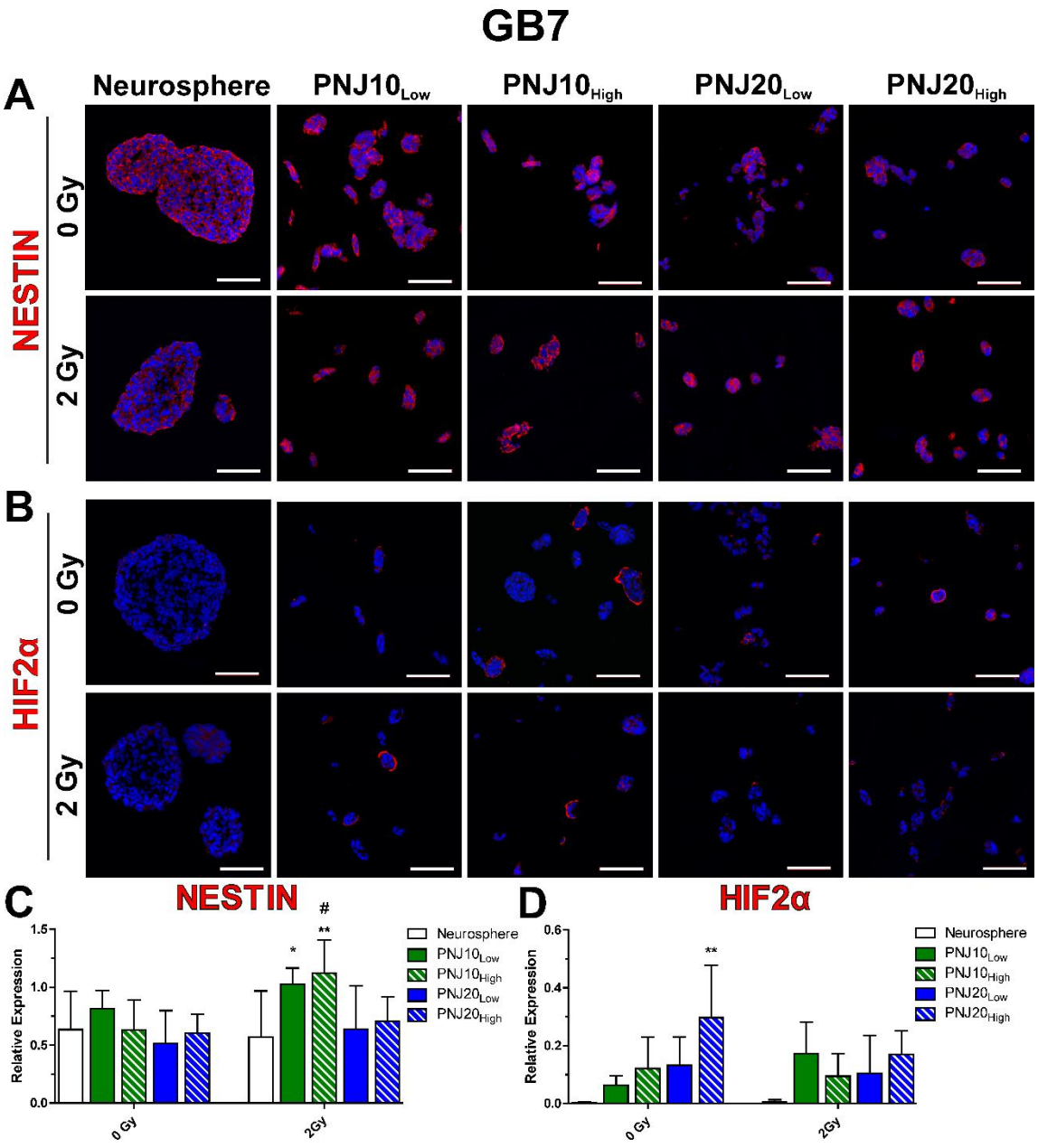

Figure 4.7 GB7 molecular response to radiation in PNJ scaffolds and neurosphere conditions. (A) Expression of NESTIN (red) and (B) HIF2α (red) was measured in untreated and radiated (2 Gy) conditions with a 48 hr recovery period following treatment. (C) Untreated (0 Gy) scaffold and neurosphere conditions produced similar expression of NESTIN. Irradiated (2 Gy) PNJ10 scaffolds exhibited increased NESTIN that was statistically significant compared to neurosphere cultures (* $p < 0.05$, ** $p <$

0.01), and for PNJ10$_{High,}$ compared untreated conditions (# $p < 0.05$). (D) Untreated (0 Gy) PNJ20$_{High}$ scaffolds produced significantly higher expression of HIF2α compared to neurosphere cultures, which did not express HIF2α (** $p < 0.01$). Irradiated (2 Gy) PNJ scaffold cultures all maintained a subset of HIF2α expressing cells, while expression in neurosphere cultures was rare. Quantification (Relative Expression) is presented as area of staining (NESTIN or HIF2α) normalized to area of nuclear counterstain (DAPI, scale bars = 100 μm).

Table 4.2: Summary of GB3 behaviors compared across PNJ scaffolds and neurosphere cultures. Color scale is represented with 0% as green, 50% as yellow, and 100% as red. Color scales are reset for each individual column other than NESTIN and HIF2α, which include both 0 Gy and 2 Gy columns.

	Self-renewing	2 Gy Functional Response			NESTIN		HIF2α	
Condition	0 Gy	TUNEL	Ki67	γH2AX	0 Gy	2 Gy	0 Gy	2 Gy
Neurosphere	0.15	0.37	0.35	0.09	0.44	0.21	0.00	0.00
PNJ10$_{Low}$	0.23	0.20	0.24	0.06	0.44	0.37	0.08	0.05
PNJ10$_{High}$	0.08	0.24	0.48	0.08	0.01	0.26	0.15	0.05
PNJ20$_{Low}$	0.26	0.19	0.33	0.05	0.56	0.38	0.03	0.01
PNJ20$_{High}$	0.07	0.42	0.47	0.16	0.02	0.47	0.02	0.08

Table 4.3: Summary of GB7 behaviors compared across PNJ scaffolds and neurosphere cultures. Color scale is represented with 0% as green, 50% as yellow, and 100% as red. Color scales are reset for each individual column other than NESTIN and HIF2α, which include both 0 Gy and 2 Gy columns.

	Self-renewing	2 Gy Functional Response			NESTIN		HIF2α	
Condition	0 Gy	TUNEL	Ki67	γH2AX	0 Gy	2 Gy	0 Gy	2 Gy
Neurosphere	0.07	0.23	0.16	0.10	0.63	0.57	0.00	0.01
PNJ10Low	0.14	0.19	0.20	0.06	0.82	1.03	0.06	0.17
PNJ10High	0.13	0.12	0.12	0.07	0.63	1.12	0.12	0.09
PNJ20Low	0.16	0.07	0.36	0.09	0.52	0.64	0.13	0.10
PNJ20High	0.25	0.10	0.11	0.06	0.60	0.71	0.30	0.17

CHAPTER 5

Conclusions and Future Directions

This final chapter describes the progress that we achieved in addressing each of our individual specific aims, and the opportunities that this work has created for future studies.

5.1. Specific Aim 1: Design a tunable 3D biomaterial model of the GBM tumor microenvironment that enables recollection of live cells under mild conditions.

In the first research chapter, we describe the steps that we took in developing a temperature responsive PNJ copolymer as a platform for 3D cell culture. The modular chemistry of the biomaterial enabled inclusion of cysteine terminated bioactive peptides, which we tested using the cell-adhesion peptide RGD. One of the key components of PNJ and PNJ-RGD copolymers is the ability to encapsulate and release cells using a mild change in environmental temperature. Characterization of non-adherent PNJ and adherent PNJ-RGD scaffold systems indicated that these copolymers remained soluble in aqueous solution at room temperature, and each exhibited a lower critical solution temperature (LCST) phase transition when heated to body temperature). Additionally, the shear modulus of the PNJ-RGD scaffolds was tunable between 40 Pa and 3 kPa, and scaffolds displayed rapid phase reversal when cooled. These properties enable PNJ-RGD scaffolds to accurately model the stiffness of brain tissue, while also quickly dissociating physical crosslinks to facilitate cell recovery. We demonstrated that PNJ-RGD scaffolds were cytocompatible over a 14 day culture using a model GBM cell line. The adherent conditions provided in PNJ-RGD scaffolds also enabled GBM invasion as opposed to non-adherent PNJ scaffolds which rarely produced invasive cells. This indicates that the PNJ-RGD platform may be useful for studying the biology of invasive cells, particularly if

they can be separated from proliferative cells in a tumor spheroid. Finally, we demonstrated that live cells could be recovered from PNJ-RGD scaffolds over the course of a 7 day culture. Efficient recollection required the use of enzymatic dissociation to detach cells from RGD binding sites, but was not necessary for recollection from non-adherent scaffolds. Interestingly, scaffold dissociation became more difficult over time, likely a result of matrix protein deposition, but viable recovery remained above 50% even for a 7 day culture. This study showed the successful development of PNJ scaffolds as a platform for transient 3D culture of GBM in both non-adherent and adherent conditions.

5.2. Specific Aim 2: Identify microenvironmental conditions that support and enrich GSC phenotypes *in vitro*.

The second research chapter describes the use of non-adherent PNJ scaffolds as microenvironmental niche models for culturing patient-derived GSCs. In this study, we chose to develop three separate PNJ formulations by altering the concentration of the NIPAAm and JAAm comonomers. We identified scaffold conditions that provided a shear modulus range that was appropriate for brain tissue engineering (153 Pa – 1240 Pa), and focused on measuring GSC responses to low stiffness (153 Pa – 325 Pa) scaffold conditions. Using two genetically distinct patient-derived GSC models, we observed that scaffold conditions significantly enriched the population of self-renewing cells compared to standard neurosphere culture conditions. Scaffold conditions also maintained GSC multipotency as shown by differentiation into three neural cell subtypes. In addition, we measured increased expression of key stem markers including NESTIN, EGFR, and CD44 in response to scaffold conditions. This led to a hypothesis that PNJ scaffolds enrich self-renewal as a result of increased autocrine and paracrine signaling, due to diffusion limitations in the physical PNJ microenvironment and interactions with the physical scaffold structure. We concluded this study by determining that scaffold

cultured GSCs were more resistant to radiation than cells cultured in neurosphere conditions. Therefore, this study provided evidence that GSC phenotypes including self-renewal, stem marker expression, and radioresistance were enriched via culture in PNJ scaffold conditions compared to traditional neurosphere cultures. These experiments provided the first evidence that PNJ scaffolds model niche microenvironmental regulation of patient-derived GSCs.

5.3. Specific Aim 3: Define the regulatory capacity of *in vitro* GSC niche models, and determine biological mechanisms that support GSC maintenance and radioresistance.

The final research chapter details measurements and interpretations of GSC responses to alterations in the physical properties of PNJ scaffold microenvironments. We characterized the diffusion of a model growth factor, EGF, and showed that diffusion was dependent on both the concentration of the scaffold and the constituent comonomers. In cell culture assays, we applied four different scaffolds with shear moduli and diffusion properties appropriate for brain tissue engineering to our two genetically distinct GSC models described in Chapter 3. PNJ scaffold cultures regulated the self-renewal of GSCs as a function of the scaffold physical properties and cell-type. The dynamic regulation that we observed enabled study of populations that were enriched or depleted of self-renewing cells simply by changing the configuration of the physical microenvironment. We also observed that a subset of GSCs strongly expressed the transcription factor HIF2α in all PNJ scaffold conditions, whereas neurosphere cultures did not produce HIF2α expressing cells. The final component of this study was to determine if PNJ scaffolds provided radio-protective microenvironmental growth conditions to GSCs *in vitro*. Here, we measured that PNJ scaffolds provided radio-protection that was most profound in conditions that also enriched self-renewal.

Interestingly, we also observed that scaffold conditions that decreased the self-renewing populations effected an increase in NESTIN expression in response to radiation. Given the role HIF2α plays in GSC maintenance and plasticity, we hypothesized that PNJ scaffolds primed an enrichment of stem behaviors as a response to radiation. Furthermore, the lack of consistent HIF2α expression in neurosphere culture suggests that PNJ scaffolds provide a unique set of microenvironmental conditions that enable analysis of its molecular mechanism of action in an *in vitro* GSC niche model. In this final study, we demonstrated the capacity for PNJ scaffolds to support microenvironmental maintenance and radioresistance of GSC phenotypes.

5.4. Future Directions

5.4.1. Engineering the Perivascular Niche

The approach that we described in Chapter 2 involved developing PNJ scaffolds with the cell adhesion peptide RGD. However, in the work presented in Chapters 3 and 4, we elected to employ non-adherent scaffold conditions to patient-derived GSC cultures. This was primarily done to enable direct comparison to neurosphere culture, which does not present any matrix adhesion sites. In the perivascular niche, GSCs are known to interact and concentrate in laminin rich regions surrounding blood vessels. It is therefore unsurprising that laminin and its corresponding integrins have been identified as regulators of various GSC phenotypes *in vitro* and *in vivo* [21,29,30,32,97,113,156]. Although non-adherent suspension cultures are standard for GSC propagation, it is also now accepted that GSCs may be maintained in culture on 2D laminin substrates [97]. Considering that RGD and a number of other cell adhesive sites are presented on different laminin isoforms (YIGSR, IKVAV, etc.), we propose that the PNJ platform would enable analysis of GSC regulation via adhesion to various laminin-derived peptides. A limitation of the currently validated scaffold system is that assays

would be restricted to cysteine terminated peptides. Incorporation of full length laminin or other ECM proteins is likely to significantly disrupt the physical gelation, and increase the LCST out of the workable range for cell culture. In work not described here (and not yet published), we have observed that GSCs increase self-renewal capacity and ECM deposition on PNJ-RGD scaffolds as compared to non-adherent PNJ formulations, which motivates further functional studies to study how these cells differentially remodel their microenvironment in response to extracellular cues. We would be interested to study the effect of various laminin derived peptides specifically on the treatment resistance of PNJ cultured GSCs. The direct evidence for perivascular protection from radiation is relatively limited *in vivo*. Thus, these *in vitro* assays may provide insight into the specific contributions of various adhesive ligands toward building a radio-protective GSC microenvironment.

Expanding on the idea of perivascular niche modeling, we also propose that the PNJ-RGD system would be useful for establishing GSC co-cultures with vascular endothelial cells. The interactions between these two cell types is well-characterized both *in vivo* and *in vivo*. However, their relationship has not been defined in response to radiation in a three-dimensional co-culture. Furthermore, a second motivating factor is that HIF2α activity in PNJ cultures would be predicted to increase recruitment and proliferation of endothelial cells. Therefore, there may be new understanding to be gained from developing this system where GSCs are encapsulated and endothelial cells are cultured on the gel surface. This test design would allow for measurements of endothelial tube formation as well as contributions to therapeutic response. These interactions described therein may lead to identification of mechanisms that are co-opted to decrease GSC and tumor associated endothelial cell radiosensitivity.

5.4.2. Characterization of GSC Derived Exosomes

In PNJ scaffold cultures we have consistently observed what appear to be vesicles concentrated around growing spheres, and immunofluorescence staining indicates that cytoplasmic NESTIN is present in these structures (results not shown or published). Importantly, we have never observed the presence of DNA in these structures (via positive DAPI staining), thus ruling out the concern that these structures are evidence of membrane blebbing associated with apoptosis. Instead, we hypothesize that these structures are exosomes, and that they may also contribute to GSC enrichment. GBM cells release exosomes containing proteins, miRNA, and mRNA that induce changes in their surrounding microenvironment [232]. One of the primary responses associated with exosome signaling is angiogenesis, and both VEGF and FGF have each been empirically identified as proteins secreted in GBM exosomes [232,233]. To identify exosomes in PNJ cultures, we propose staining PNJ derived GSCs for exosome surface markers including CD9, CD63, Lamp-1, and Lamp-2. Growth factor signaling plays a principal role in maintaining GSC phenotypes [44], and we therefore believe that the concentration of these extracellular structures around spheres may promote stem behaviors in PNJ scaffolds through growth factor pathways.

5.4.3. Microenvironmental Regulation of HIF2α

As previously described, expression of HIF2α is controlled by the microenvironment and may manifest in conditions where oxygen is not restricted [36,72,74,79]. Therefore, further characterization of the GSC-PNJ microenvironment may provide insight into the mechanisms that lead to HIF2α activity. The simplest explanation is that expression is mediated by relative hypoxia within the PNJ microenvironments. However, evidence to the contrary is provided in that HIF2α expression was not directly correlated to microenvironmental inhibition of diffusion;

also, HIF2a expression was not observed in the core of large neurospheres. Still, hypoxic microenvironments could be directly identified using a chemical probe such as pimonidazole, and could be analyzed in conjunction with staining for both HIF2α and HIF1α. Considering that HIF1α is generally observed in states of chronic hypoxia, this would provide a more complete landscape of how oxygen availability affects different GSC culture conditions.

The role of HIF2α and hypoxia in regulating GSC phenotypes indicates that PNJ scaffolds offer a platform for studying activation of this pathway and mechanistic consequences. The long-term goal of the project described in this dissertation is to identify possible methods for disrupting niche regulation of GSCs. HIF2α is an interesting GSC selective target, and we would be interested to test the effects of HIF2α inhibitory drugs such as TC-S7009 and PT2385 on GSC behaviors in PNJ scaffolds [234].

5.4.4. Preservation of Tumor Heterogeneity

A primary challenge in establishing patient-derived GBM cell lines is that cultured cells tend to converge rapidly on a single dominant genetic profile [98]. This loss of heterogeneity limits the capacity for recapitulating the genetic and phenotypic diversity of GBM cell types that are present in the original tumor tissue. In the work presented here, we demonstrated the ability to use PNJ scaffolds such that cells are segregated and unable to aggregate during culture. We therefore hypothesize that PNJ scaffold conditions may be useful for maintaining a heterogeneous mixture of tumor cell types during cell line establishment. These assays would be completed in conjunction with FACS sorting for GSC/GBM marker proteins and/or lineage tracing to determine how well different cell types are maintained. Although GSC cultures currently provide the best *in vitro* model for maintaining key features of the original tumor, there is

nonetheless always loss of heterogeneity that may be important for drug testing in the development of next generation personalized medicine strategies.

REFERENCES

[1] J.M. Heffernan, D.J. Overstreet, S. Srinivasan, L.D. Le, B.L. Vernon, R.W. Sirianni, Temperature responsive hydrogels enable transient three-dimensional tumor cultures via rapid cell recovery, J. Biomed. Mater. Res. A. 104 (2016) 17–25. doi:10.1002/jbm.a.35534.

[2] J.M. Heffernan, J.B. McNamara, S. Borwege, B.L. Vernon, N. Sanai, S. Mehta, R.W. Sirianni, PNIPAAm-co-Jeffamine® (PNJ) scaffolds as in vitro models for niche enrichment of Glioblastoma stem-like cells, Biomaterials. (2017). doi:10.1016/j.biomaterials.2017.05.007.

[3] Q.T. Ostrom, H. Gittleman, J. Xu, C. Kromer, Y. Wolinsky, C. Kruchko, J.S. Barnholtz-Sloan, CBTRUS Statistical Report: Primary Brain and Other Central Nervous System Tumors Diagnosed in the United States in 2009–2013, Neuro-Oncol. 18 (2016) v1–v75. doi:10.1093/neuonc/now207.

[4] R. Stupp, M.E. Hegi, W.P. Mason, M.J. van den Bent, M.J. Taphoorn, R.C. Janzer, S.K. Ludwin, A. Allgeier, B. Fisher, K. Belanger, P. Hau, A.A. Brandes, J. Gijtenbeek, C. Marosi, C.J. Vecht, K. Mokhtari, P. Wesseling, S. Villa, E. Eisenhauer, T. Gorlia, M. Weller, D. Lacombe, J.G. Cairncross, R.-O. Mirimanoff, Effects of radiotherapy with concomitant and adjuvant temozolomide versus radiotherapy alone on survival in glioblastoma in a randomised phase III study: 5-year analysis of the EORTC-NCIC trial, Lancet Oncol. 10 (2009) 459–466. doi:10.1016/S1470-2045(09)70025-7.

[5] Omuro A, DeAngelis LM, Glioblastoma and other malignant gliomas: A clinical review, JAMA. 310 (2013) 1842–1850. doi:10.1001/jama.2013.280319.

[6] N. Sanai, M.-Y. Polley, M.W. McDermott, A.T. Parsa, M.S. Berger, An extent of resection threshold for newly diagnosed glioblastomas, J. Neurosurg. 115 (2011) 3–8. doi:10.3171/2011.2.JNS10998.

[7] A. Giese, M.E. Berens, M. Westphal, Cost of Migration: Invasion of Malignant Gliomas and Implications for Treatment, J. Clin. Oncol. 21 (2003) 1624–1636. doi:10.1200/JCO.2003.05.063.

[8] K. Petrecca, M.-C. Guiot, V. Panet-Raymond, L. Souhami, Failure pattern following complete resection plus radiotherapy and temozolomide is at the resection margin in patients with glioblastoma, J. Neurooncol. 111 (2012) 19–23. doi:10.1007/s11060-012-0983-4.

[9] A. Giese, M. Westphal, Glioma invasion in the central nervous system, Neurosurgery. 39 (1996) 235–252.

[10] Y. Matsukado, C.S. MacCarty, J.W. Kernohan, The Growth of Glioblastoma Multiforme (Astrocytomas, Grades 3 and 4) in Neurosurgical Practice, J. Neurosurg. 18 (1961) 636–644. doi:10.3171/jns.1961.18.5.0636.

[11] R.G.W. Verhaak, K.A. Hoadley, E. Purdom, V. Wang, Y. Qi, M.D. Wilkerson, C.R. Miller, L. Ding, T. Golub, J.P. Mesirov, G. Alexe, M. Lawrence, M. O'Kelly, P.

Tamayo, B.A. Weir, S. Gabriel, W. Winckler, S. Gupta, L. Jakkula, H.S. Feiler, J.G. Hodgson, C.D. James, J.N. Sarkaria, C. Brennan, A. Kahn, P.T. Spellman, R.K. Wilson, T.P. Speed, J.W. Gray, M. Meyerson, G. Getz, C.M. Perou, D.N. Hayes, Integrated Genomic Analysis Identifies Clinically Relevant Subtypes of Glioblastoma Characterized by Abnormalities in PDGFRA, IDH1, EGFR, and NF1, Cancer Cell. 17 (2010) 98–110. doi:10.1016/j.ccr.2009.12.020.

[12] A. Sottoriva, I. Spiteri, S.G.M. Piccirillo, A. Touloumis, V.P. Collins, J.C. Marioni, C. Curtis, C. Watts, S. Tavaré, Intratumor heterogeneity in human glioblastoma reflects cancer evolutionary dynamics, Proc. Natl. Acad. Sci. 110 (2013) 4009–4014. doi:10.1073/pnas.1219747110.

[13] R. Bonavia, M.-M. Inda, W.K. Cavenee, F.B. Furnari, Heterogeneity Maintenance in Glioblastoma: A Social Network, Cancer Res. 71 (2011) 4055–4060. doi:10.1158/0008-5472.CAN-11-0153.

[14] A. Rape, B. Ananthanarayanan, S. Kumar, Engineering strategies to mimic the glioblastoma microenvironment, Adv. Drug Deliv. Rev. (2014). doi:10.1016/j.addr.2014.08.012.

[15] A.C. Bellail, S.B. Hunter, D.J. Brat, C. Tan, E.G. Van Meir, Microregional extracellular matrix heterogeneity in brain modulates glioma cell invasion, Int. J. Biochem. Cell Biol. 36 (2004) 1046–1069. doi:10.1016/j.biocel.2004.01.013.

[16] A. Ariza, D. López, J.L. Mate, M. Isamat, E. Musulen, M. Pujol, A. Ley, J. Navas-palacios, Role of CD44 in the invasiveness of glioblastoma multiforme and the noninvasiveness of meningioma: an immunohistochemistry study, Hum. Pathol. 26 (1995) 1144–1147.

[17] Y. Akiyama, S. Jung, B. Salhia, S. Lee, S. Hubbard, M. Taylor, T. Mainprize, K. Akaishi, W. van Furth, J.T. Rutka, Hyaluronate receptors mediating glioma cell migration and proliferation, J. Neurooncol. 53 (2001) 115–127.

[18] A. Merzak, S. Koocheckpour, G.J. Pilkington, CD44 mediates human glioma cell adhesion and invasion in vitro, Cancer Res. 54 (1994) 3988–3992.

[19] B. Delpech, C. Maingonnat, N. Girard, C. Chauzy, A. Olivier, R. Maunoury, J. Tayot, P. Creissard, Hyaluronan and hyaluronectin in the extracellular matrix of human brain tumour stroma, Eur. J. Cancer. 29 (1993) 1012–1017.

[20] S. Sarkar, R.K. Nuttall, S. Liu, D.R. Edwards, V.W. Yong, Tenascin-C stimulates glioma cell invasion through matrix metalloproteinase-12, Cancer Res. 66 (2006) 11771–11780.

[21] J.D. Lathia, M. Li, P.E. Hall, J. Gallagher, J.S. Hale, Q. Wu, M. Venere, E. Levy, M.R.S. Rani, P. Huang, E. Bae, J. Selfridge, L. Cheng, H. Guvenc, R.E. McLendon, I. Nakano, A.E. Sloan, H.S. Phillips, A. Lai, C.L. Gladson, M. Bredel, S. Bao, A.B. Hjelmeland, J.N. Rich, Laminin alpha 2 enables glioblastoma stem cell growth, Ann. Neurol. 72 (2012) 766–778. doi:10.1002/ana.23674.

[22] M. Wiranowska, M.V. Rojiani, Extracellular matrix microenvironment in glioma progression, INTECH Open Access Publisher, 2011. https://cdn.intechopen.com/pdfs-wm/22475.pdf.

[23] V. Umesh, A.D. Rape, T.A. Ulrich, S. Kumar, Microenvironmental Stiffness Enhances Glioma Cell Proliferation by Stimulating Epidermal Growth Factor Receptor Signaling, PLOS ONE. 9 (2014) e101771. doi:10.1371/journal.pone.0101771.

[24] B. Ananthanarayanan, Y. Kim, S. Kumar, Elucidating the mechanobiology of malignant brain tumors using a brain matrix-mimetic hyaluronic acid hydrogel platform, Biomaterials. 32 (2011) 7913–7923. doi:10.1016/j.biomaterials.2011.07.005.

[25] Y. Kim, S. Kumar, CD44-mediated Adhesion to Hyaluronic Acid Contributes to Mechanosensing and Invasive Motility, Mol. Cancer Res. MCR. 12 (2014) 1416–1429. doi:10.1158/1541-7786.MCR-13-0629.

[26] A. Pathak, S. Kumar, Independent regulation of tumor cell migration by matrix stiffness and confinement, Proc. Natl. Acad. Sci. 109 (2012) 10334–10339.

[27] J. Heffernan, D. Overstreet, L. Le, B. Vernon, R. Sirianni, Bioengineered Scaffolds for 3D Analysis of Glioblastoma Proliferation and Invasion, Ann. Biomed. Eng. (2014) 1–13. doi:10.1007/s10439-014-1223-1.

[28] S. Pedron, B.A.C. Harley, Impact of the biophysical features of a 3D gelatin microenvironment on glioblastoma malignancy, J. Biomed. Mater. Res. A. 101 (2013) 3404–3415. doi:10.1002/jbm.a.34637.

[29] J.D. Lathia, J. Gallagher, J.M. Heddleston, J. Wang, C.E. Eyler, J. MacSwords, Q. Wu, A. Vasanji, R.E. McLendon, A.B. Hjelmeland, J.N. Rich, Integrin Alpha 6 Regulates Glioblastoma Stem Cells, Cell Stem Cell. 6 (2010) 421–432. doi:10.1016/j.stem.2010.02.018.

[30] T.L. Haas, M.R. Sciuto, L. Brunetto, C. Valvo, M. Signore, M.E. Fiori, S. di Martino, S. Giannetti, L. Morgante, A. Boe, M. Patrizii, U. Warnken, M. Schnölzer, A. Ciolfi, C. Di Stefano, M. Biffoni, L. Ricci-Vitiani, R. Pallini, R. De Maria, Integrin α7 Is a Functional Marker and Potential Therapeutic Target in Glioblastoma, Cell Stem Cell. 21 (2017) 35–50.e9. doi:10.1016/j.stem.2017.04.009.

[31] M. Paolillo, M. Serra, S. Schinelli, Integrins in glioblastoma: Still an attractive target?, Pharmacol. Res. 113 (2016) 55–61. doi:10.1016/j.phrs.2016.08.004.

[32] P. Ruiz-Ontañon, J.L. Orgaz, B. Aldaz, A. Elosegui-Artola, J. Martino, M.T. Berciano, J.A. Montero, L. Grande, L. Nogueira, S. Diaz-Moralli, A. Esparís-Ogando, A. Vazquez-Barquero, M. Lafarga, A. Pandiella, M. Cascante, V. Segura, J.A. Martinez-Climent, V. Sanz-Moreno, J.L. Fernandez-Luna, Cellular Plasticity Confers Migratory and Invasive Advantages to a Population of Glioblastoma-Initiating Cells that Infiltrate Peritumoral Tissue, STEM CELLS. 31 (2013) 1075–1085. doi:10.1002/stem.1349.

[33] N.A. Charles, E.C. Holland, R. Gilbertson, R. Glass, H. Kettenmann, The brain tumor microenvironment, Glia. 59 (2011) 1169–1180. doi:10.1002/glia.21136.

[34] M. Wiranowska, A. Plaas, Cytokines and Extracellular Matrix Remodeling in the Central Nervous System, in: NeuroImmune Biol., Elsevier, 2008: pp. 167–197. doi:10.1016/S1567-7443(07)10009-0.

[35] Y. Soda, C. Myskiw, A. Rommel, I.M. Verma, Mechanisms of Neovascularization and Resistance to Anti-angiogenic Therapies in Glioblastoma Multiforme, J. Mol. Med. Berl. Ger. 91 (2013) 439–448. doi:10.1007/s00109-013-1019-z.

[36] L. Holmquist-Mengelbier, E. Fredlund, T. Löfstedt, R. Noguera, S. Navarro, H. Nilsson, A. Pietras, J. Vallon-Christersson, Å. Borg, K. Gradin, L. Poellinger, S. Påhlman, Recruitment of HIF-1α and HIF-2α to common target genes is differentially regulated in neuroblastoma: HIF-2α promotes an aggressive phenotype, Cancer Cell. 10 (2006) 413–423. doi:10.1016/j.ccr.2006.08.026.

[37] T.N. Ignatova, V.G. Kukekov, E.D. Laywell, O.N. Suslov, F.D. Vrionis, D.A. Steindler, Human cortical glial tumors contain neural stem-like cells expressing astroglial and neuronal markers in vitro, Glia. 39 (2002) 193–206. doi:10.1002/glia.10094.

[38] S.K. Singh, I.D. Clarke, M. Terasaki, V.E. Bonn, C. Hawkins, J. Squire, P.B. Dirks, Identification of a Cancer Stem Cell in Human Brain Tumors, Cancer Res. 63 (2003) 5821–5828.

[39] S. Singh, C. Hawkins, I. Clarke, J. Squire, J. Bayani, T. Hide, M. Henkelman, M. Cusimano, P. Dirks, Identification of human brain tumour initiating cells, Nature. 432 (2004) 393–396. doi:10.1038/nature03031.

[40] R. Galli, E. Binda, U. Orfanelli, B. Cipelletti, A. Gritti, S.D. Vitis, R. Fiocco, C. Foroni, F. Dimeco, A. Vescovi, Isolation and Characterization of Tumorigenic, Stem-like Neural Precursors from Human Glioblastoma, Cancer Res. 64 (2004) 7011–7021. doi:10.1158/0008-5472.CAN-04-1364.

[41] M. Venere, H.A. Fine, P.B. Dirks, J.N. Rich, Cancer stem cells in gliomas: Identifying and understanding the apex cell in cancer's hierarchy, Glia. 59 (2011) 1148–1154. doi:10.1002/glia.21185.

[42] B.T. Tan, C.Y. Park, L.E. Ailles, I.L. Weissman, The cancer stem cell hypothesis: a work in progress, Lab. Invest. 86 (2006) 1203–1207. doi:10.1038/labinvest.3700488.

[43] N. Sanai, A. Alvarez-Buylla, M.S. Berger, Neural Stem Cells and the Origin of Gliomas, N. Engl. J. Med. 353 (2005) 811–822. doi:10.1056/NEJMra043666.

[44] J. Lee, S. Kotliarova, Y. Kotliarov, A. Li, Q. Su, N.M. Donin, S. Pastorino, B.W. Purow, N. Christopher, W. Zhang, J.K. Park, H.A. Fine, Tumor stem cells derived from glioblastomas cultured in bFGF and EGF more closely mirror the phenotype and genotype of primary tumors than do serum-cultured cell lines, Cancer Cell. 9 (2006) 391–403. doi:10.1016/j.ccr.2006.03.030.

[45] K.L. Ligon, E. Huillard, S. Mehta, S. Kesari, H. Liu, J.A. Alberta, R.M. Bachoo, M. Kane, D.N. Louis, R.A. DePinho, D.J. Anderson, C.D. Stiles, D.H. Rowitch, Olig2-Regulated Lineage-Restricted Pathway Controls Replication Competence in Neural Stem Cells and Malignant Glioma, Neuron. 53 (2007) 503–517. doi:10.1016/j.neuron.2007.01.009.

[46] M.J. Son, K. Woolard, D.-H. Nam, J. Lee, H.A. Fine, SSEA-1 Is an Enrichment Marker for Tumor-Initiating Cells in Human Glioblastoma, Cell Stem Cell. 4 (2009) 440–452. doi:10.1016/j.stem.2009.03.003.

[47] J.D. Lathia, S.C. Mack, E.E. Mulkearns-Hubert, C.L.L. Valentim, J.N. Rich, Cancer stem cells in glioblastoma, Genes Dev. 29 (2015) 1203–1217. doi:10.1101/gad.261982.115.

[48] L. Ricci-Vitiani, R. Pallini, M. Biffoni, M. Todaro, G. Invernici, T. Cenci, G. Maira, E.A. Parati, G. Stassi, L.M. Larocca, R. De Maria, Tumour vascularization via endothelial differentiation of glioblastoma stem-like cells, Nature. 468 (2010) 824–828. doi:10.1038/nature09557.

[49] R. Wang, K. Chadalavada, J. Wilshire, U. Kowalik, K.E. Hovinga, A. Geber, B. Fligelman, M. Leversha, C. Brennan, V. Tabar, Glioblastoma stem-like cells give rise to tumour endothelium, Nature. 468 (2010) 829–833. doi:10.1038/nature09624.

[50] L. Cheng, Z. Huang, W. Zhou, Q. Wu, S. Donnola, J.K. Liu, X. Fang, A.E. Sloan, Y. Mao, J.D. Lathia, W. Min, R.E. McLendon, J.N. Rich, S. Bao, Glioblastoma Stem Cells Generate Vascular Pericytes to Support Vessel Function and Tumor Growth, Cell. 153 (2013) 139–152. doi:10.1016/j.cell.2013.02.021.

[51] J.D. Lathia, J.M. Heddleston, M. Venere, J.N. Rich, Deadly Teamwork: Neural Cancer Stem Cells and the Tumor Microenvironment, Cell Stem Cell. 8 (2011) 482–485. doi:10.1016/j.stem.2011.04.013.

[52] L.P. Deleyrolle, A. Harding, K. Cato, F.A. Siebzehnrubl, M. Rahman, H. Azari, S. Olson, B. Gabrielli, G. Osborne, A. Vescovi, B.A. Reynolds, Evidence for label-retaining tumour-initiating cells in human glioblastoma, Brain. 134 (2011) 1331–1343. doi:10.1093/brain/awr081.

[53] L. Zeng, Y. Zhao, T. Ouyang, T. Zhao, S. Zhang, J. Chen, J. Yu, T. Lei, Label-retaining assay enriches tumor-initiating cells in glioblastoma spheres cultivated in serum-free medium, Oncol. Lett. 12 (2016) 815–824. doi:10.3892/ol.2016.4690.

[54] L. Cheng, Q. Wu, O.A. Guryanova, Z. Huang, Q. Huang, J.N. Rich, S. Bao, Elevated invasive potential of glioblastoma stem cells, Biochem. Biophys. Res. Commun. 406 (2011) 643–648. doi:10.1016/j.bbrc.2011.02.123.

[55] J. Chen, Y. Li, T.-S. Yu, R.M. McKay, D.K. Burns, S.G. Kernie, L.F. Parada, A restricted cell population propagates glioblastoma growth after chemotherapy, Nature. 488 (2012) 522–526. doi:10.1038/nature11287.

[56] S. Bao, Q. Wu, R.E. McLendon, Y. Hao, Q. Shi, A.B. Hjelmeland, M.W. Dewhirst, D.D. Bigner, J.N. Rich, Glioma stem cells promote radioresistance by preferential

activation of the DNA damage response, Nature. 444 (2006) 756–760. doi:10.1038/nature05236.

[57] G. Liu, X. Yuan, Z. Zeng, P. Tunici, H. Ng, I.R. Abdulkadir, L. Lu, D. Irvin, K.L. Black, J.S. Yu, Analysis of gene expression and chemoresistance of CD133+ cancer stem cells in glioblastoma, Mol. Cancer. 5 (2006) 67. doi:10.1186/1476-4598-5-67.

[58] T. Strojnik, G.V. Røsland, P.O. Sakariassen, R. Kavalar, T. Lah, Neural stem cell markers, nestin and musashi proteins, in the progression of human glioma: correlation of nestin with prognosis of patient survival, Surg. Neurol. 68 (2007) 133–143. doi:10.1016/j.surneu.2006.10.050.

[59] A.-M. Bleau, D. Hambardzumyan, T. Ozawa, E.I. Fomchenko, J.T. Huse, C.W. Brennan, E.C. Holland, PTEN/PI3K/Akt Pathway Regulates the Side Population Phenotype and ABCG2 Activity in Glioma Tumor Stem-like Cells, Cell Stem Cell. 4 (2009) 226–235. doi:10.1016/j.stem.2009.01.007.

[60] R.J. Gilbertson, J.N. Rich, Making a tumour's bed: glioblastoma stem cells and the vascular niche, Nat. Rev. Cancer. 7 (2007) 733–736.

[61] J.N. Rich, Cancer Stem Cells in Radiation Resistance, Cancer Res. 67 (2007) 8980–8984. doi:10.1158/0008-5472.CAN-07-0895.

[62] M. Mannino, A.J. Chalmers, Radioresistance of glioma stem cells: Intrinsic characteristic or property of the 'microenvironment-stem cell unit'?, Mol. Oncol. 5 (2011) 374–386. doi:10.1016/j.molonc.2011.05.001.

[63] M. Jamal, B.H. Rath, P.S. Tsang, K. Camphausen, P.J. Tofilon, The Brain Microenvironment Preferentially Enhances the Radioresistance of CD133+ Glioblastoma Stem-like Cells, Neoplasia N. Y. N. 14 (2012) 150.

[64] M. Jamal, B.H. Rath, E.S. Williams, K. Camphausen, P.J. Tofilon, Microenvironmental regulation of glioblastoma radioresponse, Clin. Cancer Res. (2010) clincanres.2435.2010. doi:10.1158/1078-0432.CCR-10-2435.

[65] C. Calabrese, H. Poppleton, M. Kocak, T.L. Hogg, C. Fuller, B. Hamner, E.Y. Oh, M.W. Gaber, D. Finklestein, M. Allen, A. Frank, I.T. Bayazitov, S.S. Zakharenko, A. Gajjar, A. Davidoff, R.J. Gilbertson, A Perivascular Niche for Brain Tumor Stem Cells, Cancer Cell. 11 (2007) 69–82. doi:10.1016/j.ccr.2006.11.020.

[66] S. Bao, Q. Wu, S. Sathornsumetee, Y. Hao, Z. Li, A.B. Hjelmeland, Q. Shi, R.E. McLendon, D.D. Bigner, J.N. Rich, Stem Cell–like Glioma Cells Promote Tumor Angiogenesis through Vascular Endothelial Growth Factor, Cancer Res. 66 (2006) 7843–7848. doi:10.1158/0008-5472.CAN-06-1010.

[67] C. Folkins, Y. Shaked, S. Man, T. Tang, C.R. Lee, Z. Zhu, R.M. Hoffman, R.S. Kerbel, Glioma Tumor Stem-Like Cells Promote Tumor Angiogenesis and Vasculogenesis via Vascular Endothelial Growth Factor and Stromal-Derived Factor 1, Cancer Res. 69 (2009) 7243–7251. doi:10.1158/0008-5472.CAN-09-0167.

[68] N. Charles, T. Ozawa, M. Squatrito, A.-M. Bleau, C.W. Brennan, D. Hambardzumyan, E.C. Holland, Perivascular Nitric Oxide Activates Notch Signaling and Promotes Stem-like Character in PDGF-Induced Glioma Cells, Cell Stem Cell. 6 (2010) 141–152. doi:10.1016/j.stem.2010.01.001.

[69] E.M. Galan-Moya, A.L. Guelte, E. Lima-Fernandes, C. Thirant, J. Dwyer, N. Bidere, P.-O. Couraud, M.G.H. Scott, M.-P. Junier, H. Chneiweiss, J. Gavard, Secreted factors from brain endothelial cells maintain glioblastoma stem-like cell expansion through the mTOR pathway, EMBO Rep. 12 (2011) 470–476. doi:10.1038/embor.2011.39.

[70] K.E. Hovinga, F. Shimizu, R. Wang, G. Panagiotakos, M. Van Der Heijden, H. Moayedpardazi, A.S. Correia, D. Soulet, T. Major, J. Menon, V. Tabar, Inhibition of Notch Signaling in Glioblastoma Targets Cancer Stem Cells via an Endothelial Cell Intermediate, STEM CELLS. 28 (2010) 1019–1029. doi:10.1002/stem.429.

[71] D.L. Schonberg, D. Lubelski, T.E. Miller, J.N. Rich, Brain tumor stem cells: molecular characteristics and their impact on therapy, Mol. Aspects Med. 0 (2014) 82–101. doi:10.1016/j.mam.2013.06.004.

[72] Z. Li, S. Bao, Q. Wu, H. Wang, C. Eyler, S. Sathornsumetee, Q. Shi, Y. Cao, J. Lathia, R.E. McLendon, A.B. Hjelmeland, J.N. Rich, Hypoxia-Inducible Factors Regulate Tumorigenic Capacity of Glioma Stem Cells, Cancer Cell. 15 (2009) 501–513. doi:10.1016/j.ccr.2009.03.018.

[73] J.M. Heddleston, Z. Li, J.D. Lathia, S. Bao, A.B. Hjelmeland, J.N. Rich, Hypoxia inducible factors in cancer stem cells, Br. J. Cancer. 102 (2010) 789–795. doi:10.1038/sj.bjc.6605551.

[74] J.M. Heddleston, Z. Li, R.E. McLendon, A.B. Hjelmeland, J.N. Rich, The hypoxic microenvironment maintains glioblastoma stem cells and promotes reprogramming towards a cancer stem cell phenotype, Cell Cycle. 8 (2009) 3274–3284. doi:10.4161/cc.8.20.9701.

[75] S. Seidel, B.K. Garvalov, V. Wirta, L. von Stechow, A. Schänzer, K. Meletis, M. Wolter, D. Sommerlad, A.-T. Henze, M. Nistér, G. Reifenberger, J. Lundeberg, J. Frisén, T. Acker, A hypoxic niche regulates glioblastoma stem cells through hypoxia inducible factor 2α, Brain. 133 (2010) 983–995. doi:10.1093/brain/awq042.

[76] A. Soeda, M. Park, D. Lee, A. Mintz, A. Androutsellis-Theotokis, R.D. McKay, J. Engh, T. Iwama, T. Kunisada, A.B. Kassam, others, Hypoxia promotes expansion of the CD133-positive glioma stem cells through activation of HIF-1α, Oncogene. 28 (2009) 3949–3959.

[77] E.E. Bar, A. Lin, V. Mahairaki, W. Matsui, C.G. Eberhart, Hypoxia Increases the Expression of Stem-Cell Markers and Promotes Clonogenicity in Glioblastoma Neurospheres, Am. J. Pathol. 177 (2010) 1491–1502. doi:10.2353/ajpath.2010.091021.

[78] B. Keith, R.S. Johnson, M.C. Simon, HIF1α and HIF2α: sibling rivalry in hypoxic tumor growth and progression, Nat. Rev. Cancer. 12 (2011) 9–22. doi:10.1038/nrc3183.

[79] A.B. Hjelmeland, Q. Wu, J.M. Heddleston, G.S. Choudhary, J. MacSwords, J.D. Lathia, R. McLendon, D. Lindner, A. Sloan, J.N. Rich, Acidic stress promotes a glioma stem cell phenotype, Cell Death Differ. 18 (2011) 829–840. doi:10.1038/cdd.2010.150.

[80] T. Ishiwata, K. Teduka, T. Yamamoto, K. Kawahara, Y. Matsuda, Z. Naito, Neuroepithelial stem cell marker nestin regulates the migration, invasion and growth of human gliomas, Oncol. Rep. 26 (2011) 91–99.

[81] R. Kitai, R. Horita, K. Sato, K. Yoshida, H. Arishima, Y. Higashino, N. Hashimoto, H. Takeuchi, T. Kubota, K.-I. Kikuta, Nestin expression in astrocytic tumors delineates tumor infiltration, Brain Tumor Pathol. 27 (2010) 17–21. doi:10.1007/s10014-009-0261-0.

[82] B. Ortensi, M. Setti, D. Osti, G. Pelicci, Cancer stem cell contribution to glioblastoma invasiveness, Stem Cell Res. Ther. 4 (2013) 18. doi:10.1186/scrt166.

[83] D. Hambardzumyan, O.J. Becher, M.K. Rosenblum, P.P. Pandolfi, K. Manova-Todorova, E.C. Holland, PI3K pathway regulates survival of cancer stem cells residing in the perivascular niche following radiation in medulloblastoma in vivo, Genes Dev. 22 (2008) 436–448. doi:10.1101/gad.1627008.

[84] K.B. Kang, C. Zhu, Y.L. Wong, Q. Gao, A. Ty, M.C. Wong, Gefitinib radiosensitizes stem-like glioma cells: inhibition of epidermal growth factor receptor-Akt-DNA-PK signaling, accompanied by inhibition of DNA double-strand break repair, Int. J. Radiat. Oncol. Biol. Phys. 83 (2012) e43-52. doi:10.1016/j.ijrobp.2011.11.037.

[85] P. Knizetova, J. Ehrmann, A. Hlobilkova, I. Vancova, O. Kalita, Z. Kolar, J. Bartek, Autocrine regulation of glioblastoma cell cycle progression, viability and radioresistance through the VEGF-VEGFR2 (KDR) interplay, Cell Cycle Georget. Tex. 7 (2008) 2553–2561. doi:10.4161/cc.7.16.6442.

[86] J. Wang, T.P. Wakeman, J.D. Lathia, A.B. Hjelmeland, X.-F. Wang, R.R. White, J.N. Rich, B.A. Sullenger, Notch Promotes Radioresistance of Glioma Stem Cells, STEM CELLS. 28 (2010) 17–28. doi:10.1002/stem.261.

[87] L. Harrison, K. Blackwell, Hypoxia and Anemia: Factors in Decreased Sensitivity to Radiation Therapy and Chemotherapy?, The Oncologist. 9 (2004) 31–40. doi:10.1634/theoncologist.9-90005-31.

[88] R.S. Bhatt, D.M. Landis, M. Zimmer, J. Torregrossa, S. Chen, V.P. Sukhatme, O. Iliopoulos, S. Balk, G.J. Bubley, Hypoxia-inducible factor-2α: effect on radiation sensitivity and differential regulation by an mTOR inhibitor, BJU Int. 102 (2008) 358–363. doi:10.1111/j.1464-410X.2008.07558.x.

[89] J.A. Bertout, A.J. Majmundar, J.D. Gordan, J.C. Lam, D. Ditsworth, B. Keith, E.J. Brown, K.L. Nathanson, M.C. Simon, HIF2α inhibition promotes p53 pathway

activity, tumor cell death, and radiation responses, Proc. Natl. Acad. Sci. 106 (2009) 14391–14396. doi:10.1073/pnas.0907357106.

[90] F. Pistollato, S. Abbadi, E. Rampazzo, L. Persano, A. Della Puppa, C. Frasson, E. Sarto, R. Scienza, D. D'avella, G. Basso, Intratumoral Hypoxic Gradient Drives Stem Cells Distribution and MGMT Expression in Glioblastoma, STEM CELLS. 28 (2010) 851–862. doi:10.1002/stem.415.

[91] M. Pàez-Ribes, E. Allen, J. Hudock, T. Takeda, H. Okuyama, F. Viñals, M. Inoue, G. Bergers, D. Hanahan, O. Casanovas, Antiangiogenic Therapy Elicits Malignant Progression of Tumors to Increased Local Invasion and Distant Metastasis, Cancer Cell. 15 (2009) 220–231. doi:10.1016/j.ccr.2009.01.027.

[92] O. Keunen, M. Johansson, A. Oudin, M. Sanzey, S.A.A. Rahim, F. Fack, F. Thorsen, T. Taxt, M. Bartos, R. Jirik, H. Miletic, J. Wang, D. Stieber, L. Stuhr, I. Moen, C.B. Rygh, R. Bjerkvig, S.P. Niclou, Anti-VEGF treatment reduces blood supply and increases tumor cell invasion in glioblastoma, Proc. Natl. Acad. Sci. 108 (2011) 3749–3754. doi:10.1073/pnas.1014480108.

[93] T.N. Kreisl, L. Kim, K. Moore, P. Duic, C. Royce, I. Stroud, N. Garren, M. Mackey, J.A. Butman, K. Camphausen, J. Park, P.S. Albert, H.A. Fine, Phase II Trial of Single-Agent Bevacizumab Followed by Bevacizumab Plus Irinotecan at Tumor Progression in Recurrent Glioblastoma, J. Clin. Oncol. 27 (2008) 740–745. doi:10.1200/JCO.2008.16.3055.

[94] J. Ponten, E. Macintyre, Long term culture of normal and neoplastic human glia, Acta Pathol. Microbiol. Scand. 74 (1968) 465–486.

[95] K. Woolard, H.A. Fine, Glioma Stem Cells: Better Flat Than Round, Cell Stem Cell. 4 (2009) 466–467. doi:10.1016/j.stem.2009.05.013.

[96] A. Giese, M.A. Loo, M.D. Rief, N. Tran, M.E. Berens, Substrates for astrocytoma invasion, Neurosurgery. 37 (1995) 294-301; discussion 301-302.

[97] S.M. Pollard, K. Yoshikawa, I.D. Clarke, D. Danovi, S. Stricker, R. Russell, J. Bayani, R. Head, M. Lee, M. Bernstein, J.A. Squire, A. Smith, P. Dirks, Glioma Stem Cell Lines Expanded in Adherent Culture Have Tumor-Specific Phenotypes and Are Suitable for Chemical and Genetic Screens, Cell Stem Cell. 4 (2009) 568–580. doi:10.1016/j.stem.2009.03.014.

[98] A. Li, J. Walling, Y. Kotliarov, A. Center, M.E. Steed, S.J. Ahn, M. Rosenblum, T. Mikkelsen, J.C. Zenklusen, H.A. Fine, Genomic Changes and Gene Expression Profiles Reveal That Established Glioma Cell Lines Are Poorly Representative of Primary Human Gliomas, Mol. Cancer Res. 6 (2008) 21–30. doi:10.1158/1541-7786.MCR-07-0280.

[99] M. Allen, M. Bjerke, H. Edlund, S. Nelander, B. Westermark, Origin of the U87MG glioma cell line: Good news and bad news, Sci. Transl. Med. 8 (2016) 354re3. doi:10.1126/scitranslmed.aaf6853.

[100] C. Venugopal, N.M. McFarlane, S. Nolte, B. Manoranjan, S.K. Singh, Processing of Primary Brain Tumor Tissue for Stem Cell Assays and Flow Sorting, J. Vis. Exp. (2012). doi:10.3791/4111.

[101] S. ZHANG, R. XIE, F. WAN, F. YE, D. GUO, T. LEI, Identification of U251 glioma stem cells and their heterogeneous stem-like phenotypes, Oncol. Lett. 6 (2013) 1649–1655. doi:10.3892/ol.2013.1623.

[102] B.H. Rath, J.M. Fair, M. Jamal, K. Camphausen, P.J. Tofilon, Astrocytes Enhance the Invasion Potential of Glioblastoma Stem-Like Cells, PLoS ONE. 8 (2013) e54752. doi:10.1371/journal.pone.0054752.

[103] B.H. Rath, A. Wahba, K. Camphausen, P.J. Tofilon, Coculture with astrocytes reduces the radiosensitivity of glioblastoma stem-like cells and identifies additional targets for radiosensitization, Cancer Med. 4 (2015) 1705–1716. doi:10.1002/cam4.510.

[104] D. Del Duca, T. Werbowetski, R.F. Del Maestro, Spheroid preparation from hanging drops: characterization of a model of brain tumor invasion, J. Neurooncol. 67 (2004) 295–303.

[105] F. Pampaloni, E.G. Reynaud, E.H.K. Stelzer, The third dimension bridges the gap between cell culture and live tissue, Nat. Rev. Mol. Cell Biol. 8 (2007) 839–845. doi:10.1038/nrm2236.

[106] T.M. Fael Al-Mayhani, S.L.R. Ball, J.-W. Zhao, J. Fawcett, K. Ichimura, P.V. Collins, C. Watts, An efficient method for derivation and propagation of glioblastoma cell lines that conserves the molecular profile of their original tumours, J. Neurosci. Methods. 176 (2009) 192–199. doi:10.1016/j.jneumeth.2008.07.022.

[107] Z. Chen, A. Htay, W.D. Santos, G.T. Gillies, H.L. Fillmore, M.M. Sholley, W.C. Broaddus, In vitro angiogenesis by human umbilical vein endothelial cells (HUVEC) induced by three-dimensional co-culture with glioblastoma cells, J. Neurooncol. 92 (2009) 121–128. doi:10.1007/s11060-008-9742-y.

[108] S.S. Rao, J.J. Lannutti, M.S. Viapiano, A. Sarkar, J.O. Winter, Toward 3D Biomimetic Models to Understand the Behavior of Glioblastoma Multiforme Cells, Tissue Eng. Part B Rev. (2013) 131030093023007. doi:10.1089/ten.teb.2013.0227.

[109] S.S. Jensen, M. Meyer, S.A. Petterson, B. Halle, A.M. Rosager, C. Aaberg-Jessen, M. Thomassen, M. Burton, T.A. Kruse, B.W. Kristensen, Establishment and Characterization of a Tumor Stem Cell-Based Glioblastoma Invasion Model, PloS One. 11 (2016) e0159746. doi:10.1371/journal.pone.0159746.

[110] P.C. Huszthy, I. Daphu, S.P. Niclou, D. Stieber, J.M. Nigro, P.Ø. Sakariassen, H. Miletic, F. Thorsen, R. Bjerkvig, In vivo models of primary brain tumors: pitfalls and perspectives, Neuro-Oncol. 14 (2012) 979–993. doi:10.1093/neuonc/nos135.

[111] V.L. Jacobs, P.A. Valdes, W.F. Hickey, J.A. De Leo, Current review of in vivo GBM rodent models: emphasis on the CNS-1 tumour model, ASN NEURO. 3 (2011) 171–181. doi:10.1042/AN20110014.

[112] J.A. Hubbell, Biomaterials in Tissue Engineering, Nat Biotech. 13 (1995) 565–576. doi:10.1038/nbt0695-565.

[113] N.K.L. Ma, J.K. Lim, M.F. Leong, E. Sandanaraj, B.T. Ang, C. Tang, A.C.A. Wan, Collaboration of 3D context and extracellular matrix in the development of glioma stemness in a 3D model, Biomaterials. 78 (2016) 62–73. doi:10.1016/j.biomaterials.2015.11.031.

[114] S.S. Rao, M.T. Nelson, R. Xue, J.K. DeJesus, M.S. Viapiano, J.J. Lannutti, A. Sarkar, J.O. Winter, Mimicking white matter tract topography using core–shell electrospun nanofibers to examine migration of malignant brain tumors, Biomaterials. 34 (2013) 5181–5190. doi:10.1016/j.biomaterials.2013.03.069.

[115] J. Cha, S.-G. Kang, P. Kim, Strategies of Mesenchymal Invasion of Patient-derived Brain Tumors: Microenvironmental Adaptation, Sci. Rep. 6 (2016). doi:10.1038/srep24912.

[116] C. Jiguet Jiglaire, N. Baeza-Kallee, E. Denicolaï, D. Barets, P. Metellus, L. Padovani, O. Chinot, D. Figarella-Branger, C. Fernandez, Ex vivo cultures of glioblastoma in three-dimensional hydrogel maintain the original tumor growth behavior and are suitable for preclinical drug and radiation sensitivity screening, Exp. Cell Res. 321 (2014) 99–108. doi:10.1016/j.yexcr.2013.12.010.

[117] A.D. Rape, M. Zibinsky, N. Murthy, S. Kumar, A synthetic hydrogel for the high-throughput study of cell-ECM interactions, Nat. Commun. 6 (2015). doi:10.1038/ncomms9129.

[118] A.D. Rape, S. Kumar, A composite hydrogel platform for the dissection of tumor cell migration at tissue interfaces, Biomaterials. (2014). doi:10.1016/j.biomaterials.2014.07.003.

[119] C. E. Hoyle, A. B. Lowe, C. N. Bowman, Thiol -click chemistry: a multifaceted toolbox for small molecule and polymer synthesis, Chem. Soc. Rev. 39 (2010) 1355–1387. doi:10.1039/B901979K.

[120] S. Pedron, E. Becka, B.A.C. Harley, Regulation of glioma cell phenotype in 3D matrices by hyaluronic acid, Biomaterials. 34 (2013) 7408–7417. doi:10.1016/j.biomaterials.2013.06.024.

[121] S. Pedron, E. Becka, B.A. Harley, Spatially Gradated Hydrogel Platform as a 3D Engineered Tumor Microenvironment, Adv. Mater. 27 (2015) 1567–1572. doi:10.1002/adma.201404896.

[122] S. Pedron, J.S. Hanselman, M.A. Schroeder, J.N. Sarkaria, B.A.C. Harley, Extracellular Hyaluronic Acid Influences the Efficacy of EGFR Tyrosine Kinase Inhibitors in a Biomaterial Model of Glioblastoma, Adv. Healthc. Mater. (2017) n/a-n/a. doi:10.1002/adhm.201700529.

[123] J.-W.E. Chen, S. Pedron, B.A.C. Harley, The Combined Influence of Hydrogel Stiffness and Matrix-Bound Hyaluronic Acid Content on Glioblastoma Invasion, Macromol. Biosci. (2017) n/a-n/a. doi:10.1002/mabi.201700018.

[124] M.T. Ngo, B.A. Harley, The Influence of Hyaluronic Acid and Glioblastoma Cell Coculture on the Formation of Endothelial Cell Networks in Gelatin Hydrogels, Adv. Healthc. Mater. (2017) n/a-n/a. doi:10.1002/adhm.201700687.

[125] I.M. El-Sherbiny, M.H. Yacoub, Hydrogel scaffolds for tissue engineering: Progress and challenges, Glob. Cardiol. Sci. Pract. 2013 (2013) 316–342. doi:10.5339/gcsp.2013.38.

[126] M. Herrera-Perez, S.L. Voytik-Harbin, J.L. Rickus, Extracellular Matrix Properties Regulate the Migratory Response of Glioblastoma Stem Cells in Three-Dimensional Culture, Tissue Eng. Part A. 21 (2015) 2572–2582. doi:10.1089/ten.tea.2014.0504.

[127] W. Xiao, A. Sohrabi, S.K. Seidlits, Integrating the glioblastoma microenvironment into engineered experimental models, Future Sci. OA. (2017) FSO189. doi:10.4155/fsoa-2016-0094.

[128] A.I. Teixeira, J.K. Duckworth, O. Hermanson, Getting the right stuff: Controlling neural stem cell state and fate in vivo and in vitro with biomaterials, Cell Res. Lond. 17 (2007) 56–61. doi:http://dx.doi.org.ezproxy1.lib.asu.edu/10.1038/sj.cr.7310141.

[129] K. Saha, A.J. Keung, E.F. Irwin, Y. Li, L. Little, D.V. Schaffer, K.E. Healy, Substrate Modulus Directs Neural Stem Cell Behavior, Biophys. J. 95 (2008) 4426–4438. doi:10.1529/biophysj.108.132217.

[130] Y. Soen, A. Mori, T.D. Palmer, P.O. Brown, Exploring the regulation of human neural precursor cell differentiation using arrays of signaling microenvironments, Mol. Syst. Biol. 2 (2006) 37. doi:10.1038/msb4100076.

[131] M. Nakajima, T. Ishimuro, K. Kato, I.-K. Ko, I. Hirata, Y. Arima, H. Iwata, Combinatorial protein display for the cell-based screening of biomaterials that direct neural stem cell differentiation, Biomaterials. 28 (2007) 1048–1060. doi:10.1016/j.biomaterials.2006.10.004.

[132] Q. Shen, S.K. Goderie, L. Jin, N. Karanth, Y. Sun, N. Abramova, P. Vincent, K. Pumiglia, S. Temple, Endothelial Cells Stimulate Self-Renewal and Expand Neurogenesis of Neural Stem Cells, Science. 304 (2004) 1338–1340. doi:10.1126/science.1095505.

[133] F. Yang, R. Murugan, S. Wang, S. Ramakrishna, Electrospinning of nano/micro scale poly(l-lactic acid) aligned fibers and their potential in neural tissue engineering, Biomaterials. 26 (2005) 2603–2610. doi:10.1016/j.biomaterials.2004.06.051.

[134] T.-Y. Cheng, M.-H. Chen, W.-H. Chang, M.-Y. Huang, T.-W. Wang, Neural stem cells encapsulated in a functionalized self-assembling peptide hydrogel for brain tissue engineering, Biomaterials. 34 (2013) 2005–2016. doi:10.1016/j.biomaterials.2012.11.043.

[135] C.P. Addington, J.M. Heffernan, C.S. Millar-Haskell, E.W. Tucker, R.W. Sirianni, S.E. Stabenfeldt, Enhancing neural stem cell response to SDF-1α gradients through hyaluronic acid-laminin hydrogels, Biomaterials. 72 (2015) 11–19. doi:10.1016/j.biomaterials.2015.08.041.

[136] C.P. Addington, S. Dharmawaj, J.M. Heffernan, R.W. Sirianni, S.E. Stabenfeldt, Hyaluronic acid-laminin hydrogels increase neural stem cell transplant retention and migratory response to SDF-1α, Matrix Biol. (2017). doi:10.1016/j.matbio.2016.09.007.

[137] A.R. Safa, M.R. Saadatzadeh, A.A. Cohen-Gadol, K.E. Pollok, K. Bijangi-Vishehsaraei, Glioblastoma stem cells (GSCs) epigenetic plasticity and interconversion between differentiated non-GSCs and GSCs, Genes Dis. 2 (2015) 152–163. doi:10.1016/j.gendis.2015.02.001.

[138] P. Dahan, J. Martinez Gala, C. Delmas, S. Monferran, L. Malric, D. Zentkowski, V. Lubrano, C. Toulas, E. Cohen-Jonathan Moyal, A. Lemarie, Ionizing radiations sustain glioblastoma cell dedifferentiation to a stem-like phenotype through survivin: possible involvement in radioresistance, Cell Death Dis. 5 (2014) e1543. doi:10.1038/cddis.2014.509.

[139] S.J. Florczyk, K. Wang, S. Jana, D.L. Wood, S.K. Sytsma, J.G. Sham, F.M. Kievit, M. Zhang, Porous chitosan-hyaluronic acid scaffolds as a mimic of glioblastoma microenvironment ECM, Biomaterials. 34 (2013) 10143–10150. doi:10.1016/j.biomaterials.2013.09.034.

[140] F.M. Kievit, S.J. Florczyk, M.C. Leung, K. Wang, J.D. Wu, J.R. Silber, R.G. Ellenbogen, J.S.H. Lee, M. Zhang, Proliferation and enrichment of CD133+ glioblastoma cancer stem cells on 3D chitosan-alginate scaffolds, Biomaterials. 35 (2014) 9137–9143. doi:10.1016/j.biomaterials.2014.07.037.

[141] F.M. Kievit, K. Wang, A.E. Erickson, S.K. Lan Levengood, R.G. Ellenbogen, M. Zhang, Modeling the tumor microenvironment using chitosan-alginate scaffolds to control the stem-like state of glioblastoma cells, Biomater Sci. (2016). doi:10.1039/C5BM00514K.

[142] S. J. Florczyk, F. M. Kievit, K. Wang, A. E. Erickson, R. G. Ellenbogen, M. Zhang, 3D porous chitosan–alginate scaffolds promote proliferation and enrichment of cancer stem-like cells, J. Mater. Chem. B. 4 (2016) 6326–6334. doi:10.1039/C6TB01713D.

[143] N.K.L. Ma, J.K. Lim, M.F. Leong, E. Sandanaraj, B.T. Ang, C. Tang, A.C.A. Wan, Collaboration of 3D Context and Extracellular Matrix in the Development of Glioma Stemness in a 3D Model, Biomaterials. (2016). doi:10.1016/j.biomaterials.2015.11.031.

[144] A. Bez, E. Corsini, D. Curti, M. Biggiogera, A. Colombo, R.F. Nicosia, S.F. Pagano, E.A. Parati, Neurosphere and neurosphere-forming cells: morphological and ultrastructural characterization, Brain Res. 993 (2003) 18–29. doi:10.1016/j.brainres.2003.08.061.

[145] D. Beier, J. Wischhusen, W. Dietmaier, P. Hau, M. Proescholdt, A. Brawanski, U. Bogdahn, C.P. Beier, CD133 Expression and Cancer Stem Cells Predict Prognosis in High-grade Oligodendroglial Tumors, Brain Pathol. 18 (2008) 370–377. doi:10.1111/j.1750-3639.2008.00130.x.

[146] M.-Y. Yang, M.-T. Chiao, H.-T. Lee, C.-M. Chen, Y.-C. Yang, C.-C. Shen, H.-I. Ma, An innovative three-dimensional gelatin foam culture system for improved study of glioblastoma stem cell behavior, J. Biomed. Mater. Res. B Appl. Biomater. (2014) n/a-n/a. doi:10.1002/jbm.b.33214.

[147] Y. Oh, J. Cha, S.-G. Kang, P. Kim, A polyethylene glycol-based hydrogel as macroporous scaffold for tumorsphere formation of glioblastoma multiforme, J. Ind. Eng. Chem. (2016). doi:10.1016/j.jiec.2016.05.012.

[148] Q. Li, H. Lin, O. Wang, X. Qiu, S. Kidambi, L.P. Deleyrolle, B.A. Reynolds, Y. Lei, Scalable Production of Glioblastoma Tumor-initiating Cells in 3 Dimension Thermoreversible Hydrogels, Sci. Rep. 6 (2016) 31915. doi:10.1038/srep31915.

[149] K. Wang, F.M. Kievit, A.E. Erickson, J.R. Silber, R.G. Ellenbogen, M. Zhang, Culture on 3D Chitosan-Hyaluronic Acid Scaffolds Enhances Stem Cell Marker Expression and Drug Resistance in Human Glioblastoma Cancer Stem Cells, Adv. Healthc. Mater. 5 (2016) 3173–3181. doi:10.1002/adhm.201600684.

[150] M.E. Berens, A. Giese, "...those left behind." Biology and Oncology of Invasive Glioma Cells, Neoplasia. 1 (1999) 208–219.

[151] Y. Chonan, S. Taki, O. Sampetrean, H. Saya, R. Sudo, Endothelium-induced three-dimensional invasion of heterogeneous glioma initiating cells in a microfluidic coculture platform, Integr. Biol. (2017). doi:10.1039/C7IB00091J.

[152] T.A. Ulrich, E.M. de Juan Pardo, S. Kumar, The Mechanical Rigidity of the Extracellular Matrix Regulates the Structure, Motility, and Proliferation of Glioma Cells, Cancer Res. 69 (2009) 4167–4174. doi:10.1158/0008-5472.CAN-08-4859.

[153] P.A. Netti, D.A. Berk, M.A. Swartz, A.J. Grodzinsky, R.K. Jain, Role of Extracellular Matrix Assembly in Interstitial Transport in Solid Tumors, Cancer Res. 60 (2000) 2497–2503.

[154] P.C. Georges, W.J. Miller, D.F. Meaney, E.S. Sawyer, P.A. Janmey, Matrices with Compliance Comparable to that of Brain Tissue Select Neuronal over Glial Growth in Mixed Cortical Cultures, Biophys. J. 90 (2006) 3012–3018. doi:10.1529/biophysj.105.073114.

[155] A. Buxboim, K. Rajagopal, A.E.X. Brown, D.E. Discher, How deeply cells feel: methods for thin gels, J. Phys. Condens. Matter. 22 (2010) 194116. doi:10.1088/0953-8984/22/19/194116.

[156] S.Y. Wong, T.A. Ulrich, L.P. Deleyrolle, J.L. MacKay, J.-M.G. Lin, R.T. Martuscello, M.A. Jundi, B.A. Reynolds, S. Kumar, Constitutive Activation of Myosin-Dependent Contractility Sensitizes Glioma Tumor-Initiating Cells to Mechanical Inputs and Reduces Tissue Invasion, Cancer Res. 75 (2015) 1113–1122. doi:10.1158/0008-5472.CAN-13-3426.

[157] T.J. Grundy, E. De Leon, K.R. Griffin, B.W. Stringer, B.W. Day, B. Fabry, J. Cooper-White, G.M. O'Neill, Differential response of patient-derived primary glioblastoma cells to environmental stiffness, Sci. Rep. 6 (2016) 23353. doi:10.1038/srep23353.

[158] G. Fernandez-Fuente, P. Mollinedo, L. Grande, A. Vazquez-Barquero, J.L. Fernandez-Luna, Culture Dimensionality Influences the Resistance of Glioblastoma Stem-like Cells to Multikinase Inhibitors, Mol. Cancer Ther. 13 (2014) 1664–1672. doi:10.1158/1535-7163.MCT-13-0854.

[159] C.G. Hubert, M. Rivera, L.C. Spangler, Q. Wu, S.C. Mack, B.C. Prager, M. Couce, R.E. McLendon, A.E. Sloan, J.N. Rich, A Three-Dimensional Organoid Culture System Derived from Human Glioblastomas Recapitulates the Hypoxic Gradients and Cancer Stem Cell Heterogeneity of Tumors Found In Vivo, Cancer Res. 76 (2016) 2465–2477. doi:10.1158/0008-5472.CAN-15-2402.

[160] S.S. Rao, J. DeJesus, A.R. Short, J.J. Otero, A. Sarkar, J.O. Winter, Glioblastoma Behaviors in Three-Dimensional Collagen-Hyaluronan Composite Hydrogels, ACS Appl. Mater. Interfaces. 5 (2013) 9276–9284. doi:10.1021/am402097j.

[161] S.G. Jin, Y.I. Jeong, S. Jung, H.H. Ryu, Y.H. Jin, I.Y. Kim, The effect of hyaluronic acid on the invasiveness of malignant glioma cells: comparison of invasion potential at hyaluronic acid hydrogel and matrigel, J. Korean Neurosurg. Soc. 46 (2009) 472–478.

[162] M. Tamaki, W. McDonald, V.R. Amberger, E. Moore, R.F. Del Maestro, Implantation of C6 astrocytoma spheroid into collagen type I gels: invasive, proliferative, and enzymatic characterizations, J. Neurosurg. 87 (1997) 602–609. doi:10.3171/jns.1997.87.4.0602.

[163] C. Wang, X. Tong, F. Yang, Bioengineered 3D Brain Tumor Model To Elucidate the Effects of Matrix Stiffness on Glioblastoma Cell Behavior Using PEG-Based Hydrogels, Mol. Pharm. 11 (2014) 2115–2125. doi:10.1021/mp5000828.

[164] Y. Yang, S. Motte, L.J. Kaufman, Pore size variable type I collagen gels and their interaction with glioma cells, Biomaterials. 31 (2010) 5678–5688. doi:10.1016/j.biomaterials.2010.03.039.

[165] T.A. Ulrich, A. Jain, K. Tanner, J.L. MacKay, S. Kumar, Probing cellular mechanobiology in three-dimensional culture with collagen-agarose matrices, Biomaterials. 31 (2010) 1875–1884. doi:10.1016/j.biomaterials.2009.10.047.

[166] I. Eke, K. Storch, I. Kästner, A. Vehlow, C. Faethe, W. Mueller-Klieser, G. Taucher-Scholz, A. Temme, G. Schackert, N. Cordes, Three-dimensional Invasion of Human Glioblastoma Cells Remains Unchanged by X-ray and Carbon Ion Irradiation In Vitro, Int. J. Radiat. Oncol. 84 (2012) e515–e523. doi:10.1016/j.ijrobp.2012.06.012.

[167] H.-D. Kim, T.W. Guo, A.P. Wu, A. Wells, F.B. Gertler, D.A. Lauffenburger, Epidermal Growth Factor–induced Enhancement of Glioblastoma Cell Migration in 3D Arises from an Intrinsic Increase in Speed But an Extrinsic Matrix- and Proteolysis-dependent Increase in Persistence, Mol. Biol. Cell. 19 (2008) 4249–4259. doi:10.1091/mbc.E08-05-0501.

[168] N. Cordes, B. Hansmeier, C. Beinke, V. Meineke, D. van Beuningen, Irradiation differentially affects substratum-dependent survival, adhesion, and invasion of

glioblastoma cell lines, Br. J. Cancer. 89 (2003) 2122–2132. doi:10.1038/sj.bjc.6601429.

[169] Y. Fan, D.T. Nguyen, Y. Akay, F. Xu, M. Akay, Engineering a Brain Cancer Chip for High-throughput Drug Screening, Sci. Rep. 6 (2016) 25062. doi:10.1038/srep25062.

[170] F.M. Kievit, S.J. Florczyk, M.C. Leung, O. Veiseh, J.O. Park, M.L. Disis, M. Zhang, Chitosan–alginate 3D scaffolds as a mimic of the glioma tumor microenvironment, Biomaterials. 31 (2010) 5903–5910. doi:10.1016/j.biomaterials.2010.03.062.

[171] A. Jain, M. Betancur, G.D. Patel, C.M. Valmikinathan, V.J. Mukhatyar, A. Vakharia, S.B. Pai, B. Brahma, T.J. MacDonald, R.V. Bellamkonda, Guiding intracortical brain tumour cells to an extracortical cytotoxic hydrogel using aligned polymeric nanofibres, Nat. Mater. 13 (2014) 308–316. doi:10.1038/nmat3878.

[172] L. Ma, J. Barker, C. Zhou, W. Li, J. Zhang, B. Lin, G. Foltz, J. Küblbeck, P. Honkakoski, Towards personalized medicine with a three-dimensional micro-scale perfusion-based two-chamber tissue model system, Biomaterials. (2012). http://www.sciencedirect.com/science/article/pii/S0142961212002591 (accessed January 10, 2013).

[173] B.M. Baker, C.S. Chen, Deconstructing the third dimension–how 3D culture microenvironments alter cellular cues, J. Cell Sci. 125 (2012) 3015–3024.

[174] L.G. Griffith, M.A. Swartz, Capturing complex 3D tissue physiology in vitro, Nat. Rev. Mol. Cell Biol. 7 (2006) 211–224. doi:10.1038/nrm1858.

[175] M.W. Tibbitt, K.S. Anseth, Hydrogels as extracellular matrix mimics for 3D cell culture, Biotechnol. Bioeng. 103 (2009) 655–663. doi:10.1002/bit.22361.

[176] M.J. Bissell, D. Radisky, Putting tumours in context, Nat. Rev. Cancer. 1 (2001) 46–54.

[177] M.J. Paszek, N. Zahir, K.R. Johnson, J.N. Lakins, G.I. Rozenberg, A. Gefen, C.A. Reinhart-King, S.S. Margulies, M. Dembo, D. Boettiger, D.A. Hammer, V.M. Weaver, Tensional homeostasis and the malignant phenotype, Cancer Cell. 8 (2005) 241–254. doi:10.1016/j.ccr.2005.08.010.

[178] P.A. Kenny, G.Y. Lee, C.A. Myers, R.M. Neve, J.R. Semeiks, P.T. Spellman, K. Lorenz, E.H. Lee, M.H. Barcellos-Hoff, O.W. Petersen, The morphologies of breast cancer cell lines in three-dimensional assays correlate with their profiles of gene expression, Mol. Oncol. 1 (2007) 84–96.

[179] H.G. Schild, Poly (N-isopropylacrylamide): experiment, theory and application, Prog. Polym. Sci. 17 (1992) 163–249.

[180] D.J. Overstreet, R.Y. McLemore, B.D. Doan, A. Farag, B.L. Vernon, Temperature-Responsive Graft Copolymer Hydrogels for Controlled Swelling and Drug Delivery, Soft Mater. 11 (2013) 294–304. doi:10.1080/1539445X.2011.640731.

[181] D.J. Overstreet, R. Huynh, K. Jarbo, R.Y. McLemore, B.L. Vernon, In situ forming, resorbable graft copolymer hydrogels providing controlled drug release, J. Biomed. Mater. Res. A. 101A (2013) 1437–1446. doi:10.1002/jbm.a.34443.

[182] K.-H. Park, K. Yun, Immobilization of Arg-Gly-Asp (RGD) sequence in a thermosensitive hydrogel for cell delivery using pheochromocytoma cells (PC12), J. Biosci. Bioeng. 97 (2004) 374–377.

[183] K.-H. Park, K. Na, S.W. Kim, S.Y. Jung, K.H. Park, H.-M. Chung, Phenotype of Hepatocyte Spheroids Behavior within Thermo-Sensitive Poly(NiPAAm-co-PEG-g-GRGDS) Hydrogel as a Cell Delivery Vehicle, Biotechnol. Lett. 27 (2005) 1081–1086. doi:10.1007/s10529-005-8453-0.

[184] K.-H. Park, K. Na, H.-M. Chung, Enhancement of the adhesion of fibroblasts by peptide containing an Arg-Gly-Asp sequence with poly (ethylene glycol) into a thermo-reversible hydrogel as a synthetic extracellular matrix, Biotechnol. Lett. 27 (2005) 227–231.

[185] R.A. Stile, K.E. Healy, Thermo-Responsive Peptide-Modified Hydrogels for Tissue Regeneration, Biomacromolecules. 2 (2001) 185–194. doi:10.1021/bm0000945.

[186] K.-H. Park, K. Na, S.Y. Jung, S.W. Kim, K.H. Park, K.Y. Cha, H.-M. Chung, Insulinoma cell line (MIN6) adhesion and spreading mediated by Arg-Gly-Asp (RGD) sequence conjugated in thermo-reversible gel, J. Biosci. Bioeng. 99 (2005) 598–602. doi:10.1263/jbb.99.598.

[187] K. Na, K.-H. Park, Conjugation of Arg-Gly-Asp sequence into thermo-reversible gel as an extracellular matrix for 3T3-L1 fibroblast cell culture, Biotechnol. Lett. 22 (2000) 1553–1556. doi:10.1023/A:1005680800420.

[188] T. Okano, N. Yamada, H. Sakai, Y. Sakurai, A novel recovery system for cultured cells using plasma-treated polystyrene dishes grafted with poly(N-isopropylacrylamide), J. Biomed. Mater. Res. 27 (1993) 1243–1251. doi:10.1002/jbm.820271005.

[189] M.R. Kim, J.H. Jeong, T.G. Park, Swelling Induced Detachment of Chondrocytes Using RGD-Modified Poly(N-isopropylacrylamide) Hydrogel Beads, Biotechnol. Prog. 18 (2002) 495–500. doi:10.1021/bp020287z.

[190] K. Nishida, M. Yamato, Y. Hayashida, K. Watanabe, N. Maeda, H. Watanabe, K. Yamamoto, S. Nagai, A. Kikuchi, Y. Tano, T. Okano, Functional bioengineered corneal epithelial sheet grafts from corneal stem cells expanded ex vivo on a temperature-responsive cell culture surface:, Transplantation. 77 (2004) 379–385. doi:10.1097/01.TP.0000110320.45678.30.

[191] M. Nitschke, S. Gramm, T. Götze, M. Valtink, J. Drichel, B. Voit, K. Engelmann, C. Werner, Thermo-responsive poly(NiPAAm-co-DEGMA) substrates for gentle harvest of human corneal endothelial cell sheets, J. Biomed. Mater. Res. A. 80A (2007) 1003–1010. doi:10.1002/jbm.a.31098.

[192] K. Haraguchi, T. Takehisa, M. Ebato, Control of Cell Cultivation and Cell Sheet Detachment on the Surface of Polymer/Clay Nanocomposite Hydrogels, Biomacromolecules. 7 (2006) 3267–3275. doi:10.1021/bm060549b.

[193] R. Stupp, W.P. Mason, M.J. Van Den Bent, M. Weller, B. Fisher, M.J. Taphoorn, K. Belanger, A.A. Brandes, C. Marosi, U. Bogdahn, Radiotherapy plus concomitant and adjuvant temozolomide for glioblastoma, N. Engl. J. Med. 352 (2005) 987–996.

[194] B.H. Lee, B. West, R. McLemore, C. Pauken, B.L. Vernon, In-Situ Injectable Physically and Chemically Gelling NIPAAm-Based Copolymer System for Embolization, Biomacromolecules. 7 (2006) 2059–2064. doi:10.1021/bm060211h.

[195] X.Z. Shu, K. Ghosh, Y. Liu, F.S. Palumbo, Y. Luo, R.A. Clark, G.D. Prestwich, Attachment and spreading of fibroblasts on an RGD peptide–modified injectable hyaluronan hydrogel, J. Biomed. Mater. Res. A. 68 (2004) 365–375.

[196] D.J. Siegwart, J.K. Oh, H. Gao, S.A. Bencherif, F. Perineau, A.K. Bohaty, J.O. Hollinger, K. Matyjaszewski, Biotin-, Pyrene-, and GRGDS-Functionalized Polymers and Nanogels via ATRP and End Group Modification, Macromol. Chem. Phys. 209 (2008) 2179–2193. doi:10.1002/macp.200800337.

[197] A. Guzman, M.J. Ziperstein, L.J. Kaufman, The effect of fibrillar matrix architecture on tumor cell invasion of physically challenging environments, Biomaterials. 35 (2014) 6954–6963. doi:10.1016/j.biomaterials.2014.04.086.

[198] R.A. Weiss-Malik, F.J. Solis, B.L. Vernon, Independent control of lower critical solution temperature and swelling behavior with pH for poly(N-isopropylacrylamide-co-maleic acid), J. Appl. Polym. Sci. 94 (2004) 2110–2116. doi:10.1002/app.21000.

[199] G. Chen, A.S. Hoffman, Graft co-polymers that exhibit temperature induced phase transitions over a wide range of pH, Nature. 373 (1995).

[200] J.F. Pollock, K.E. Healy, Mechanical and swelling characterization of poly(N-isopropyl acrylamide -co- methoxy poly(ethylene glycol) methacrylate) sol–gels, Acta Biomater. 6 (2010) 1307–1318. doi:10.1016/j.actbio.2009.11.027.

[201] B. Vernon, S.W. Kim, Y.H. Bae, Thermoreversible copolymer gels for extracellular matrix, J. Biomed. Mater. Res. 51 (2000) 69–79.

[202] A. Eramo, L. Ricci-Vitiani, A. Zeuner, R. Pallini, F. Lotti, G. Sette, E. Pilozzi, L.M. Larocca, C. Peschle, R. De Maria, Chemotherapy resistance of glioblastoma stem cells, Cell Death Differ. 13 (2006) 1238–1241. doi:10.1038/sj.cdd.4401872.

[203] A. Murat, E. Migliavacca, T. Gorlia, W.L. Lambiv, T. Shay, M.-F. Hamou, N. de Tribolet, L. Regli, W. Wick, M.C.M. Kouwenhoven, J.A. Hainfellner, F.L. Heppner, P.-Y. Dietrich, Y. Zimmer, J.G. Cairncross, R.-C. Janzer, E. Domany, M. Delorenzi, R. Stupp, M.E. Hegi, Stem Cell–Related "Self-Renewal" Signature and High Epidermal Growth Factor Receptor Expression Associated With Resistance to Concomitant Chemoradiotherapy in Glioblastoma, J. Clin. Oncol. 26 (2008) 3015–3024. doi:10.1200/JCO.2007.15.7164.

[204] S.K. Singh, R. Fiorelli, R. Kupp, S. Rajan, E. Szeto, C. Lo Cascio, C.L. Maire, Y. Sun, J.A. Alberta, J.M. Eschbacher, K.L. Ligon, M.E. Berens, N. Sanai, S. Mehta, Post-translational Modifications of OLIG2 Regulate Glioma Invasion through the TGF-β Pathway, Cell Rep. 16 (2016) 950–966. doi:10.1016/j.celrep.2016.06.045.

[205] R. Kupp, L. Shtayer, A.-C. Tien, E. Szeto, N. Sanai, D.H. Rowitch, S. Mehta, Lineage-Restricted OLIG2-RTK Signaling Governs the Molecular Subtype of Glioma Stem-like Cells, Cell Rep. 16 (2016) 2838–2845. doi:10.1016/j.celrep.2016.08.040.

[206] Y. Hu, G.K. Smyth, ELDA: Extreme limiting dilution analysis for comparing depleted and enriched populations in stem cell and other assays, J. Immunol. Methods. 347 (2009) 70–78. doi:10.1016/j.jim.2009.06.008.

[207] A. Higuchi, Q.-D. Ling, S. Suresh Kumar, Y. Chang, A. A. Alarfaj, M. A. Munusamy, K. Murugan, S.-T. Hsu, A. Umezawa, Physical cues of cell culture materials lead the direction of differentiation lineages of pluripotent stem cells, J. Mater. Chem. B. 3 (2015) 8032–8058. doi:10.1039/C5TB01276G.

[208] A. Kawaguchi, T. Miyata, K. Sawamoto, N. Takashita, A. Murayama, W. Akamatsu, M. Ogawa, M. Okabe, Y. Tano, S.A. Goldman, H. Okano, Nestin-EGFP Transgenic Mice: Visualization of the Self-Renewal and Multipotency of CNS Stem Cells, Mol. Cell. Neurosci. 17 (2001) 259–273. doi:10.1006/mcne.2000.0925.

[209] D. Park, A.P. Xiang, F.F. Mao, L. Zhang, C.-G. Di, X.-M. Liu, Y. Shao, B.-F. Ma, J.-H. Lee, K.-S. Ha, N. Walton, B.T. Lahn, Nestin Is Required for the Proper Self-Renewal of Neural Stem Cells, STEM CELLS. 28 (2010) 2162–2171. doi:10.1002/stem.541.

[210] A. Soeda, A. Inagaki, N. Oka, Y. Ikegame, H. Aoki, S. Yoshimura, S. Nakashima, T. Kunisada, T. Iwama, Epidermal Growth Factor Plays a Crucial Role in Mitogenic Regulation of Human Brain Tumor Stem Cells, J. Biol. Chem. 283 (2008) 10958–10966. doi:10.1074/jbc.M704205200.

[211] A. Chakravarti, A. Chakladar, M.A. Delaney, D.E. Latham, J.S. Loeffler, The Epidermal Growth Factor Receptor Pathway Mediates Resistance to Sequential Administration of Radiation and Chemotherapy in Primary Human Glioblastoma Cells in a RAS-dependent Manner, Cancer Res. 62 (2002) 4307–4315.

[212] J.N. Sarkaria, B.L. Carlson, M.A. Schroeder, P. Grogan, P.D. Brown, C. Giannini, K.V. Ballman, G.J. Kitange, A. Guha, A. Pandita, C.D. James, Use of an Orthotopic Xenograft Model for Assessing the Effect of Epidermal Growth Factor Receptor Amplification on Glioblastoma Radiation Response, Am. Assoc. Cancer Res. 12 (2006) 2264–2271. doi:10.1158/1078-0432.CCR-05-2510.

[213] K.L. Ligon, J.A. Alberta, A.T. Kho, J. Weiss, M.R. Kwaan, C.L. Nutt, D.N. Louis, C.D. Stiles, D.H. Rowitch, The Oligodendroglial Lineage Marker OLIG2 Is Universally Expressed in Diffuse Gliomas, J. Neuropathol. Exp. Neurol. 63 (2004) 499–509. doi:10.1093/jnen/63.5.499.

[214] M.E. Hardee, A.E. Marciscano, C.M. Medina-Ramirez, D. Zagzag, A. Narayana, S.M. Lonning, M.H. Barcellos-Hoff, Resistance of Glioblastoma-Initiating Cells to

Radiation Mediated by the Tumor Microenvironment Can Be Abolished by Inhibiting Transforming Growth Factor-β, Cancer Res. 72 (2012) 4119–4129. doi:10.1158/0008-5472.CAN-12-0546.

[215] D. Uribe, Á. Torres, J.D. Rocha, I. Niechi, C. Oyarzún, L. Sobrevia, R. San Martín, C. Quezada, Multidrug resistance in glioblastoma stem-like cells: Role of the hypoxic microenvironment and adenosine signaling, Mol. Aspects Med. (2017). doi:10.1016/j.mam.2017.01.009.

[216] M.-J. Kim, R.-K. Kim, C.-H. Yoon, S. An, S.-G. Hwang, Y. Suh, M.-J. Park, H.Y. Chung, I.G. Kim, S.-J. Lee, Importance of PKCδ signaling in fractionated-radiation-induced expansion of glioma-initiating cells and resistance to cancer treatment, J Cell Sci. 124 (2011) 3084–3094. doi:10.1242/jcs.080119.

[217] S.M. van Neerven, M. Tieken, L. Vermeulen, M.F. Bijlsma, Bidirectional interconversion of stem and non-stem cancer cell populations: A reassessment of theoretical models for tumor heterogeneity, Mol. Cell. Oncol. 3 (2015). doi:10.1080/23723556.2015.1098791.

[218] E.L. Cussler, Diffusion: mass transfer in fluid systems, Cambridge University Press, 1997.

[219] H. Guerrero-Cázares, K.L. Chaichana, A. Quiñones-Hinojosa, Neurosphere Culture and Human Organotypic Model to Evaluate Brain Tumor Stem Cells, Methods Mol. Biol. Clifton NJ. 568 (2009) 73–83. doi:10.1007/978-1-59745-280-9_6.

[220] R.G. Thorne, S. Hrabětová, C. Nicholson, Diffusion of Epidermal Growth Factor in Rat Brain Extracellular Space Measured by Integrative Optical Imaging, J. Neurophysiol. 92 (2004) 3471–3481. doi:10.1152/jn.00352.2004.

[221] N. Cordes, J. Seidler, R. Durzok, H. Geinitz, C. Brakebusch, β1-integrin-mediated signaling essentially contributes to cell survival after radiation-induced genotoxic injury, Oncogene. 25 (2005) 1378–1390. doi:10.1038/sj.onc.1209164.

[222] S. Osuka, O. Sampetrean, T. Shimizu, I. Saga, N. Onishi, E. Sugihara, J. Okubo, S. Fujita, S. Takano, A. Matsumura, H. Saya, IGF1 Receptor Signaling Regulates Adaptive Radioprotection in Glioma Stem Cells, STEM CELLS. 31 (2013) 627–640. doi:10.1002/stem.1328.

[223] M. Kioi, H. Vogel, G. Schultz, R.M. Hoffman, G.R. Harsh, J.M. Brown, Inhibition of vasculogenesis, but not angiogenesis, prevents the recurrence of glioblastoma after irradiation in mice, J. Clin. Invest. 120 (2010) 694–705. doi:10.1172/JCI40283.

[224] N. Goffart, A. Lombard, F. Lallemand, J. Kroonen, J. Nassen, E.D. Valentin, S. Berendsen, M. Dedobbeleer, E. Willems, P. Robe, V. Bours, D. Martin, P. Martinive, P. Maquet, B. Rogister, CXCL12 mediates glioblastoma resistance to radiotherapy in the subventricular zone, Neuro-Oncol. (2016) now136. doi:10.1093/neuonc/now136.

[225] H. Xu, S. Rahimpour, C.L. Nesvick, X. Zhang, J. Ma, M. Zhang, G. Zhang, L. Wang, C. Yang, C.S. Hong, A.V. Germanwala, J.B. Elder, A. Ray-Chaudhury, Y. Yao, M.R.

Gilbert, R.R. Lonser, J.D. Heiss, R.O. Brady, Y. Mao, J. Qin, Z. Zhuang, Activation of hypoxia signaling induces phenotypic transformation of glioma cells: implications for bevacizumab antiangiogenic therapy, Oncotarget. 6 (2015) 11882–11893.

[226] J. Kolenda, S.S. Jensen, C. Aaberg-Jessen, K. Christensen, C. Andersen, N. Brünner, B.W. Kristensen, Effects of hypoxia on expression of a panel of stem cell and chemoresistance markers in glioblastoma-derived spheroids, J. Neurooncol. 103 (2010) 43–58. doi:10.1007/s11060-010-0357-8.

[227] A. Jagielska, A.L. Norman, G. Whyte, K.J.V. Vliet, J. Guck, R.J.M. Franklin, Mechanical Environment Modulates Biological Properties of Oligodendrocyte Progenitor Cells, Stem Cells Dev. 21 (2012) 2905–2914. doi:10.1089/scd.2012.0189.

[228] N.D. Leipzig, M.S. Shoichet, The effect of substrate stiffness on adult neural stem cell behavior, Biomaterials. 30 (2009) 6867–6878. doi:10.1016/j.biomaterials.2009.09.002.

[229] L.J. Kuo, L.-X. Yang, γ-H2AX - A Novel Biomarker for DNA Double-strand Breaks, In Vivo. 22 (2008) 305–309.

[230] D. Klokov, S.M. MacPhail, J.P. Banáth, J.P. Byrne, P.L. Olive, Phosphorylated histone H2AX in relation to cell survival in tumor cells and xenografts exposed to single and fractionated doses of X-rays, Radiother. Oncol. 80 (2006) 223–229. doi:10.1016/j.radonc.2006.07.026.

[231] K. Takahashi, K. Tanabe, M. Ohnuki, M. Narita, T. Ichisaka, K. Tomoda, S. Yamanaka, Induction of Pluripotent Stem Cells from Adult Human Fibroblasts by Defined Factors, Cell. 131 (2007) 861–872. doi:10.1016/j.cell.2007.11.019.

[232] J. Skog, T. Wurdinger, S. van Rijn, D. Meijer, L. Gainche, M. Sena-Esteves, W.T. Curry, R.S. Carter, A.M. Krichevsky, X.O. Breakefield, Glioblastoma microvesicles transport RNA and protein that promote tumor growth and provide diagnostic biomarkers, Nat. Cell Biol. 10 (2008) 1470–1476. doi:10.1038/ncb1800.

[233] P. Kucharzewska, H.C. Christianson, J.E. Welch, K.J. Svensson, E. Fredlund, M. Ringnér, M. Mörgelin, E. Bourseau-Guilmain, J. Bengzon, M. Belting, Exosomes reflect the hypoxic status of glioma cells and mediate hypoxia-dependent activation of vascular cells during tumor development, Proc. Natl. Acad. Sci. 110 (2013) 7312–7317. doi:10.1073/pnas.1220998110.

[234] T. Yu, B. Tang, X. Sun, Development of Inhibitors Targeting Hypoxia-Inducible Factor 1 and 2 for Cancer Therapy, Yonsei Med. J. 58 (2017) 489–496. doi:10.3349/ymj.2017.58.3.489.

APPENDIX A

CO-AUTHOR APPROVAL OF PUBLICATION USAGE

The co-authors of prior published works (described in the Preface) have given their consent for this material to be reproduced in this dissertation.